Friedrich Miescher Institute
Novartis Research Foundation
Basel, Switzerland

Optical analysis of synaptic plasticity in rat hippocampus

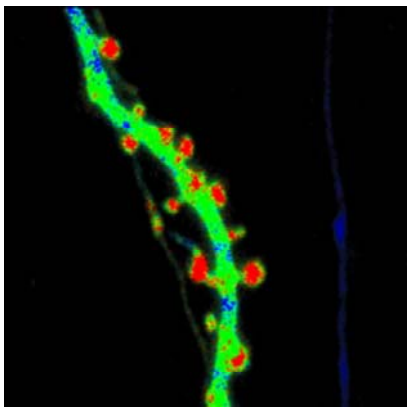

Inauguraldissertation

zur

Erlangung der Würde eines Doktors der Philosophie

vorgelegt der

Philosophisch-Naturwissenschaftlichen Fakultät

der Universität Basel

von

Yan-Ping Zhang

aus Shanghai, China

Basel, 2008

Genehmigt von der Philosophisch-Naturwissenschaftlichen Fakultät

Auf Antrag von

Prof. Dr. Markus A. Rüegg
Dr. Thomas G. Oertner
Prof. Dr. Andreas Lüthi
Prof. Dr. Carl Petersen

Basel, den 11. 12. 2007

Dekan

Prof. Dr. Hans-Peter Hauri

Contents

Summary

Long-term potentiation (LTP) in the CA1 region of the hippocampus is dependent on NMDA receptor activation. Downstream of NMDA receptor signaling, the activation of α-calcium/calmodulin-dependent protein kinase II (αCaMKII) is both necessary and sufficient for the induction of this form of LTP. It has been shown that αCaMKII accumulates in spines after glutamate application or 'chemical LTP'. This postsynaptic accumulation of αCaMKII could be a key step for the induction of LTP, because it localizes the activated kinase close to the substrates of synaptic potentiation. It is not clear, however, what the threshold, time course of αCaMKII translocation are, and whether it is specific to the stimulated synapses only.

To address these three questions, I combined optical stimulation techniques (Channelrhodopsin-2 stimulation and two-photon glutamate uncaging) with optical measurements of calcium transients and αCaMKII concentration. This 'all-optical' approach made it possible to investigate synapse-specific changes during the induction of LTP. I could show that coincident activity of pre- and postsynaptic cells was needed to trigger the translocation of αCaMKII. Functional potentiation could be measured immediately after stimulation, whereas αCaMKII accumulation reached its peak ~10 min later. This points to an additional structural role of αCaMKII at the postsynaptic density. Both αCaMKII fractions, the cytoplasmic fraction and postsynaptic bound αCaMKII, increased after optical LTP induction. These changes were restricted to stimulated spines. In spines that showed a persistent volume increase, the amount of bound αCaMKII was increased by a factor of two after 30-40 minutes.

A second very interesting finding was the close correlation between spine volume changes and LTP, in terms of the time course, induction threshold and specificity. The optical LTP protocol led to a lasting volume increase only in the stimulated spines, but not in directly neighboring spines on the same dendrite. Spine volume reached its maximum immediately after stimulation.

Since my all-optical approach relied heavily on the use of a newly identified light-gated cation channel (Channelrhodopsin-2, ChR2), I finally also characterized light activation of ChR2 in hippocampal pyramidal cells in detail. Neuronal activity could be controlled by blue light with millisecond precision. No direct activation of ChR2 was observed by two-photon imaging lasers, making it possible to combine the ChR2 stimulation technique with two-photon imaging. This led to a third important finding: the release probability of ChR2-expressing axonal terminals was increased if the action potential was induced by light. As a result, pairing of light stimulation with postsynaptic depolarization induced reliable long-term potentiation at CA1 synapses.

In summary, the new all-optical approach that combines ChR2 stimulation, two-photon glutamate uncaging, and optical measurements of calcium transients and protein concentration, provides a new avenue for investigating plasticity at the level of single synapses. The induction of LTP in single synapses revealed that accumulation of αCaMKII is input specific thus validating Hebb's postulate on a micrometer scale.

Chapter 1. General introduction

The basic structural units of the nervous system are individual neurons. In the human nervous system there are about 10^{12} neurons. They accomplish the fundamental task of the nervous system, which is to communicate and process information. Neurons communicate with one another through specialized contact zones, called synapses. There are about 10^{15} synapses in the human brain. Synapses can be either electrical or chemical. Electrical synapses are gap junctions, which consist of specialized proteins that form channels bridging the interiors of two neurons and allow current flow from one neuron to the other. The typical chemical synapses consist of 3 main parts: synaptic vesicles in the presynaptic neuron, membrane thickening in the postsynaptic neuron and the synaptic cleft, the region separating the pre- and postsynaptic membrane. In the adult mammalian central nervous system, electrical synapses among principal cell types (e.g., pyramidal neurons) are rare. Information is passed from one neuron to another mainly through chemical synapses. Moreover, the strength of the communication can be enhanced or diminished by cellular activity. This plasticity is crucial to learning and memory.

A. Rat hippocampus

The hippocampus is one of the most widely studied regions of the brain and is attractive to a wide spectrum of neuroscientists, ranging from psychologists, synaptic physiologists to computational neuroscientists. The hippocampal formation consists of the dentate gyrus, the *Cornu Ammonis* fields CA1-CA3, subiculum, presubiculum, parasubiculum, and entorhinal cortex (Fig 1.1). Although the volume of the hippocampus is about 100 times larger in humans than in rats, the basic layout of cells and fiber pathways is much the same. The dentate gyrus receives its major input from the entorhinal cortex via the perforant pathway. The axons that project from the dentate gyrus to CA3 are called the mossy fibers. The dentate projection to CA3 stops precisely at the border between CA3 and CA2, and the lack of granule cell input is one of the main features that distinguish CA3 from CA2 pyramidal cells. CA3 pyramidal cells give rise to highly collateralized axons. The CA3 projections to CA3 and CA2 are typically called the associated connections, and the CA3 projections to the CA1 field are typically called the Schaffer collaterals. Axons of CA1 pyramidal

cells descend into the stratum oriens or the alveus and bend sharply toward the subiculum (Per Andersen, 2007).

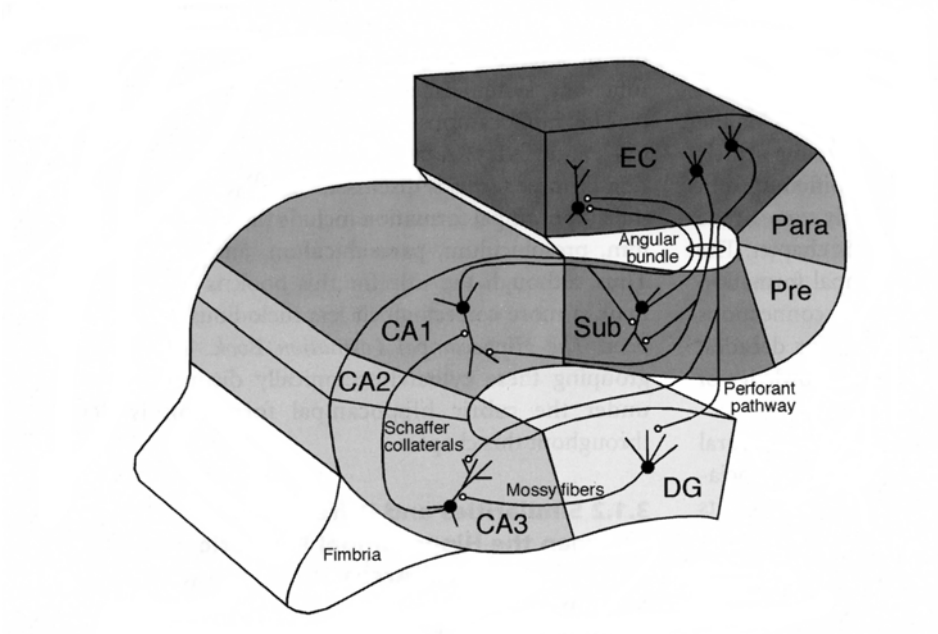

Figure 1.1. ***The hippocampal formation.***

Neurons in the entorhinal cortex (EC) project to the dentate gyrus (DG) and the CA3 field of the hippocampus proper via the perforant pathway. The granule cells of the dentate gyrus project to the CA3 field of the hippocampus via mossy fiber projections. Pyramidal neurons in the CA3 filed of the hippocampus project to CA1 via Schaffer collaterals. Pyramidal cells in CA1 project to the subiculum (Sub). Both CA1 and the subiculum project back to the deep layers of the entorhinal cortex (EC). (Adapted from Per Andersen, 2007).

It is generally agreed that the hippocampus has an essential role in the formation of new memories about experienced events. Damage to the hippocampus affects new long-term memory formation, but does not affect recall of long-term memories that existed well before the damage (Scoville and Milner, 1957). The discovery of place cells in rat hippocampus led to the idea that the hippocampus is involved in storing and processing spatial information (O'Keefe and Dostrovsky, 1971; Muller et al., 1987). Selective tests for the spatial functions of the hippocampus have been widely used, including the Olton radial arm maze (Olton, 1987) and the Morris watermaze (Morris, 1984). An intact hippocampus is required for these simple spatial memory tasks (Cassel et al., 1998; Xavier et al., 1999).

B. Hebb's learning rule

In 1949, Donald Hebb published "Organization of Behaviour: A Neuropsychological Theory". This groundbreaking book set forth a theory to explain behaviour in terms of brain function. In this book he introduced a famous idea, which is also called Hebb's learning rule:

"When an axon of cell A is near enough to excite a cell B and repeatedly or persistently takes part in firing it, some growth process or metabolic change takes place in one or both cells such that A's efficiency, as one of the cells firing B, is increased. "

It describes a basic mechanism for synaptic plasticity — an increase in synaptic efficacy arises from the presynaptic cell's repeated and persistent stimulation of the postsynaptic cell. Hebb predicted that learning and memory would involve synaptic strengthening elicited by the coordinated firing of pre- and postsynaptic cells.

C. Long-term potentiation (LTP)

LTP, a persistent increase in synaptic strength following high-frequency stimulation of a chemical synapse, was first discovered in the rabbit hippocampus by Terje Lømo in 1966 and first described in two papers published in 1973 (Bliss and Gardner-Medwin, 1973; Bliss and Lomo, 1973). Since then, it has been observed at many synapses in other brain areas, including neocortex (Markram and Tsodyks, 1996; Feldman, 2000), amygdala (Huang and Kandel, 1998) and cerebellum (Salin et al., 1996; Lev-Ram et al., 2002). Indeed, by enhancing synaptic transmission, LTP improves the ability of two neurons to communicate with one another across a synapse. LTP shares many features with long-term memory that make it an attractive candidate for a cellular mechanism of learning (Bliss and Collingridge, 1993). For example, LTP and long-term memory are rapidly induced and can potentially last for many months. Both depend upon the synthesis of new proteins and both have properties of associativity. But whether LTP is really triggered during learning and is causally related to memory formation is still a matter of debate (Zamanillo et al., 1999; Martin et al., 2000; Whitlock et al., 2006). Nevertheless, the basic properties of LTP have been intensively studied in the past thirty years. Although some forms of

LTP (e.g. at the mossy fibre synapse in the hippocampus (Nicoll and Malenka, 1995)) show different properties, the LTP at CA1 synapses, the synapses between the Schaffer collateral and the apical dendrites of CA1 pyramidal cells, appears to be identical or very similar to the LTP observed at glutamatergic excitatory synapses throughout the mammalian brain.

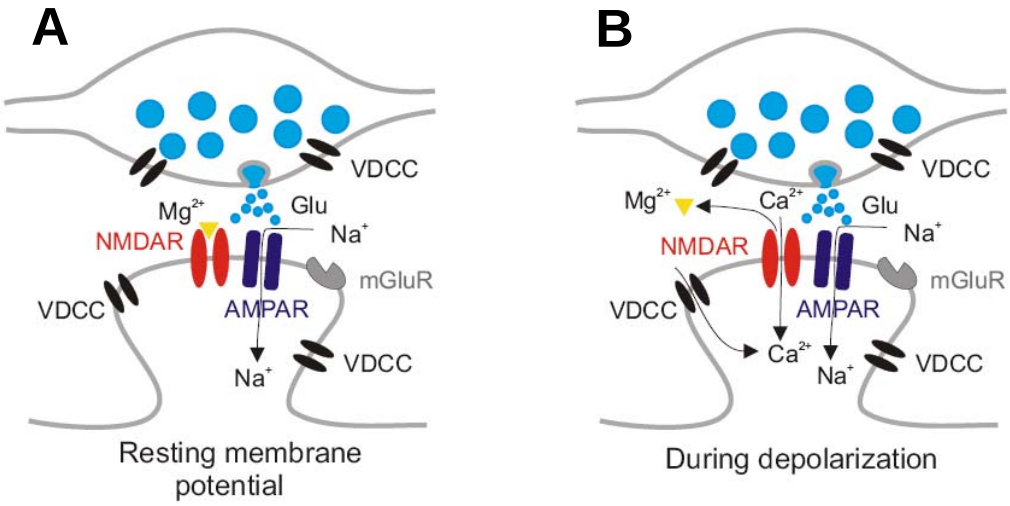

Figure 1.2. ***Model for the induction of LTP.***

A. *During normal synaptic transmission, glutamate (Glu) is released from the presynaptic bouton and acts on both AMPA receptors (AMPARs) and NMDA receptors (NMDARs). However, Na^+ flows only through the AMPA receptor, but not the NMDA receptor, because Mg^{2+} blocks the channel of the NMDA receptor.* ***B****. Depolarization of the postsynaptic cell relieves the Mg^{2+} block of the NMDA receptor channel, allowing Na^+ and Ca^{2+} to flow into the dendritic spine by means of the NMDA receptor. Another source of Ca^{2+} influx is through voltage sensitive Ca^{2+} channels (VDCCs). The resulting rise in Ca^{2+} within the dendritic spine is the critical trigger for LTP.*

In the CA1 region of the hippocampus, LTP is cooperative, which means a crucial number of presynaptic fibres must be simultaneously activated. This property is explained by the fact that, to trigger LTP, the postsynaptic cell must be sufficiently depolarized to allow current (particularly Ca^{2+}) to flow through the NMDA (N-methyl-D-aspartate) receptors. LTP is also associative, that is, strong activation of one set of synapses can facilitate LTP at an independent set of adjacent synapses on the same cell if both sets are activated within a finite temporal window. It is easy to envision how this property makes LTP an attractive mechanism for associative learning or classical conditioning. Moreover, LTP is input-specific. This property

refers the fact that when LTP is elicited at one set of synapses, adjacent synapses that were not activated during the induction protocol do not show LTP. This property is probably most advantageous because it greatly increases the storage capacity of individual neurons. However, it presents major challenges for experimental investigation.

In fact, all of these properties can be explained mechanistically by the biophysical properties of the NMDA receptors that are required to trigger this form of LTP (Nicoll and Malenka, 1999) (Fig 1.2). NMDA receptor exhibits profound voltage dependence because of the blocking of its channel by extracellular Mg^{2+} at resting or hyperpolarized potential, such that it contributes little to the basal synaptic transmission (Collingridge et al., 1983; Johnson and Ascher, 1987; Bliss and Collingridge, 1993). However, when the postsynaptic cell is strongly depolarized such as during LTP induction, Mg^{2+} dissociates from its binding site, allowing Ca^{2+} as well as Na^{+} to enter the dendritic spine. The consequent rise of intracellular calcium is the critical trigger for LTP (Malenka et al., 1989). Cooperativity and associativity occur because strong activation depolarizes adjacent regions of the dendritic tree. The localized calcium within the dendritic spine accounts for the input specificity.

D. Structural plasticity of dendritic spines

The term spine ("espinas" in Spanish) was first introduced by Ramon Cajal in 1888 in his description of small twig-like appendages arising from the branchlets of Purkinje cell dendrites. The substantial structural diversity of dendritic spines has attracted the attention of neuroscientists ever since. Because most spines are beyond the range of normal light microscopy, the dimensions were first measured by electron-microscopical reconstructions. Typical ranges for spines of pyramidal neurons in rodents are 0.004 – 2 μm^3 for total spine volume and 0.1 – 0.7 μm^2 for total surface area (Harris and Kater, 1994). Most glutamatergic synapses are made on the heads of dendritic spines. Immunogold labelling of AMPA-sensitive glutamate receptors, which mediate the fast component of glutamate-mediated synaptic transmission, revealed that spines with larger postsynaptic densities (PSDs) tend to exhibit a higher level of AMPA-receptor immunoreactivity than those with smaller PSDs (Nusser et al., 1998; Takumi et al., 1999). Given that the size of PSDs is correlated with that of

spine heads (Harris and Stevens, 1989), this implies that large spines express a greater number of glutamate receptors than small ones (Matsuzaki et al., 2001b). In addition, the spine neck resistance provides significant electrical isolation of the synapse from its parent dendrite (Araya et al., 2006). Therefore, a dendritic spine not only creates a site of synaptic connection, but also creates a structural, biochemical, and physiological compartment that is specific for that individual synapse.

The idea that the spine might be well suited as a site for neural plasticity was suggested by Ramon Cajal (1911), Donald Hebb (1949) and Bliss & Collingridge (1993). Alteration in spine number or shape could provide a mechanism for the storage of memories, by strengthening or weakening particular synaptic connections in response to experience. This hypothesis stimulated a number of studies attempting to correlate changes in spine morphology with induced changes in synaptic potency, such as induction of LTP (Harris et al., 1992; Engert and Bonhoeffer, 1999; Maletic-Savatic et al., 1999; Toni et al., 1999; Stewart et al., 2005). A pronounced characteristic of the dendritic spine is an enrichment of cytoskeletal actin. Spines from cultured hippocampal neurons exhibit a rapid actin-based motility that is regulated by glutamate receptor activation (Matus, 2000). But how cytoskeletal actin in the dendritic spine could contribute to synaptic plasticity is unclear. EM studies of the neuropil were used to make population comparisons of the structure of dendritic spines across plasticity states. Indeed, increases in the number or volume of dendritic spines or changes in spine shape have been observed (Yuste and Bonhoeffer, 2001; Harris et al., 2003). It is not possible, however, to establish a close correlation between specific changes and the induction of LTP.

E. The role of CaMKII in synaptic plasticity

Calcium/calmodulin-dependent protein kinase II (CaMKII) is expressed at high levels in the central nervous system (Bennett et al., 1983), where it constitutes ~2% of total protein (Erondu and Kennedy, 1985). This enzyme is highly concentrated in the postsynaptic density (PSD), a structure directly attached to the cytoplasmic face of the postsynaptic membrane (Kennedy et al., 1983; Petersen et al., 2003). Several lines of evidence implicate CaMKII as a key component of the molecular machinery of LTP. Postsynaptic injection of inhibitors of CaMKII or genetic deletion of a critical

CaMKII subunit (αCaMKII) blocks the ability to generate LTP (Malinow et al., 1989; Silva et al., 1992b; Silva et al., 1992a; Giese et al., 1998). By increasing the

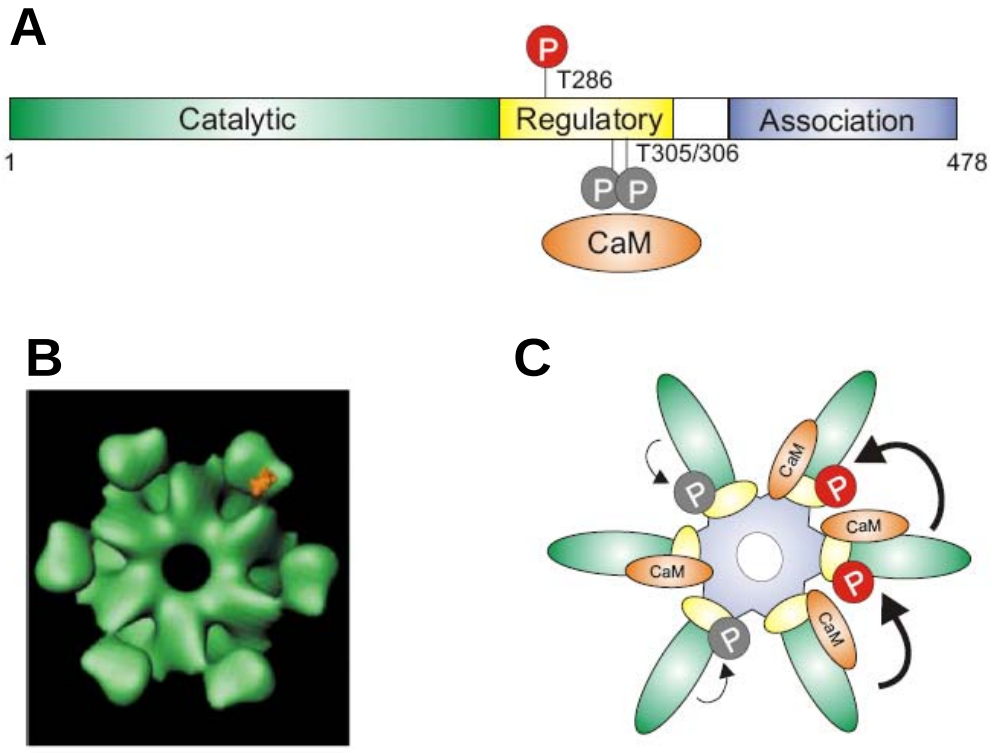

Figure 1.3. ***Structure and regulation of CaMKII.***

A. *The different functional domains in the primary structure of calcium/calmodulin-dependent protein kinase II (CaMKII). T286, T305, T306 are threonine residues that are crucial phosphorylation sites.* ***B.*** *Three-dimensional structure of CaMKII. This view shows only one of the hexameric rings formed by the catalytic regions of six subunits.* ***C.*** *The C-terminal association domains assemble subunits into a holoenzyme that is a stacked pair of hexameric rings with regulatory and catalytic domains projecting outward. Each subunit can be independently activated by binding of Ca^{2+}/calmodulin (CaM). Activation of adjacent subunits results in rapid trans-autophosphorylation at T286 (Red circled 'P', thick arrows), generating autonomous kinase activity. Intrasubunit autophosphorylation at T305, T306 blocks calmodulin binding (grey circled 'P', thin arrows).(Adapted from Lisman et al., 2002; Colbran and Brown, 2004)*

concentration of constitutively active CaMKII in CA1 cells, synaptic transmission is enhanced and LTP is occluded (Lledo et al., 1995). As a holoenzyme, neuronal CaMKII is made up of 12 subunits, primarily the 52 kDa α isoform and the 60 kDa β isoform (Bennett et al., 1983; Miller and Kennedy, 1985). The subunits of the holoenzyme are held together by association domains in their C-terminal, from which the N-termials extend radially (Kanaseki et al., 1991; Kolodziej et al., 2000). The N-

terminal contains the catalytic sites of the kinase as well as the autoinhibitory domains that bind to the catalytic sites in the basal state (Fig 1.3). CaMKII regulation has been reviewed in detail (Hudmon and Schulman, 2002b, a; Lisman et al., 2002; Colbran and Brown, 2004). The binding of Ca^{2+}/calmodulin releases this autoinhibition, allowing phosphorylation to take place at a critical threonine residue, Thr^{286} in α and Thr^{287} in β, and results in the activation of CaMKII. The resulting autonomously active CaMKII autophosphorylates at Thr^{305} and Thr^{306}, blocks Ca^{2+}/calmodulin from re-binding. Moreover, the unique holoenzyme configuration allows for intersubunit phosphorylation, thus its kinase activity continues long after the Ca^{2+} signal has returned to baseline (Mukherji and Soderling, 1994).

It was first shown that treatment of hippocampal slices with K^+-channel blocker TEA led to an enhancement of transmission at CA3-CA1 synapses, which was accompanied by increased CaMKII activity and a 70-80% increase of CaMKII protein in the PSD-enriched fraction (Strack et al., 1997). Soon after, using immunogold labeling with antibody against CaMKII, Reese and his colleagues showed that exposure of cultured hippocampal neurons to high K^+ resulted in 5-fold increase of PSD-associated CaMKII and 1.7-fold increase after glutamate/glycine treatment (Dosemeci et al., 2001). Different treatments seem to have various influences on postsynaptic accumulation of CaMKII. One criticism of these studies is that they relied on population comparisons and were not able to examine the same set of spines before and after the manipulation. The observed differences might simpliy come from the error of population comparisons. Time-lapse imaging of neurons transfected with green fluorescent protein (GFP) tagged proteins has provided a complementary approach to track CaMKII translocation in real time. Applications of glutamate or NMDA to cultured rat hippocampal neurons redistributed αCaMKII from cytosol to synaptic sites likely to PSDs (Shen and Meyer, 1999; Shen et al., 2000; Fong et al., 2002). These findings have created a lot of excitement. It has been suggested that postsynaptic accumulation of αCaMKII could be responsible for the induction of LTP, because it localizes the activated kinase close to the substrates of synaptic potentiation (Lisman and McIntyre, 2001; Lisman and Zhabotinsky, 2001; Soderling et al., 2001). However, a central assumption of this theory has never been tested

experimentally, namely that αCaMKII accumulates specifically and exclusively at synapses that did experience coincident activity.

Another problem has to be kept in mind while interpreting CaMKII translocation results from fluorescence measurements. For small structures like spines, fluorescence measurements in a single color channel are not sufficient to quantify protein concentration, not even relative to the dendrite. Since the size of the spine is below the resolution limit of the light microscopy, the fluorescence intensity of labeled αCaMKII in individual spines is determined by two unknown variables: the concentration of αCaMKII in the spine, and the volume of that spine. In addition, the dynamic changes in spine volume shown in the previous section make single-color measurements over time even more difficult to interpret. The presence of the bound faction increases the CaMKII concentration. Two recent studies have attempted to measure bound CaMKII in individual spines more quantitatively: the first one included a volume marker while studying the translocation of CaMKII (Otmakhov et al., 2004); the second one performed photobleaching of tagged CaMKII in individual dendritic spines and followed fluorescence recovery for up to 30 min (Sharma et al., 2006) to quantify the bound fraction. Consistently, both studies showed that the bound CaMKII fraction in spines was increased after non-physiological strong stimulation. However, whether physiological stimulation, namely coincident activity can increase the bound fraction of postsynaptic CaMKII is still unknown.

F. New advances in technology

New advances in technology have allowed the detection of changes in spine structure and density that may accompany stimulus-induced synaptic plasticity. First, time-lapse microscopy, especially two-photon excitation fluorescence microscopy, allows for comparison of the morphology of spines before and after a manipulation both *in vitro* and *in vivo (Maletic-Savatic et al., 1999; Zuo et al., 2005; Holtmaat et al., 2006)*. Second, two-photon glutamate uncaging allows the experimenter to select nearly any visualized spine and deliver an arbitrary pattern of glutamate stimulation to the postsynaptic terminal of the selected spine (Matsuzaki et al., 2001a). Last, genetic manipulation of neurons with a light sensitive channel, Channelrhodopsin-2 (ChR2), allows for remote control of neuronal activity with millisecond precision (Boyden et al., 2005).

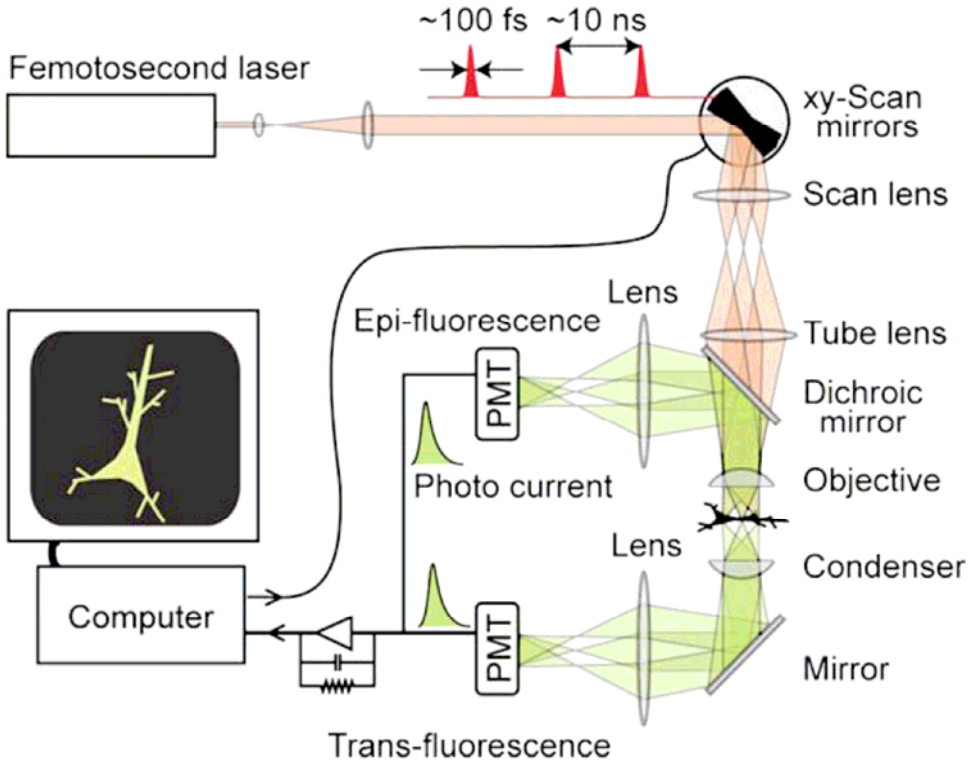

Figure 1.4. ***Two-Photon Excitation Microscopy.***

Schematic drawing of a two-photon microscope with epifluorescence and transfluorescence detection. (Adapted from Svoboda and Yasuda, 2006)

F.1 Two-photon excitation fluorescence microscopy

A two-photon microscope is a laser-scanning microscope that uses a long wavelength laser (near infrared, 800-1000 nm) to excite fluorescence. Fluorescence is generated when a molecule is electronically excited from its ground state to an excited state by absorption of a photon of the corresponding energy and then relaxes rapidly by emission of a red-shifted photon again to its ground state. One photon excitation is not the only possibility to excite a fluorophore. Two-photon excitation was first described theoretically by Göppert-Mayer in 1931. A fluorophore can also absorb two photons of approximately half the energy or twice the wavelength simultaneously, combining their energy to make the transition to the excited state. In 1990, Denk *et al.* described two-photon excitation fluorescence microscopy for imaging biological specimens (Denk et al., 1990). Since then a large number of studies have employed this technique to image fluorescent probes and to measure ionic concentration in small neuronal compartments in intact brain slices and even in deep brain tissue of living

animals (Denk et al., 1996; Svoboda et al., 1997; Helmchen et al., 2001). A detailed description of the physical principles relevant to two-photon micrsocopy can be found in a paper by Denk *et al*. (1995), and practical issues of microscope design are discussed by Denk & Svoboda (Denk and Svoboda, 1997; Svoboda and Yasuda, 2006) (see Fig 1.4).

What is the advantage of using two-photon absorption to excite fluorescence? In a focused laser, the intensity is highest in the vicinity of the focus and drops off quadratically with distance. The probability of two-photon absorption depends on the second power of the light intensity. As a result, fluorophores are excited almost exclusively in a tiny diffraction limited focal volume. In practice a focal volume can be as small as ~0.1 μm^3 (for a 1.4 NA objective) (Zipfel et al., 2003). Since all emitted photons originate from the focal volume, there is no need for a confocal pinhole to reject out-of-focus fluorescence. Wide-field detection can be used to capture as many emitted photons as possible, even the ones exiting the preparation through the condenser (Fig 1.4). Localization of excitation also guarantees that bleaching and phototoxicity, undesirable effects of the illumination, will be restricted to the small focal volume only. In addition, the longer wavelength will be less scattered in tissue, allowing for deeper penetration in the intact tissue. Depending on the properties of the tissue, two-photon excitation microscopy can image up to 1 mm deep in tissue (Oheim et al., 2001; Theer et al., 2003). As a third advantage, most fluorescent probes have a much broader two-photon excitation spectrum, which means that different fluorescent probes can be excited simultaneously by the same laser beam. Moreover, there are no endogenous fluorophores in nerve cells that can be excited by two-photon excitation at long wavelength. Therefore, extremely low levels of autofluorescence are detected.

F.2 Two-photon glutamate uncaging

Electrophysiological analysis of synaptic currents has been a valuable tool to study synaptic transmission, but it has been difficult to isolate the responses of individual synapses. The development of caged compounds with a good two-photon cross-section has facilitated the understanding of synaptic physiology at the single synapse level. For example, MNI-caged glutamate provides a sufficiently large two-photon

cross-section (0.06 GM) so that glutamate can be photoreleased in synaptic clefts to mimic unitary synaptic currents (Matsuzaki et al., 2001b; Carter and Sabatini, 2004; Sobczyk et al., 2005). Using glutamate uncaging, the number and properties of glutamate receptors in single postsynaptic densities have been measured (Matsuzaki et al., 2001b; Andrasfalvy et al., 2003; Smith et al., 2003; Carter and Sabatini, 2004; Sobczyk et al., 2005). The measurement of calcium influx through NMDA receptors and calcium-permeable AMPA receptors in single spines was done by combining two-photon glutamate uncaging with two-photon calcium imaging (Carter and Sabatini, 2004; Noguchi et al., 2005; Sobczyk et al., 2005). Repetitive two-photon uncaging in zero-Mg^{2+} solution has been used to induce synaptic plasticity at single synapses (Matsuzaki et al., 2004). Synaptic integration in dendrites was studied by stimulation of multiple spines using a fast uncaging method (Gasparini and Magee, 2006). In summary, two-photon glutamate uncaging allows for excellent spatial and temporal resolution. However, this technique completely bypasses the presynaptic terminal and is therefore restricted to the investigation of postsynaptic mechanisms.

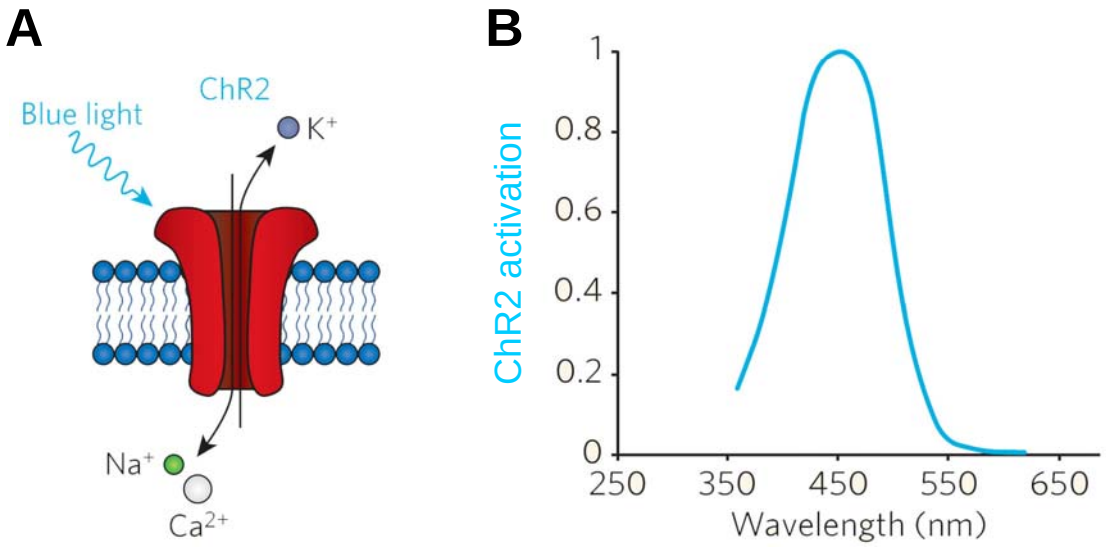

Figure 1.5. ***Light activation of channeldhodopsin-2 (ChR2).***

A. *Blue light activates ChR2, a cation channel, which depolarizes the cell and causes action potentials.*
B. *The absorption spectrum of ChR2.(Adapted from Hausser and Smith, 2007)*

F.3 Controlling neural activity with light

The traditional approach for controlling neural activity uses an extracellular stimulation electrode. Although the timing of the electrode stimulation is very precise,

its specificity and spatial control are poor because all neurons within a certain range are affected. Taking advantage of a newly identified light-gated cation channel, Channelrhodopsin-2 (ChR2) (Fig 1.5), it is now possible to control neuronal activity with blue light. ChR2 was discovered in the green alga *Chlamydomonas reinhardtii*, where it triggers photon-orientation movements that allow the alga to find optimal conditions for photosynthesis (Sineshchekov et al., 2002; Nagel et al., 2003). ChR2 is related to rhodopsin, the light-sensitive protein in mammalian vision. Like rhodospin, it requires all-trans retinal, a vitamin-A based chromophore cofactor, in order to be activated by light. But unlike rhodopsin, which activates a chemical cascade that eventually results in neural activity, ChR2 is a self-contained, light-sensitive channel that allows Na^+ and Ca^{2+} ions to enter the cell following exposure to ~470 nm blue light (Nagel et al., 2003; Nagel et al., 2005). Because the cation conductance of ChR2 is confined to the N-terminal 315 amino acids, ChR2 can be readily expressed in mammalian neurons through genetic methods (Boyden et al., 2005; Arenkiel et al., 2007; Petreanu et al., 2007; Zhang and Oertner, 2007). Conveniently, mammalian brain tissue normally contains enough all-trans retinal, which means adding retinal is not necessary. Due to its rapid kinetics, ChR2 enables driving of spikes or synaptic transmission with millisecond precision.

G. Scope of the thesis

Long-term potentiation, one form of synaptic plasticity, has captured the attention of neuroscientists for over three decades (Chapter 1). Synaptic plasticity allows bi-directional control of synaptic strength and empowers neuronal circuits with much greater flexibility. Much remains to be learned about this fascinating phenomenon.

Donald Hebb predicted that synaptic strengthening could be elicited by the coordinated activity of pre- and postsynaptic cells (Chapter 1). LTP has been reliably elicited and studied in brain slice preparation *in vitro*. However, it has been very difficult to demonstrate that LTP is accompanied or even caused by morphological changes on the subcellular level. Are synapse-specific associative changes involved? Should we view synapses as independent units of information processing or do neighboring synapses cooperate? Spines show great diversity in shape and size. Do they change their transmission characteristics according to the same rule? Finally, what is the temporal profile of LTP induction or expression? What

biochemical/molecular changes allow the initial increase in synaptic strength to be maintained?

To address these questions, I focused on the connection between hippocampal CA3 pyramidal cells and CA1 pyramidal cells, a well-defined system for studying synaptic plasticity. Most of these synapses are formed on dendritic spines, which show a rich, dynamic diversity of shape and size. Understanding the functional implication of this diversity is the key motivation of my PhD thesis work.

To examine the properties of individual synapses in intact brain tissue, I used two-photon laser scanning microscopy to optically record the amplitude of postsynaptic calcium transients in dendritic spines. In vitro transfection technique allowed us to study morphology and function of genetically modified neurons within a network of wildtype cells. Optical monitoring and manipulation of a number of fluorescently labeled proteins enabled us to study synaptic plasticity at the level of single synapses. In Chapter 2, a new method that we have developed to induce LTP of synaptic connections in CA1 using the light stimulation technique is described (Zhang and Oertner, 2007). To stimulate individually identified axons in a slice culture, we transfected neurons with a light sensitive cation channel, Channelrhosopsin-2 (ChR2). As compared to stimulation by extracellular electrodes, light stimulation is very selective. Compared to multiple patch-clamp recordings, light stimulation has a much higher throughput and allows contacts to be visualized with ease.

To answer the question whether synapse-specific associative changes are involved, we have further improved our optical stimulation technique, which is discussed in Chapter 3. We used channelrhodopsin-2 to optically depolarize CA1 pyramidal cells while stimulating individual excitatory synapses on dendritic spines by two-photon glutamate uncaging. Repetitive pairing of light with MNI-glutamate uncaging led to a lasting increase of spine volume and translocation of αCaMKII to stimulated synapses, but not to neighboring spines. Although two-photon glutamate uncaging allows for excellent spatial resolution, this technique completely bypasses the presynaptic terminal and is therefore restricted to the investigation of postsynaptic mechanisms.

Thus, in Chapter 4, an all-optical method for identification of functional synaptic contacts in intact brain tissue is introduced. To control glutamate release and postsynaptic depolarization non-invasively, we expressed Channelrhodopsin-2 both pre- and post-synaptically. Our strategy to validate functional synapses was to monitor the fluorescence changes of a genetically encoded Ca^{2+} indicator (GCaMP2) postsynaptically. This all-optical method has no time limitation for plasticity experiments, thus has the great potential to visualize individual synapses as they undergo LTP and ask directly whether both pre- and postsynaptic growth occurs.

Although our research is focused mainly on excitatory synapses, we have started to investigate G-protein coupled $GABA_B$ receptors, which induce slow inhibitory potentials by activating K^+ -channels. In collaboration with Dr. Bernhard Bettler, we investigated specific targeting of GFP-labeled $GABA_B$ receptor variants in organotypic slice cultures (Vigot et al., 2006). Chapter 5 gives a description of this collaborative work. Interestingly, $GABA_{B1a}$ subunit and $GABA_{B1b}$ subunit showed distinct distribution in the axons and dendrites, even at the individual dendrite spines level. This differential distribution may underlie the functional diversity of the knockout mice.

Chapter 6 provides a general discussion of the advantages as well as limitations of using optical methods to study synaptic plasticity. The biological significance of our studies will be discussed and future experiments will be proposed in this chapter. This thesis also includes four appendixes. The first one describes the use of site-directed mutagenesis to generate non-clumpy GFP and YFP fusion proteins. The method is useful to generate point mutations of any gene of interest. Appendix B summarizes the generation and optimization of two-promoter vectors. This strategy is useful to express two genes of interest simultaneously at a constant ratio. Appendix C shows the common problem of making red fusion proteins and highlights advantages of using tdimer2RFP. Two-photon excitation spectra of commonly used fluorophores are presented in appendix D.

Chapter 2. Optical induction of synaptic plasticity using a light-sensitive channel

Yan-Ping Zhang & Thomas G Oertner

Nature Methods. 2007 Feb;4(2):139-41.

Abstract

We have combined millisecond activation of channelrhodopsin-2 (ChR2), a light-gated ion channel, with two-photon calcium imaging to investigate active synaptic contacts in rat hippocampal slice cultures. Calcium influx was larger during light-induced action potentials than during action potentials induced by somatic current injection, leading to highly reproducible synaptic transmission. Pairing of light stimulation with postsynaptic depolarization induced long-term potentiation, making this technique ideal for genetic and pharmacological dissection of synaptic plasticity.

Introduction

Long-term potentiation, a form of synaptic plasticity, is a primary experimental model for the study of cellular and molecular mechanisms underlying learning and memory. Several reports have suggested that there might be considerable heterogeneity in the expression of plasticity at individual synapses (Isaac et al., 1998; Petersen et al., 1998; Debanne et al., 1999), but it has been difficult to measure both functional and morphological parameters of synapses at the same time (Koester and Sakmann, 1998; Engert and Bonhoeffer, 1999; Holthoff et al., 2002). Laser uncaging of glutamate has recently been used to study synaptic plasticity at identified spines (Matsuzaki et al., 2004; Bagal et al., 2005). Although it allows for excellent spatial resolution, this technique completely bypasses the presynaptic terminal and is therefore restricted to the investigation of postsynaptic mechanisms. Here we have developed a new approach that allows us to observe presynaptic varicosities and postsynaptic spines first, and then stimulate visually identified synaptic contacts precisely and uninvasively. We took advantage of a newly identified light-gated cation channel, ChR2, that can control neuronal activity with millisecond precision (Nagel et al., 2003; Boyden et al., 2005). We modified a previously published construct (Boyden et al., 2005) by tagging it with the red fluorescent protein tdimer2 (Campbell et al.,

2002) (see Supplementary Methods online). Red labeling is advantageous for visualizing ChR2-positive neurons without activating the channel: under 546-nm illumination, ChR2 absorption is only ~ 4% of the maximum (Nagel et al., 2003). Using particle-mediated gene transfer, we obtained strong, stable expression of ChR2-tdimer2 in a small number of neurons in rat hippocampal slice cultures (Supplementary Fig. 2.1).

Results

Light-induced responses in ChR2-expressing CA1 pyramdial cells

First, we examined the light dependence of ChR2 currents in the presence of tetrodotoxin (TTX) to block action potentials. We recorded the membrane potential from ChR2-positive neurons using three standard filter sets for excitation: a green fluorescent protein (GFP) filter set (470/40, blue), a yellow fluorescent protein (YFP) filter set (500/20, blue) and a *Discosoma* red fluorescent protein (DsRed) filter set (546/11, green). Consistent with the published excitation spectrum of ChR2 (Nagel et al., 2003), blue light was most efficient in activating the channel (Fig. 2.1a). In regular recording solution without TTX, the spike threshold was reached at 0.3 mW for blue light (5-ms light pulses) and at 7 mW for green light (DsRed filter set). Thus, we had a large safety margin to inspect the ChR2-tdimer2-transfected slice cultures in epifluorescence mode without triggering any spikes. Using the DsRed filter set, we could select cultures with a favorable expression pattern and target ChR2-postive cells for patch-clamp recordings.

As a standard stimulus, we used 5-ms pulses of blue light, which reliably triggered action potentials up to 10 Hz. At higher frequencies, action potentials became unreliable owing to permanent depolarization of the cell (Supplementary Fig. 2.1). We were interested in potential differences between light-evoked action potentials (AP_L) and action potentials evoked by brief somatic current injection (AP_C). Recording the somatic membrane potential during AP_L revealed a long-lasting depolarization after the action potential (Fig. 2.1b), suggesting that the ChR2 conductance outlasted and counteracted the repolarizing K^+ current. We investigated the time course of ChR2 currents in voltage-clamp recordings, and measured a decay time constant (τ_{decay}) of 32 ms in K^+-based intracellular solution (Fig. 2.1c). In Cs^+-

based intracellular solution, which provides better space clamping of the cell, decay was 10 ± 3 ms, and restricting the illumination to the soma further shortened τ_{decay} to 5 ± 1 ms, very similar to the turning-off rate of ChR2-YFP measured in a tumor cell line (PC12 cells) (Ishizuka et al., 2006). Thus, the long-lasting depolarization after the action potential (Fig. 2.1b) is mostly due to the large capacitance of the cells used, pyramidal cells of hippocampal area CA1.

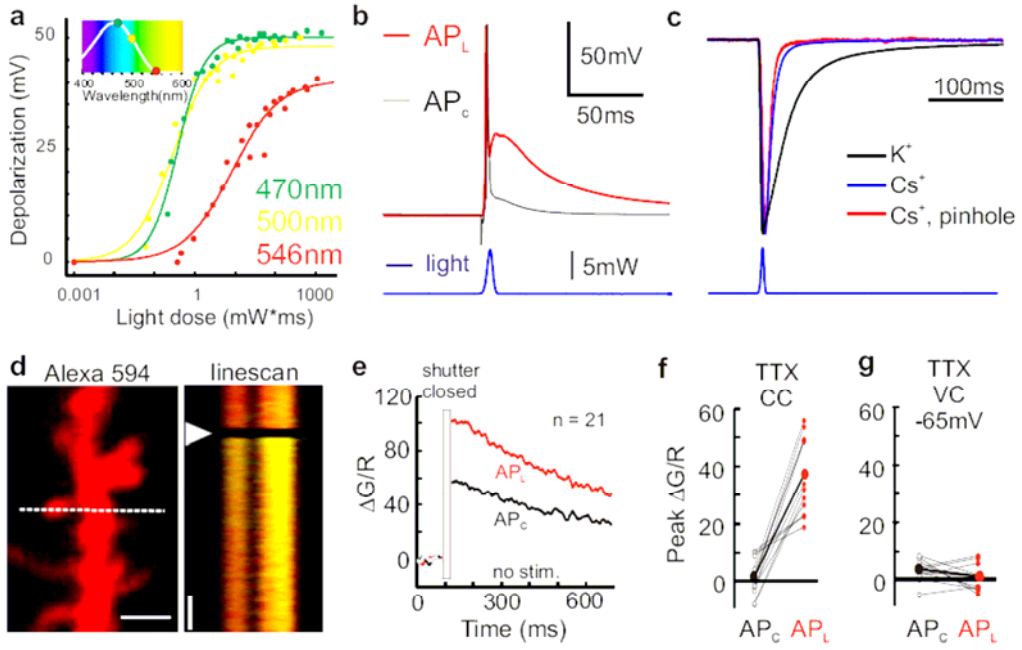

Figure 2.1. ***Light-induced responses in ChR2-expressing CA1 pyramidal cells.***

(a) *ChR2-mediated membrane depolarization depends on light dose (light intensity × pulse duration) and wavelength (1 μmM TTX, n = 3 cells). Curves are exponential fits to the data points.* ***(b)*** *Comparison of light-evoked action potential (AP_L) and action potential evoked by somatic current injection (2 nA, 4 ms, AP_C) in a ChR2-expressing pyramidal cell. Blue trace, measured light pulse.* ***(c)*** *Currents produced by ChR2 in the presence of TTX (average of six traces each), recorded using K^+ internal solution (black, τ = 32 ms), Cs^+ internal solution with wide field (blue, τ = 9 ms) and local illumination (red, τ = 6 ms).* ***(d)*** *Oblique dendrite with spines, filled with Alexa 594 (left). Scale bar, 2.5 mm. Line scan across spine and dendrite (dashed line in Alexa 594 image; right). Overlay of green (Fluo-5F) and red fluorescence (Alexa 594). Arrowhead indicates light-induced action potential.* ***(e)*** *Dendritic Ca^{2+} transients evoked by a single AP_L (red trace), single AP_C (black) and no stimulation (gray). Average of 21 dendrites, 4 cells.* ***(f)*** *Effect of TTX on peak dendritic calcium transients during AP_C and AP_L (n = 12, averaged over ten trials each; thick line, average of all experiments).* ***(g)*** *Peak Ca^{2+} transients measured in voltage clamp at –65 mV in the presence of TTX (n = 10, ten trials each; thick line, average).*

As ChR2 is known to be permeable to Ca^{2+} ions (Nagel et al., 2003), we set out to compare AP_L and AP_C with respect to the peak calcium levels reached in the cell.

ChR2-positive neurons were loaded with a mixture of Fluo-5F and Alexa 594 through a patch-clamp electrode and imaged using two-photon excitation at 810 nm. At the intensities we used for calcium imaging (<30 mW), we did not detect any direct activation of ChR2 by the imaging laser (Supplementary Fig. 2.1). Action potentials induced by blue light pulses (5 ms) triggered simultaneous fluorescence changes in basal dendrites and spines (Fig. 2.1d). To compare calcium transient amplitudes, we normalized the fluorescence change of Fluo-5F to the fluorescence intensity in the red channel (ΔG/R) (Yasuda et al., 2004). ΔG/R was significantly larger when the action potential was trigged by light (Fig. 2.1e; $P < 0.05$). To investigate the mechanism of the additional calcium influx, we applied the Na^+ channel blocker TTX (1 μM), which completely blocked AP_C and the subsequent calcium influx (Fig. 2.1f). The light pulse, in contrast, still caused a calcium transient, which was similar in amplitude to the difference between the calcium transients during AP_C and AP_L. In case of direct calcium influx through ChR2 channels, preventing the cell depolarization should increase the calcium influx owing to the increased driving force on Ca^{2+} ions at more negative potentials. Light stimulation under voltage-clamp conditions (-65 mV), however, did not evoke any detectable calcium influx (Fig. 2.1g), although the rapid depolarizing current recorded at the soma indicated that the ChR2 channel was still functional (data not shown). We concluded that the additional calcium influx seen during light-induced action potentials was mainly due to activation of voltage-gated calcium channels during the after-depolarization following an AP_L (Fig. 2.1b), not to calcium influx through the pore of ChR2 itself.

High release probability in ChR2-expressing axonal terminals

Because of the high degree of connectivity in mature hippocampal slice cultures (Debanne et al., 1999), it was straightforward to record light-induced excitatory postsynaptic currents ($EPSC_L$) in ChR2-negative CA1 neurons in cultures containing at least one ChR2-expressing neuron in area CA3. Moving the illuminated spot from CA3 to CA1 changed the latency of the $EPSC_L$ from ~ 7 ms to 0 ms (Supplementary Fig. 2.2), indicating the generation of a local AP_L in the axon. For comparison, we performed intracellular recordings of connected pairs of a CA3 and a CA1 pyramidal cell. Paired recordings resulted in excitatory postsynaptic currents ($EPSC_P$) of rather uniform amplitude (23 ± 6 pA), whereas $EPSC_L$ often had larger amplitudes (54 ± 33

pA; Supplementary Fig. 2.2), probably owing to the stimulation of more than one connected axon. The coefficient of variation was significantly smaller in $EPSC_L$ (CV_L

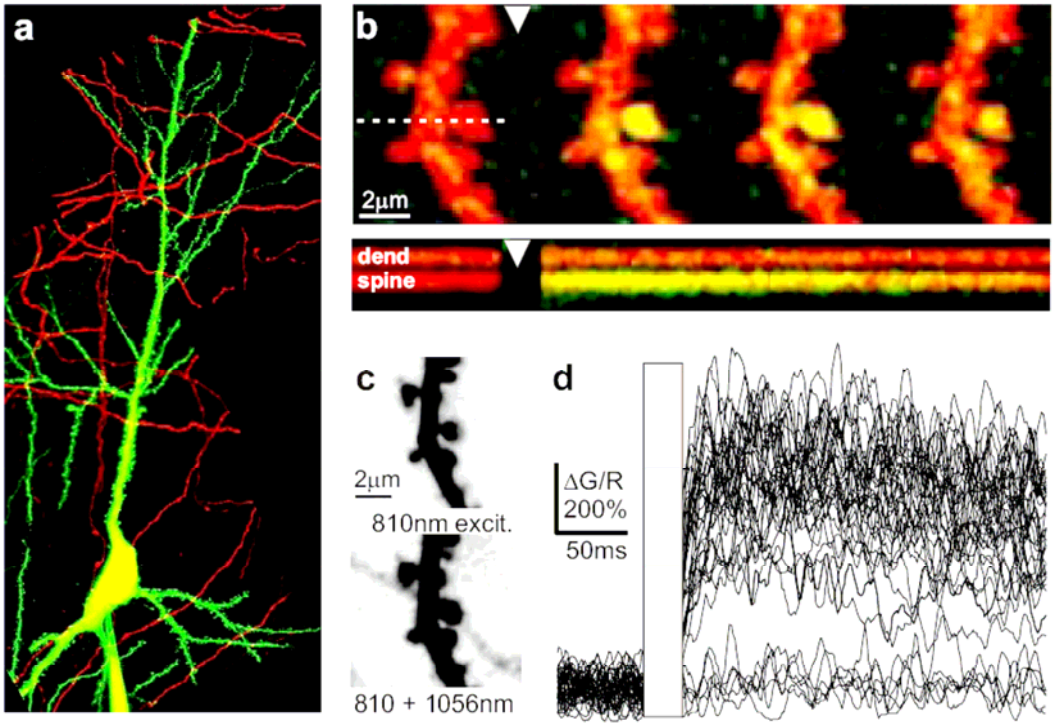

Figure 2.2. ***Imaging postsynaptic calcium transients following light-induced action potentials in the presynaptic axon.***

(a) *Single CA1 pyramidal cell filled with Fluo-5F and Alexa 594 in proximity to ChR2-expressing axons (red). Overlay of 810-nm excitation image (green) and 1,056-nm excitation image (red). Scale bar, 10 mm.* ***(b)*** *Top, overlay of green (Fluo-5F) and red fluorescence (Alexa 594). Ca^{2+} transient after light stimulation (arrowhead) is restricted to a single spine (yellow). White line indicates position of line scan. Scale bar, 2 mm. Bottom, line scan (single trial) across dendrite (dend) and spine head (spine). Scale bar, 50 ms.* ***(c)*** *Visualization of potential synaptic contacts by simultaneous imaging of ChR2-tdimer2–expressing axon (1,056-nm excitation) contacting Alexa 594–labeled spine (810 nm). Scale bar, 2 mm* ***(d)*** *Spine calcium transients and transmission failures evoked by 5-ms light pulses (42 consecutive trials).*

= 0.24 ± 0.09, CV_P = 0.48 ± 0.20, $P < 0.05$, Mann-Whitney *U* test), suggesting that there is an increased release probability, p_r, after an AP_L. The light-induced responses were well fit by a Monte Carlo simulation of glutamate release assuming quantal size q = 15 pA and p_r = 0.8 (Supplementary Fig. 2.2). Artificially depressing *Pr* by adding 2-chloroadenosine to the recording solution increased the variability of $EPSC_L$ to values similar to those for $EPSC_P$ (Supplementary Fig. 2.2). We conclude that AP_L increases the synaptic release probability, which is corroborated by the strong paired-pulse depression that we always observed with light stimulation.

The most direct way to measure release probabilities at individual synaptic contacts is spine calcium imaging. *N*-Methyl-*D*-aspartate (NMDA) receptors activated by presynaptic glutamate release trigger calcium transients in dendritic spines, which can be readily detected by two-photon microscopy (Oertner et al., 2002). We identified potential points of contact between the dendrite of a dye-filled CA1 pyramidal cell and ChR2-positive axons (Fig. 2.2). Testing 33 potential contacts by two-photon calcium imaging, we found three functional synapses (Fig. 2.2b). At functional synapses, successes and failures of glutamate release could be clearly distinguished (Fig. 2.2d; 42 trials, 6 failures). Release probability was very high in all cases (p_r = 0.89 ± 0.09, n = 3), in line with the low variability of $EPSC_L$ (Supplementary Fig. 2.2). Clearly, ChR2-expressing axonal terminals provide a highly reliable and precisely timed source of glutamate, and two-photon calcium imaging can be used to verify putative synaptic contacts without the need for electron microscopic reconstruction.

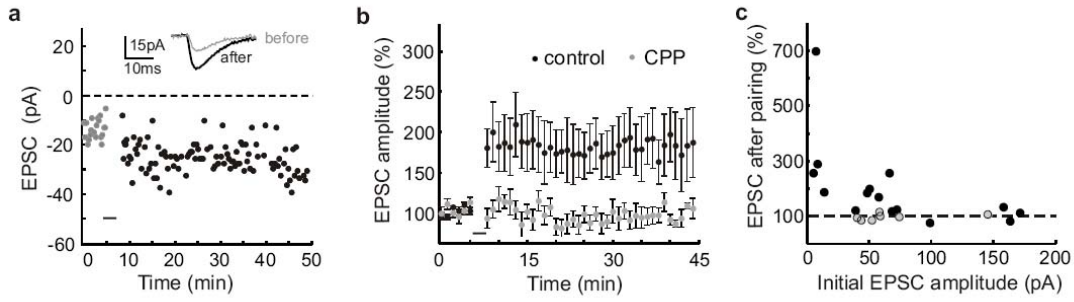

Figure 2.3. ***Potentiation of light-induced synaptic responses.***

(a) *Amplitude of light-induced synaptic responses plotted as a function of time. After 6 min of baseline recording, ten light-induced EPSCs were paired with brief postsynaptic depolarizations (voltage step to –15 mV for 100 ms) at 0.1 Hz, resulting in a stable increase in response amplitude to 187% of baseline. Horizontal bar indicates time of pairing. Inset, average EPSCs before and after pairing.* ***(b)*** *The pairing protocol led to stable long-term potentiation of 168% ± 29% (black markers, mean ± s.e.m., n = 22 cells). Blockade of NMDA receptors with dCPP prevented the potentiation of light-induced responses (gray markers, n = 9 cells).* ***(c)*** *Potentiation plotted as a function of initial EPSC amplitude. EPSCs were averaged in a 10-min time window, 20–30 min after pairing. Black, significant change (P < 0.05, Student's t-test, two-tailed); gray, change not significant.*

Potentiation of light-induced synaptic responses

We were interested in whether the light stimulation technique could be used to induce long-term potentiation of synaptic connections in CA1. Our induction protocol consisted of $EPSC_L$ paired with brief postsynaptic depolarizations (100 ms to V_m = -15 mV) at 0.1 Hz. After ten pairings, $EPSC_L$ amplitudes increased significantly (Fig. 2.3a; $P < 0.05$). The increase was stable for the duration of the recording (up to 90 min). On average, the excitatory postsynaptic current was potentiated to 168% ± 29% (mean ± s.e.m., n = 22 cells) of the control amplitude (Fig. 2.3b). Potentiation was completely prevented in recording solution containing 10 μM dCPP, an NMDA receptor blocker, suggesting that the potentiation was NMDA receptor dependent (Fig. 2.3b). The magnitude of potentiation was inversely correlated with the amplitude of the excitatory postsynaptic current before potentiation: all connections with initial excitatory postsynaptic current amplitudes <40 pA, but only half of the connections between 40 and 170 pA, showed significant potentiation (Fig. 2.3c; $P < 0.05$). The inverse correlation might indicate that strong synaptic connections have already undergone potentiation during the culture period. Our results are virtually identical to those of published long-term potentiation experiments carried out on connected pairs of CA3-CA1 pyramidal cells using dual patch-clamp recordings (Debanne et al., 1999), suggesting that the development of synaptic connections proceeds undisturbed in cells expressing ChR2.

Supplementary Figures:

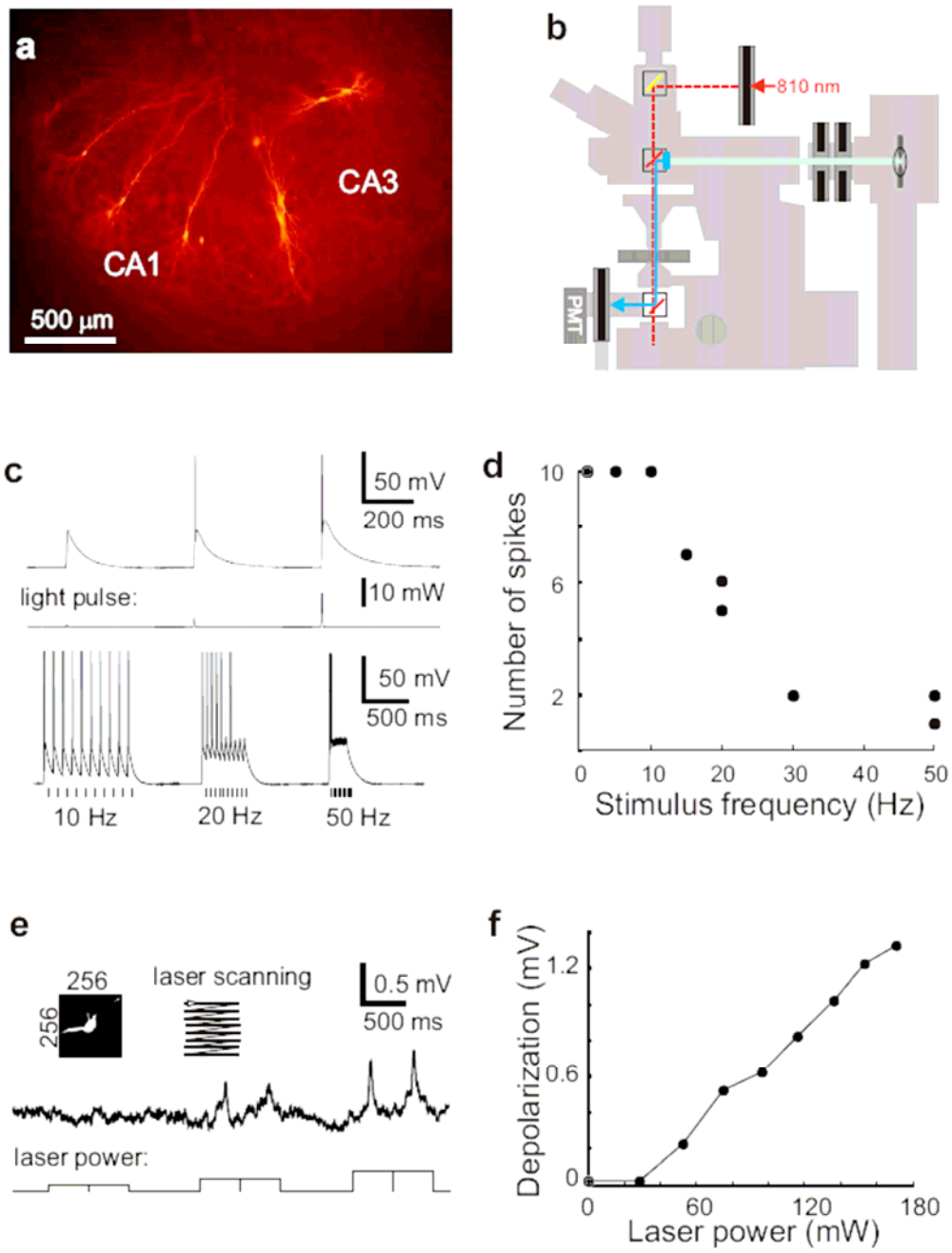

Supplementary Figure 2.1. ***Light stimulation using single-photon and two-photon excitation.*** ***(a)*** *Hippocampal neurons expressing ChR2-tdimer2.* ***(b)*** *Schematic drawing of the shutter system used to combine light stimulation with two-photon imaging.* ***(c)*** *Top: Voltage trace showing subthreshold depolarization and action potential generation in a ChR2 expressing neuron evoked by 470 nm light pulses (5 ms) at different intensities (stimulus trace below). Bottom: Responses to repetitive stimulation by 5 ms light pulses at 10, 20, and 50 Hz.* ***(d)*** *In response to a burst of 10 light pulses, action potentials were reliably induced up to 10 Hz. At higher frequencies, cells became permanently depolarized and failed to spike reliably.* ***(e)*** *Voltage trace showing membrane depolarization of a ChR2 expressing cell in response to laser scanning across the soma at 810 nm (2 frame scans, 500 ms each) at 30, 80, and 140 mW average laser power. Only at high laser intensities, small depolarizations were detectable.* ***(f)*** *Membrane depolarization depends on laser power (810 nm). Typical intensities used for calcium imaging were < 30 mW.*

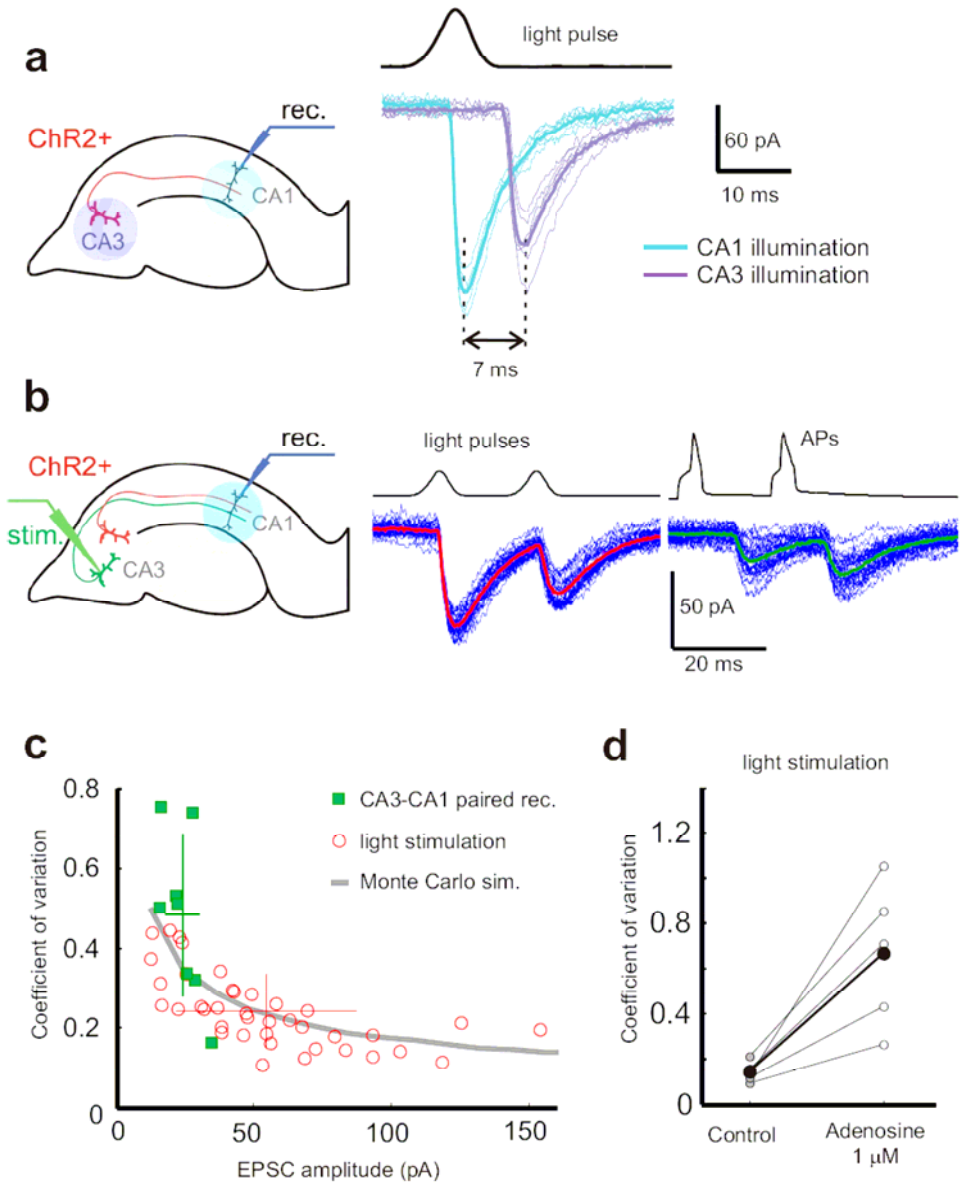

Supplementary Figure 2.2. ***Comparison of light-evoked synaptic responses and paired recordings.*** ***(a)*** *Illuminating a ChR2-expressing cell in CA3 caused delayed EPSCs in a synaptically connected CA1 pyramidal cell (blue traces). Illuminating CA1 at the same intensity led to instantaneous EPSCs in the same postsynaptic CA1 pyramidal cell (green traces), indicating local action potential generation in the axon.* ***(b)*** *Simultaneous patch clamp recording of a connected pair of non-transfected CA3 and CA1 pyramidal cells in a slice culture containing also ChR2-expressing cells (red). EPSCs recorded in single CA1 cell in response to stimulation of presynaptic axons by a pair of light pulses (left, duration = 5 ms, ISI = 20 ms) and by a pair of APs in a single connected CA3 cell (right). Note small trial-to-trial variability, paired-pulse depression, and short latency of the light-evoked responses.* ***(c)*** *Summary of paired recording experiments (green squares, n = 8 pairs) and stimulation of presynaptic axons by light (red circles, n = 39 cells). Crosses indicate mean ± s.d. Gray line: Result of Monte-Carlo simulation with q =15 pA and pr = 0.8. Note that many paired recordings have higher CV, indicating release probabilities < 0.8.* ***(d)*** *Variability of light-evoked synaptic response strongly increases after decreasing synaptic release probability by 1 μM 2-Chloroadenosine (n = 5 cells, thick line: average).*

Discussion

Remote control of synaptic transmission by light combined with two-photon imaging provides a new avenue for investigating plasticity at the single-synapse level. As compared to stimulation by extracellular electrodes, light stimulation is very selective. This mitigates the typical problems with recurrent excitation in organotypic slice cultures and makes it unnecessary to reduce excitability by adenosine receptor agonists (Shi et al., 2001). Compared to multiple patch-clamp recordings, light stimulation has a much higher throughput and allows contacts to be visualized with ease; however, in densely transfected cultures wide-field illumination may activate multiple axons. Light stimulation is not limited to excitatory synapses: in cultures with ChR2-positive interneurons, we frequently observed inhibitory postsynaptic responses (data not shown). The increased calcium influx during ChR2 activation reported here (Fig. 2.1) has important consequences, especially for the design of transgenic animals expressing ChR2; unfocused blue light not only will trigger spikes, but also might induce synaptic plasticity by providing (i) a high release probability at ChR2-positive axons and (ii) additional calcium influx at ChR2-positive dendrites and spines. In summary, ChR2 is a powerful tool to selectively activate neurons and to modify neuronal circuits by changing synaptic efficacy.

Methods

Plasmid construction: The cDNA encoding ChR2-YFP, a gift from Karl Deisseroth, was subcloned into a neuron-specific expression vector (Synapsin-1 promoter vector (Kugler et al., 2001)) via *Nhe*I and *Bam*HI restriction sites by PCR with primers: 5'-ATT*GCTAGC*CACCATGGATTATGGAGGCGCCCTG-3' and 5'-ATT*GGATCC*TTACTTGTACAGCTCGTCCATGCC-3'. The ChR2-tdimer2 construct was then generated by replacing the YFP gene with tdimer2 (Campbell et al., 2002) via *Not*I and *Sal*I restrictions sites using PCR with primers: 5'-ATT*GCGGCCGC*CATGGTGGCCTCCTCCGAGGACG-3' and 5'-ATT*GTCGAC*CTACAGGAACAGGTGGTGGCGG-3'. The constructs were verified by DNA sequencing, amplified and purified using MaxiPrep Kits (Qiagen).

Slice culture and transfection: Organotypic hippocampal slices were prepared from Wistar rat at postnatal day 5 as described (Stoppini et al., 1991), in accordance with

the animal care and use guidelines of the Veterinary Department Basel-Stadt. After 7-10 days *in vitro*, cultures were biolistically transfected with the synapsin-ChR2-tdimer2 construct, using a Helios Gene Gun (BioRad). Light stimulation experiments were performed 2-3 weeks after transfection. No extra retinal was added to either culture medium or recording solution.

Electrophysiology: Hippocampal slice cultures were placed in the recording chamber of the microscope and superfused with artificial cerebrospinal fluid (ACSF) containing (in mM): 119 NaCl, 2.5 KCl, 4 $CaCl_2$, 4 $MgCl_2$, 26.2 $NaHCO_3$, 1 NaH_2PO_4, 11 glucose. The solution was gassed with 95% O_2, 5% CO_2, pH was adjusted to 7.2. Single and dual whole-cell recordings were performed using Axopatch 200B and MultiClamp 700B amplifiers (Axon Instruments). For current-clamp experiments, the recording pipettes (4.5 - 5.5 MΩ) were filled with intracellular solution containing (in mM): 140 K-$MeSO_4$, 10 HEPES, 4 $MgCl_2$, 4 Na_2-ATP, 0.4 Na_2-GTP, 10 Na_2-phosphocreatine, 3 ascorbate, 0.03 Alexa Fluor 594 and 0.6 fluo-5F. Voltage-clamp experiments were compensated for series resistance and whole-cell capacitance, and K^+ was replaced by Cs^+. For imaging of postsynaptic calcium transients, cells were voltage-clamped at +40 mV. For LTP experiments, EGTA (0.6 mM) was used instead of fluo-5F. Measurements are given as mean ± standard deviation, unless indicated otherwise.

Light stimulation and 2-photon imaging: The custom-build 2-photon imaging setup was based on an Olympus BX51WI microscope equipped with a LUMPlan W-IR2 60 × 0.9 NA objective, controlled by a free software package (Pologruto et al., 2003) written in Matlab (The MathWorks). Emitted fluorescence was detected through an oil immersion condenser (1.4 NA, Olympus). A recording chamber with a 1 mm quartz glass bottom (wzw-optic AG) was used to minimize glass phosphorescence after the blue light pulse. We used two mechanical shutters (VS25, Uniblitz) in front of a 100W Hg arc lamp (Olympus) to deliver light pulses for ChR2 activation. Two shutters were needed to keep millisecond timing in spite of intense heat build-up by the arc lamp. Time course and intensity of the light pulse were measured below the condenser using a photomultiplier protected by neutral density filters. The shortest pulses we could produce were 5 ms full-width at halfmaximum. To calibrate the

intensity measurements for each wavelength, we measured the light intensity at the back aperture of the objective with a commercial power meter (LaserCheck, Coherent). Two PMTs below the condenser were used to detect red and green emission (R3896, Hamamatsu). During the light pulse, they were protected by an additional VS25 shutter (see Supplementary Fig. 1B). Two ultrafast IR lasers (ChameleonXR, Coherent; GLX-200, Time-Bandwidth Products) controlled by electrooptic modulators (350-80, Conoptics) were combined by a polarizing beamsplitting cube (Thorlabs) to excite the synthetic dyes (810 nm) and ChR2-tdimer2 (1056 nm) simultaneously. To combine the blue light used for stimulation with the IR lasers, we used a 470/40 bandpass and a 725DCXR dichoic mirror (Chroma).

Chapter 3. Single synapse LTP reveals input-specific accumulation of αCaMKII

Yan-Ping Zhang, Niklaus Holbro and Thomas G. Oertner

Submitted 2007

Abstract

Long-term potentiation (LTP), a form of synaptic plasticity, is a primary experimental model for understanding learning and memory formation. Synaptic strength between hippocampal pyramidal cells can be potentiated when depolarization of a postsynaptic cell is repeatedly coincident with activity of a presynaptic cell. However, it has been difficult to study the sequence of molecular events that occur during LTP at the level of individual synapses. Here we use channelrhodopsin-2 (ChR2) to optically depolarize CA1 pyramidal cells while stimulating individual excitatory synapses on dendritic spines by two-photon glutamate uncaging. Repetitive pairing of light with MNI-glutamate uncaging led to a lasting increase of spine volume and translocation of αCaMKII to stimulated synapses, but not to neighboring spines. Our results provide evidence that αCaMKII accumulation at postsynaptic sites is a synapse-specific memory trace of coincident activity.

Introduction

Activity-dependent changes in synaptic strength are generally considered to be the cellular basis of learning and memory (Bliss and Collingridge, 1993; Malenka and Nicoll, 1999). Long-term potentiation (LTP), the most extensively studied form of such synaptic plasticity, can be trigged within seconds by coincident activity in pre- and postsynaptic cells. The possible structural modifications that occur at synapses where LTP has been induced are poorly known due to the difficulty of simultaneously measuring functional and morphological parameters at individual synapses. Furthermore, it is controversial whether neighboring synapses can be modified independent of each other (Engert and Bonhoeffer, 1997; Bi and Poo, 2001; Matsuzaki et al., 2004). Whether individual synapses can be regarded as the

elementary unit of information storage is of fundamental importance from a computational point of view.

A key player in the signaling cascade that is activated during LTP induction and eventually leads to potentiation of synaptic currents is αCaMKII. The αCaMKII holoenzyme is thought to act as a molecular switch: Following activation by Ca^{2+}-calmodulin, it can stay active for prolonged periods of time via autophosphorylation (Giese et al., 1998; Lisman and Zhabotinsky, 2001). Reports that brief application of glutamate or NMDA to rat hippocampal neurons in culture induces accumulation of CaMKII in spines (Shen and Meyer, 1999; Shen et al., 2000; Merrill et al., 2005) have created much interest because αCaMKII activation is both necessary and sufficient to induce synaptic plasticity (Lledo et al., 1995; Giese et al., 1998). It has been suggested that postsynaptic accumulation of αCaMKII could be responsible for the synapse specificity of LTP, because it localizes the putative activated kinase close to the substrates of synaptic potentiation (Soderling and Derkach, 2000; Lisman and Zhabotinsky, 2001). However a crucial condition of this hypothesis, namely that αCaMKII accumulates specifically and exclusively at synapses that experience coincident activity, has never been tested experimentally.

To address the question of synaptic specificity, we set out to monitor the concentration of αCaMKII in individual spines during the induction of LTP. Long-term imaging of fluorescently labeled CaMKII in live cells is not compatible with simultaneous whole-cell patch clamp, since this technique leads to dialysis of the cytoplasm and rapid wash-out of soluble proteins (Supp. Fig. 3.1). Previously, we have shown that channelrodopsin-2 (ChR2), a light-gated cation channel, can be used presynaptically to induce LTP at identified synapses in the hippocampus (Zhang and Oertner, 2007). Here, we combine three optical methods for an all-optical pairing protocol in order to investigate synapse-specific changes during the induction of LTP. First, 2-photon uncaging of MNI-glutamate allows us to stimulate individual synapses with high temporal precision. Second, we use ChR2 to depolarize individual postsynaptic cells in CA1, thus avoiding the wash-out problems typically associated with whole-cell patch clamp. Third, we measure spine morphology and protein concentration before and after paired stimulation by time-lapse two-photon

ratiometry. We show that αCaMKII accumulation occurs specifically at synapses exposed to LTP-inducing stimuli, providing compelling evidence that αCaMKII functions as a memory molecule.

Results

A strategy for non-invasive LTP induction and protein concentration measurements

In the classical electrophysiological pairing protocol, postsynaptic depolarization is provided by somatic current injection via a patch electrode (Chen et al., 1999), which has the disadvantage that soluble proteins are washed out (Supp. Fig. 3.1). Since our goal was to optically monitor potential concentration changes of fluorescently labeled αCaMKII during the induction of plasticity, it was essential not to disturb the cytoplasm during the experiment. We therefore used the light-gated cation channel ChR2 (Boyden et al., 2005) to depolarize individual postsynaptic cells in a non-invasive fashion.

Comparing protein concentrations in dendrites and spines presented a second challenge: Most dendritic spines were substantially smaller than the point spread function of our microscope. As a result, the fluorescence intensity of labeled αCaMKII in individual spines was determined by two unknown variables: The concentration of αCaMKII in the spine, and the volume of that spine. Thus, fluorescence intensity measurements in a single color channel were not sufficient to quantify differences in protein concentration between spines and dendrites. We solved this problem by co-transfection with a freely diffusible dimeric RFP which served as a marker of cytosolic volume. We then used a ratiometric approach (green/red fluorescence intensity ratio) to compare the concentration of αCaMKII in spines of different size.

A fluorescently labeled version of ChR2 would have resulted in staining of the cell membrane and thus interfered with our αCaMKII measurements. To be able to assess the expression level of ChR2 in individual cells, we combined unlabeled ChR2 and soluble RFP in a single plasmid with separate promoters, which resulted in very reliable co-expression (see methods). Using particle-mediated gene transfer, we co-

transfected hippocampal neurons with 2 vectors encoding 3 different proteins: ChR2 / RFP, and Dronpa-αCaMKII (Fig. 3.1 A-C). In response to blue light illumination (200 ms, 470 nm LED), transfected cells produced large inward currents (1395 pA ± 115

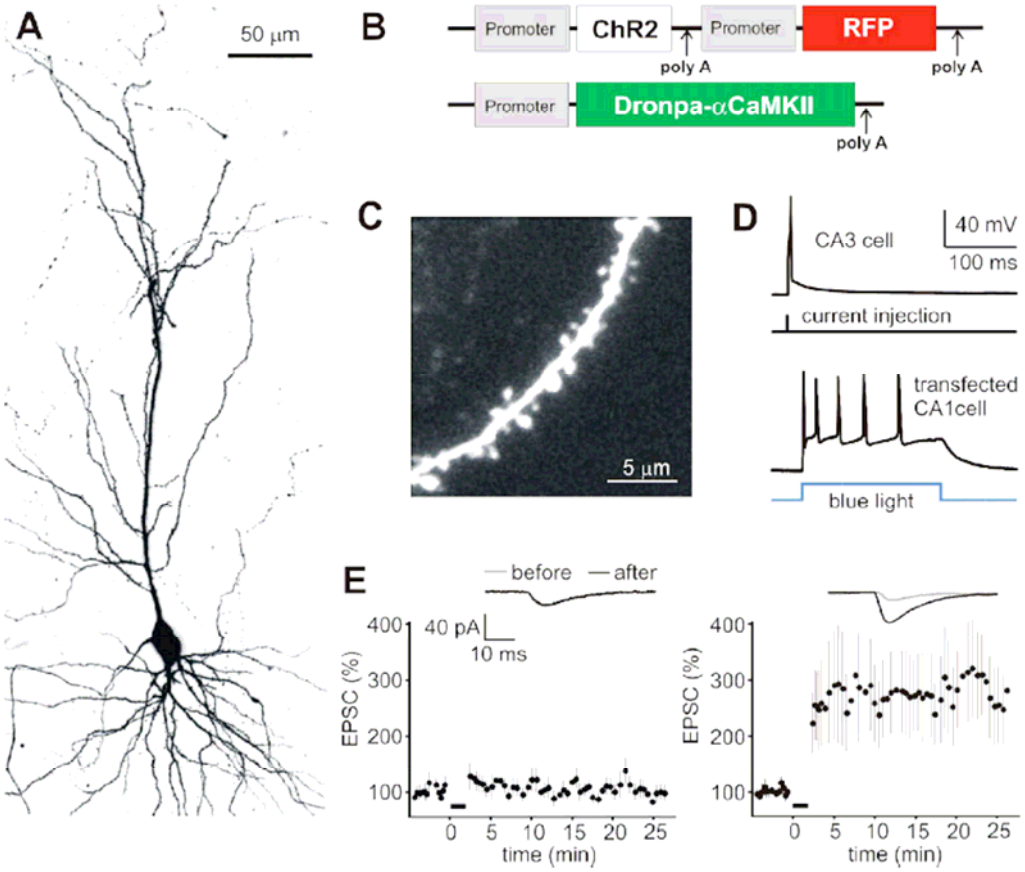

Figure 3.1. ***LTP induction by ChR2-mediated depolarization of the postsynaptic cell.***
A, *CA1 pyramidal cell in organotypic slice culture expressing ChR2, RFP and Dronpa-αCaMKII (maximum intensity projection).* ***B,*** *Schematic drawing of the two vectors used for triple transfection by gene gun. Promoter denotes synapsin-I promoter, poly A denotes SV40 poly A sequence.* ***C,*** *High magnification RFP fluorescence image showing spiny oblique dendrite.* ***D,*** *LTP induction protocol. A single AP evoked by current injection (2 nA, 5 ms) into a patch-clamped CA3 pyramidal cell was paired with a short burst of 5 APs elicited by blue light illumination (200 ms) of a triple-transfected CA1 pyramidal cell (Δt = 6 ms). Pairing was repeated 20 times at 0.1 Hz.* ***E,*** *Pairing stimulation induces synaptic plasticity in connected CA3-CA1 pairs. Left panel: Postsynaptic depolarization alone (black bar: 200 ms light pulses, 20 repetitions at 0.1 Hz) did not significantly change EPSC amplitudes in triple-transfected CA1 pyramidal cells (107% ± 16%, n = 7 pairs). Insert: example traces before and after pairing. Right panel: Pairing stimulation as described in D induced 274% ± 76% potentiation (n = 7 pairs). Error bars indicate SEM.*

pA at peak and 804 pA ± 89 pA at steady-state, n = 21). In current clamp mode, the same blue light stimulation induced robust spiking (5.4 ± 0.5 spikes, Fig. 3.1 D).

We next examined whether the light stimulation technique could be used to induce long-term potentiation of Schaffer collateral synapses. We performed dual patch-clamp recordings of connected pairs of untransfected CA3 and transfected CA1 pyramidal cells. Our induction protocol consisted of repetitive pairing of single presynaptic action potentials with brief postsynaptic bursts induced by 200 ms blue light pulses (Fig. 3.1 D). To compensate for the propagation delay from CA3 to CA1, we started the light pulse with a delay of Δt = 6 ms relative to the presynaptic current injection (Fig. 3.1 D). After 20 pairings at 0.1 Hz, excitatory postsynaptic currents (EPSCs) increased to 274 % ± 76 % (Fig. 3.1 E). In control experiments in which blue light stimulation was not paired with presynaptic activation, postsynaptic response amplitudes remained unchanged (107 % ± 16 %, Fig. 3.1 E). These results indicate that LTP was induced by coincident activity of pre- and postsynaptic cell, as in previous experiments using electrophysiogical pairing (Petersen et al., 1998; Debanne et al., 1999).

Spine volume changes induced by repetitive pairing of light with uncaging of MNI-glutamate

Having established optical depolarization of postsynaptic cells with ChR2, the next step was to replace the electrophysiological stimulation of CA3 axons by 2-photon glutamate uncaging on individual spines. For each experiment, uncaging laser power (725 nm) was first adjusted on several spines of a neighboring, patch-clamped cell, such that uncaging-evoked excitatory postsynaptic currents (uEPSCs) had amplitudes of ~24 pA (laser power, ~50 mW, pulse duration, 0.5 ms). To induce LTP at individual spines of transfected cells, we paired single uncaging pulses with 200 ms postsynaptic depolarization by blue light (20 pairings at 0.07 Hz, Δt = 0, Fig. 3.2 B). In experiments where the spine head increased its size during the low-frequency pairing protocol, the uncaging location was adjusted accordingly to avoid direct illumination of the spine head by the uncaging laser. In 4 control experiments, we verified by patch clamp recordings from transfected cells that this pairing protocol, but not glutamate uncaging alone, resulted in a lasting increase in uEPSC amplitude (Fig. 3.2 C). Before and after optical LTP induction, we acquired stacks of images at 5 min intervals to monitor spine morphology in 3D. The integrated intensity of the spine head was used as a measure of spine volume (see supplemental methods). Stimulated

spines responded with a rapid volume expansion by a factor of 2.4, on average. Spine volume partially decreased again during the following 15 min, but most stimulated spines (11/16) remained enlarged 30-40 min after stimulation (Fig. 3.2 D-G). When

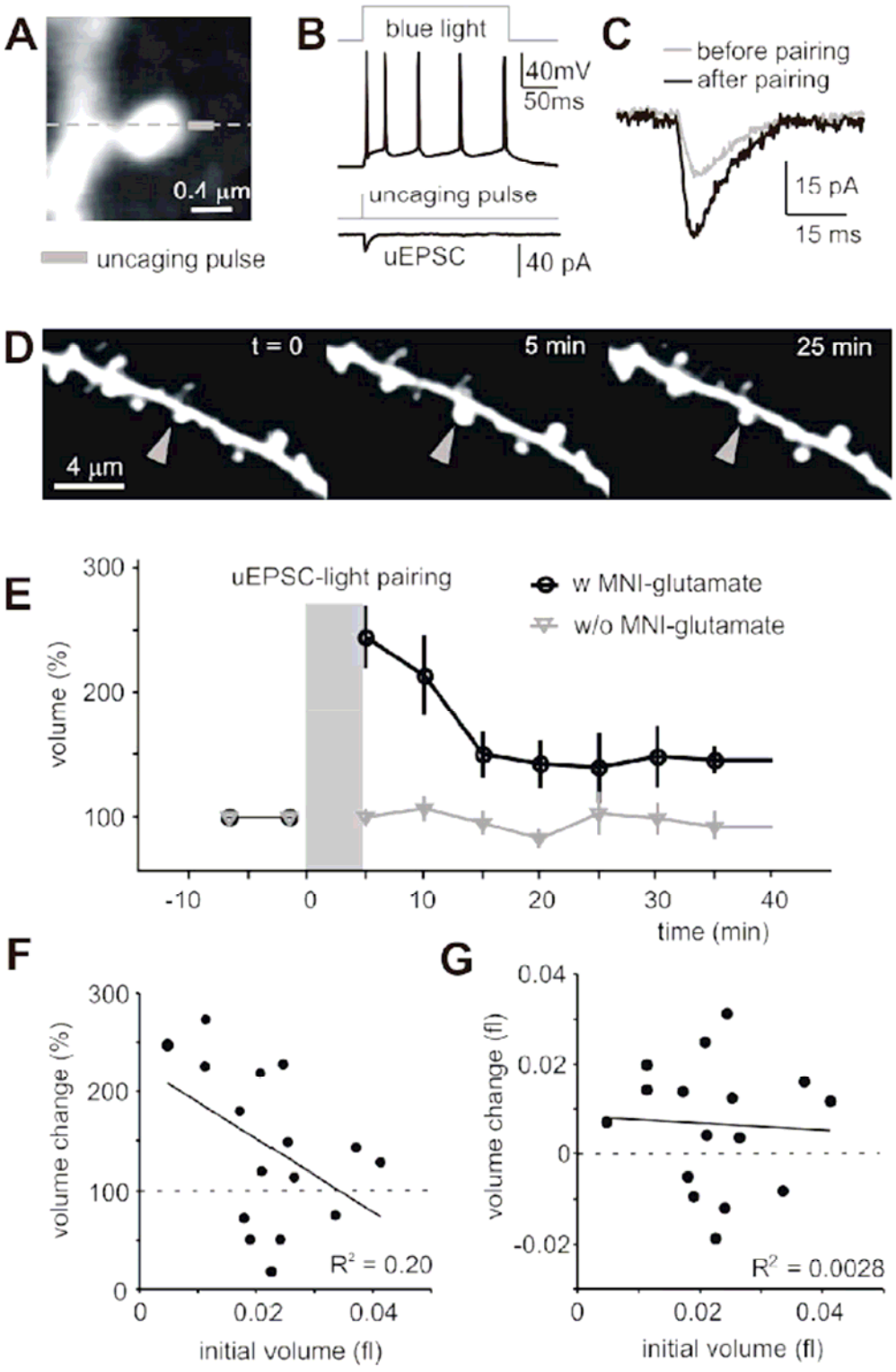

Figure 3.2. ***Spine volume increase induced by pairing of glutamate uncaging and ChR2 activation.***

Figure 3.2. ***Continues***

A, *Simultaneous two-photon imaging and two-photon MNI-glutamate uncaging at a single spine. Grey bar indicates glutamate uncaging pulse (0.5 ms).* ***B,*** *Optical pairing protocol. Postsynaptic responses to 200 ms blue light pulse (current clamp) and to single uncaging pulse (uEPSC, voltage clamp at -65 mV) are shown in isolation. To induce plasticity at individual synapses, these two stimuli were paired 20 times at 0.07 Hz in current clamp (Δt = 0).* ***C****, uEPSCs before and 20 min after optical pairing protocol as described in B (averages of 5 consecutive responses).* ***D,*** *RFP fluorescence images (maximum projections) before and after optical pairing protocol. Arrowhead indicates stimulated spine.* ***E,*** *Spine volume changes induced by optical pairing protocol in the presence of MNI-glutamate (black circles, n = 16 spines, 8 cells) and without MNI-glutamate (gray triangles, n = 12 spines, 5 cells). Error bars indicate SEM.* ***F,*** *Persistent spine volume change, 30 ~ 40 min. after optical pairing protocol, expressed as percent of initial spine volume, was larger in smaller spines (n = 16). Solid line: linear fit to data points.* ***G,*** *Absolute volume change did not depend on initial spine volume. Solid line: linear fit to data. Dashed line: no change in volume.*

expressed as fractional change, the lasting volume increase was larger in spines that were initially small (Fig. 3.2 F), consistent with a previous study (Matsuzaki et al., 2004). The absolute increase in volume, however, did not depend on initial spine size (Fig. 3.2 G), suggesting that small and large spines both have the capacity to further increase their volume. In a separate set of control experiments, we performed identical pairing of light-induced depolarization and uncaging laser pulses in the absence of MNI-glutamate (Fig. 3.2 E). We did not detect any spine enlargement after pairing without MNI-glutamate and thus could rule out any unspecific effects induced by the uncaging laser pulse itself.

αCaMKII concentration in dendritic spines

By calculating the fluorescence intensity ratio between YPF-αCaMKII and RFP on a pixel-by-pixel basis (*Y*/*R*), we were able to compare the concentration of αCaMKII in compartments below the resolution limit of the microscope (Fig. 3.3 A). This strategy is analogous to the use of two different dyes for ratiometric calcium measurements (Yasuda et al., 2004). To pool spine data from cells with different relative expression levels of YPF-αCaMKII and RFP, we normalized the *Y*/*R* ratio in the spine by *Y*/*R* ratio in the dendrite (*S*/*D* ratio). The *S*/*D* ratio is a measure of αCaMKII enrichment in spines independent of spine volume. Under baseline conditions, αCaMKII in spines was enriched by a factor of 1.7 relative to the dendrite, suggesting that about 41% of total αCaMKII in spines was bound to postsynaptic sites (see methods). To test whether binding was dependent on the phosphorylation state of αCaMKII, we

generated a double mutant (TT305/6VA) where two inhibitory autophosphorylation sites were removed. The threshold for kinase activation and for LTP induction is known to be lowered in the TT305/6VA mutant (Hanson and Schulman, 1992; Elgersma et al., 2002; Thalhammer et al., 2006). Indeed, cells transfected with mutant

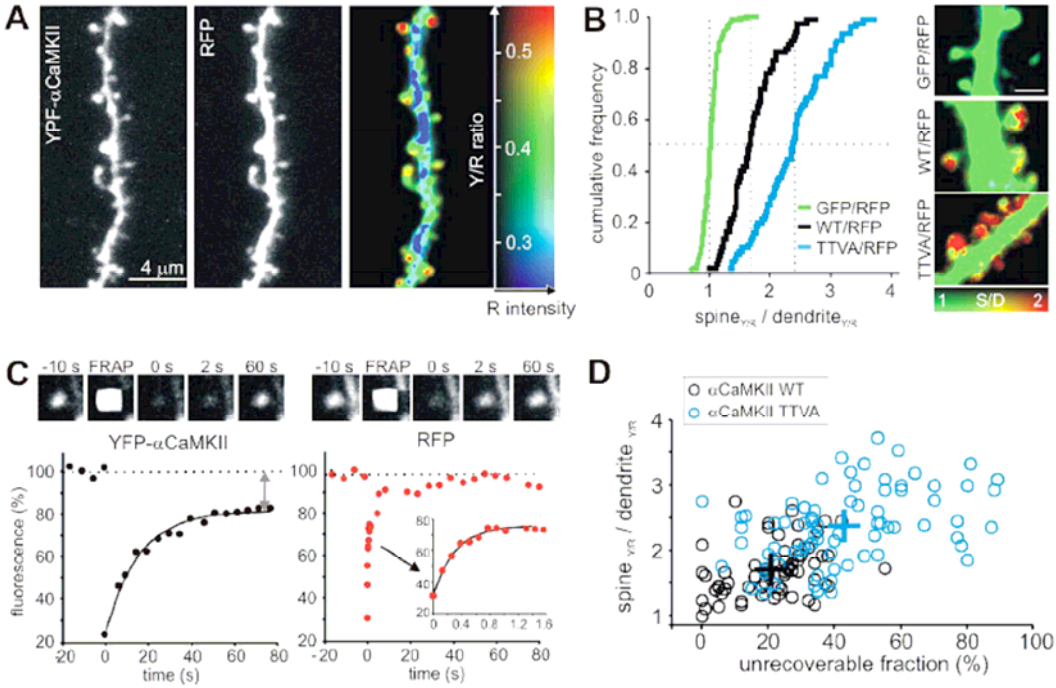

Figure 3.3. ***Enrichment of CaMKII in spines.***

A, *CA1 pyramidal cell dendrite expressing YFP-αCaMKII and RFP (maximum intensity projection). Left: YFP-αCaMKII signal. Middle: Cytoplasmic volume (RFP). Right: Color-coded ratio of αCaMKII/volume (Y/R), indicating elevated αCaMKII concentration in spines. To mask background ratios, pixel brightness was scaled by total intensity in volume channel.* ***B,*** *Cumulative distribution of Y/R ratio (protein concentration) in spines relative to parent dendrite (S/D ratio). αCaMKII, but not GFP, is enriched in dendritic spines. GFP, n = 286 spines, 3 cells; YFP-αCaMKII (wild type), n = 80 spines, 4 cells; YFP-αCaMKII (TT305/6VA mutant), n = 82 spines, 4 cells. Examples of cells transfected with the three different constructs and RFP are shown on the left, false color indicates S/D ratio. Scale bar: 1 µm.* ***C,*** *FRAP analysis on a dendritic spine expressing YFP-αCaMKII and RFP. Black dots: YFP-αCaMKII fluorescence intensity in spine. Black line: single exponential fit. Note ~20% unrecoverable fraction. Red dots: RFP fluorescence. Note rapid (insert) and complete recovery of fluorescence. RFP showed much faster recovery following photobleaching than YFP-αCaMKII (RFP = 0.31 s, YFP-αCaMKII = 16 s).* ***D,*** *Correlation between FRAP and spine/dendrite ratio measurements in individual spines. YFP-αCaMKII TT305/306VA mutant showed higher unrecoverable fraction and higher enrichment in spines compared to wild type αCaMKII. Wild type: S/D ratio, 1.7± 0.4, unrecoverable fraction, 21% ±12%, n = 80 spines, 4 cells. TT305/6VA mutant: S/D ratio, 2.38± 0.06, unrecoverable fraction, 42%± 28%, n = 82 spines, 4 cells (all values given as mean± SD).*

αCaMKII had higher spine/dendrite ratios (*S*/*D* = 2.4), indicating a higher bound fraction of ~58% (Fig. 3.1 B). To test for potential measurement artifacts due to the different signal-to-noise ratio in spines and dendrites, we also determined *S*/*D* ratios of soluble EGFP/RFP. *S*/*D* ratios were normally distributed with a mean of 1.0 (Fig. 3.1 B), indicating that our ratiometric approach was indeed volume-independent.

An alternative method to distinguish bound and soluble fraction is fluorescence recovery after photobleaching (FRAP). After a brief laser pulse that bleached 70-80% of the fluorescent molecules in the spine, fluorescence in the red color channel recovered rapidly to its initial value, indicating free diffusion of the dimeric RFP (Fig. 3.3 C). YFP-αCaMKII fluorescence, on the other hand, did not fully recover, indicating a fraction of αCaMKII molecules that were bound to postsynaptic sites and were thus not replaced by unbleached molecules from the dendrite. To quantify the unrecoverable fraction, we fit a single exponential function to the normalized fluorescence recovery data *F*(*t*):

$$F(t) = 1 - f_U - f_S e^{-\frac{t}{\tau}} \qquad \text{(Eq. 4)}$$

where f_U and f_S are the unrecoverable and soluble fraction of total αCaMKII, respectively, and τ is the recovery time constant. For clarity, values are reported as percentages rather than fractions. For wild-type YFP-αCaMKII, the unrecoverable fraction was 21% ± 12% (mean ± SD). We also bleached spines of cells transfected with the TT305/6VA mutant, which had a significantly higher unrecoverable fraction of 42% ± 28% ($p < 0.05$). Time constants of recovery, on the other hand, were not significantly different for WT and mutant αCaMKII (median τ_{WT} = 12.5 s; τ_{TTVA} = 14.3 s), suggesting that the mobility of the soluble fraction was not influenced by the mutation. As expected, the *S*/*D* ratio and the unrecoverable fraction were correlated in individual spines (Fig. 3.3 D), but the two different methods led to different estimates of the bound fraction: According to the FRAP experiments; about 21% of WT αCaMKII in spines was bound to postsynaptic sites, on average. The estimate from the *S*/*D* ratio measurements was 41%. This difference suggests that the assumption of a single, uniform population of bound αCaMKII molecules, which was the basis our FRAP analysis, is probably an oversimplification. More likely, subpopulations of bound αCaMKII in the spine head turn over on multiple time scales. Based on these

considerations, we decided to rely on ratio measurements rather than FRAP to asses the effects of LTP on αCaMKII binding.

Spine enlargement precedes the input-specific accumulation of αCaMKII

Previous studies have demonstrated unspecific αCaMKII translocation into spines after induction of chemical LTP. Here, our question was whether αCaMKII translocation is detectable, specific, and persistent following potentiation of a single synapse. A concern for optical concentration measurements of fluorescently labeled proteins are potential bleaching artifacts during time-lapse imaging and glutamate uncaging. To minimize this problem, we labeled αCaMKII with the photoswitchable green fluorescent protein Dronpa, which can be reactivated after bleaching by brief UV illumination (Ando et al., 2004). From a series of control experiments, we estimated that ~95% of bleached Dronpa-αCaMKII could be reactivated by 405 nm illumination (Supp. Fig. 3.3). As described above (Fig. 3.1 A-C), we co-transfected CA1 pyramidal cells with Dronpa-αCaMKII, RFP, and unlabeled ChR2. Image stacks were obtained every 4 minutes, and Dronpa fluorescence was reactivated before each acquisition. We verified that UV illumination did not induce spiking of ChR2-transfected cells (Supp. Fig. 3.3). The optical LTP induction protocol consisted of 20 pairings of a single glutamate uncaging pulse with postsynaptic bursting by 200 ms blue light illumination. The majority of spines (18 / 23 experiments) responded to pairing stimulation with a rapid increase in spine head volume. 10 out of these 18 spines that did increase their volume were still enlarged 30-40 min after stimulation (Fig. 3.4 A, right example). We split our sample of stimulated spines in 2 different groups, spines that responded with a persistent volume increase to the pairing protocol and spines that did not (Fig. 3.4 B). As a third group, we analyzed neighboring spines on the same dendrite that were not directly stimulated (average distance from the stimulated spine: 5.5 µm). We then compared αCaMKII enrichment (spine/dendrite) in the three groups (Fig. 3.4 C). Only in the group of spines with persistent volume increase, we detected a significant increase in the concentration αCaMKII at t = 10 min ($p < 0.05$, Fig. 3.4 C). Interestingly, all groups had the same αCaMKII concentration before stimulation, indicating that the initial αCaMKII level had no predictive value for the type of change (transient vs. persistent) induced by pairing stimulation. In neighboring spines, we did not detect an increase in αCaMKII

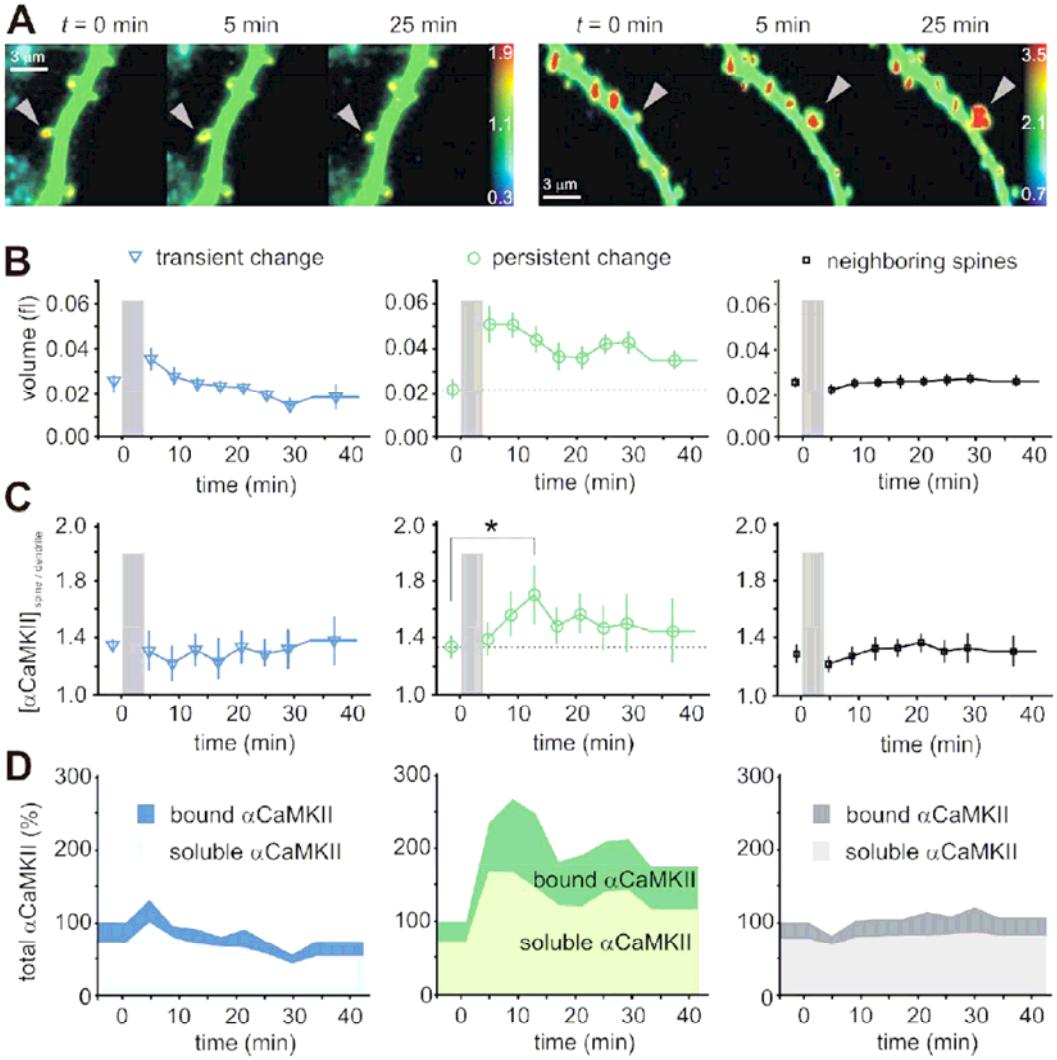

Figure3. 4. ***Spine enlargement precedes input-specific accumulation of αCaMKII.***

A, *Ratio images of CA1 pyramidal cell dendrites expressing ChR2/RFP and Dronpa-αCaMKII before and after optical pairing protocol. Arrow head marks stimulated spine. Left example: Stimulated spine shows transient volume increase. Right example: Stimulated spine shows persistent increase in volume and αCaMKII concentration.* ***B,*** *Spine volume changes in response to optical pairing protocol. Stimulated spines were sorted into 2 groups according to their volume 30-40 min after pairing (Transient spines: < 30% change, n = 13; Persistent spines, >30% change, n = 10). Note similar absolute volume of the two groups before stimulation. Right panel: neighboring, non-stimulated spines on the same dendrite show no significant volume change (mean distance from stimulated spine: 5.5 µm ± 0.9 µm, n = 110).* ***C,*** *α CaMKII concentration changes following pairing. Spines were sorted according to persistence of volume change as described in B. Significant increase in αCaMKII concentration was detected in persistently enlarged spines (asterisk, p < 0.05), but not in the group that responded only with transient swelling. Note identical αCaMKII concentration in both groups before stimulation. Right panel: Neighboring, non-stimulated spines showed noαCaMKII increase.* ***D,*** *Soluble and bound fraction calculated from data shown in C and B (see methods). In the spines that responded with persistent volume change to paired stimulation (middle panel), the amount of both soluble and bound αCaMKII is persistently increased.*

concentration, indicating a high spatial specificity of the αCaMKII enrichment. We noted that spine enlargement preceded the input-specific accumulation of αCaMKII: Whereas spine volume reached its maximum immediately after stimulation, αCaMKII concentration reached its peak ~10 min later. Using the spine/dendrite ratio before stimulation as a starting point, we could estimate changes in the amount of bound and soluble αCaMKII in stimulated and non-stimulated spines (Fig. 3.4 D). This analysis revealed that in the spines that showed a persistent increase in volume (middle panel), the absolute amount of bound αCaMKII in the spine had doubled 30-40 min after stimulation. The bound *fraction*, on the other hand, peaked transiently ~10 min after stimulation, but later returned to baseline (29% before stimulation, 33% 30-40 min after stimulation). These experiments suggests that the disturbance caused by paired stimulation did move 10 of 23 spines to a new equilibrium state, characterized by an increased amount of both soluble and bound αCaMKII and a larger volume. No significant volume or αCaMKII changes were detected in neighboring spines on the same dendrite.

Induction of long-term plasticity by synaptic activation

Glutamate uncaging is a convenient way to stimulate individual dendritic spines, but the amplitude of the postsynaptic response depends on laser intensity. Therefore, the question remained whether synaptic activity would be sufficient to induce spine volume changes and CaMKII translocation. To address this question, we imaged spiny dendrites of double-transfected CA1 pyramidal cells (YFP-αCaMKII + RFP, Fig. 3.5 A) while stimulating Schaffer collateral axons at high frequency (3 x 1 s, 100 Hz, Fig. 3.5 B). Simultaneously, we performed electrophysiological recordings from a neighboring cell to verify LTP induction (Fig. 3.5 D). Following time-lapse imaging of the undisturbed transfected cell for 40 min, we introduced a calcium sensitive dye (Fluo 4FF) and Alexa-Fluor 594 via patch pipette. Although the plasticity-inducing tetanic stimulation was applied under blind conditions, re-activation of the stimulation electrode allowed us to identify synaptically stimulated spines *post hoc* by Ca^{2+} imaging in 4 experiments (Fig. 3.5 C). The fluorescent proteins in the cell did not interfere with optical Ca^{2+} measurements since they were not excited at the wavelength we used for Ca^{2+} imaging (810 nm). Analysis of head volume of synaptically stimulated spines revealed a rapid volume increase with a large persistent

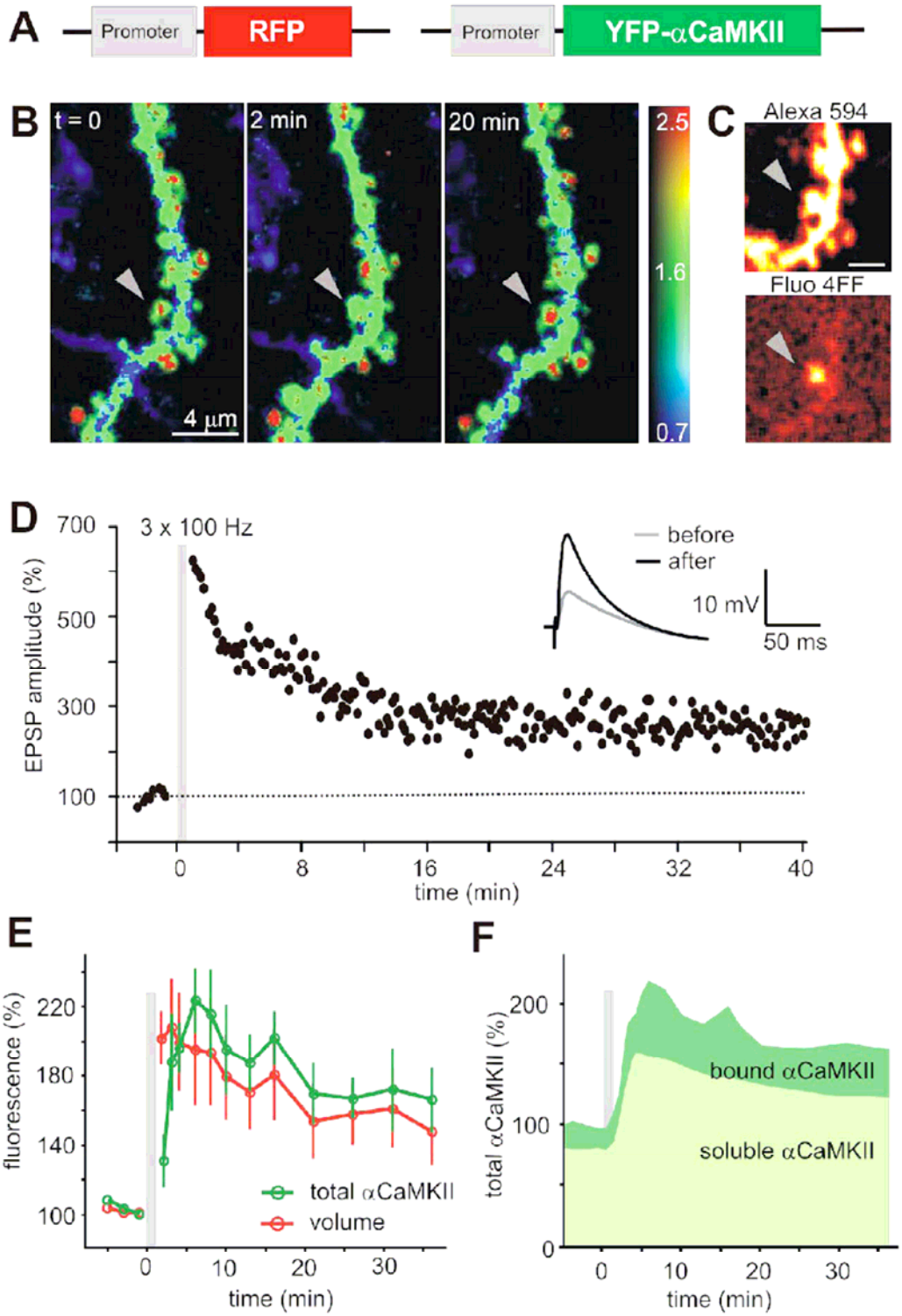

Figure 3.5. ***Input-specific accumulation of αCaMKII induced by high frequency stimulation of Schaffer collaterals.***

A, *Schematic drawing of the two vectors used for double transfection by gene gun. Promoter denotes synapsin-I promoter.* **B,** *Ratio images of cells expressing YFP-αCaMKII and RFP before (t = 0) and after (2 min, 20 min) repetitive stimulation of Schaffer collateral fibers at high frequency (3 x 100 Hz, 1 s, at 0.1 Hz). Warm colors indicate high CaMKII concentration. At t = 0, the high frequency protocol was applied. The spine marked by the arrow head was the stimulated spine identified by post hoc*

Figure 3.5. Continues

calcium imaging (see B). ***C,*** *Post-hoc identification of the stimulated spine using calcium imaging. Upper image: Alexa 594 fluorescence. Lower image: Fluo 4FF signal (Δf) after synaptic stimulation at depolarized membrane potential (0 mV), indicating localized calcium influx at stimulated spine. Scale bar: 2 µm. D, Tetanic stimulation induces LTP at Schaffer collateral synapses. Grey bar indicates high frequency stimulation (3 x 1 s, 100 Hz).* ***E,*** *Tetanic stimulation induces rapid spine volume increase (red curve) and delayed increase in total αCaMKII (green curve) in the stimulated spines (n = 4 spines, 4 cells).* ***F,*** *Tetanic stimulation leads to an increase in the total number of soluble and bound αCaMKII molecules in the stimulated spines (2.0 fold change in bound αCaMKII, 1.5 fold change in soluble αCaMKII).*

component (Fig. 3.5 E). Total αCaMKII also increased in the stimulated spines, peaking 6 min after stimulation (Fig. 3.5 E). The increase in total αCaMKII was slightly larger than the relative volume change. This overshoot reflects binding of αCaMKII to postsynaptic sites. Analysis of the soluble and bound fraction revealed an increase in bound αCaMKII in the tetanized spines by a factor of 2.1 (Fig. 3.5 F). Due to the brief stimulation protocol and the different label (YFP instead of Dronpa), we achieved a higher temporal resolution of the early phase of spine expansion in these experiments. Spine volume increase was rapid and preceded αCaMKII enrichment, leading to a transient decrease in αCaMKII concentration in the first 4 minutes after tetanic stimulation (Fig. 3.5 B, E). We conclude that synaptic stimulation at high frequency is sufficient to induce LTP at Schaffer collateral synapses, causes persistent spine volume changes and binding of additional αCaMKII to postsynaptic sites. Taken together, the physiological and morphological consequences of high frequency stimulation were remarkably similar to the changes we observed after pairing of glutamate uncaging with postsynaptic depolarization by ChR2 (Fig. 3.4).

Supplementary figures:

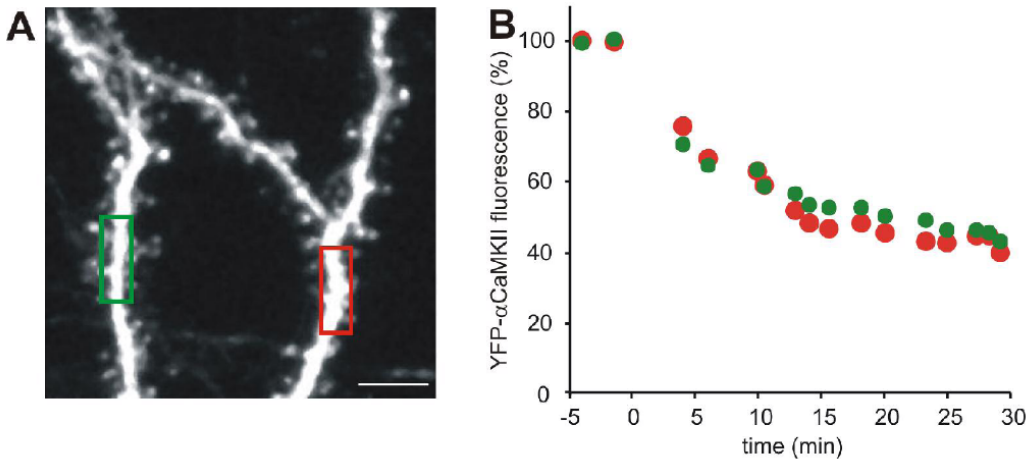

Supplementary Figure 3.1. ***Example of αCaMKII wash-out following whole-cell patch clamp.***

A, *Image of YFP-αCaMKII transfected cell before patch clamp. CA1 pyramidal cell, oblique dendrites. Scale bar: 5 µm.* ***B,*** *Decay of YFP-αCaMKII fluorescence in oblique dendrites after formation of the whole-cell configuration at t = 0.*

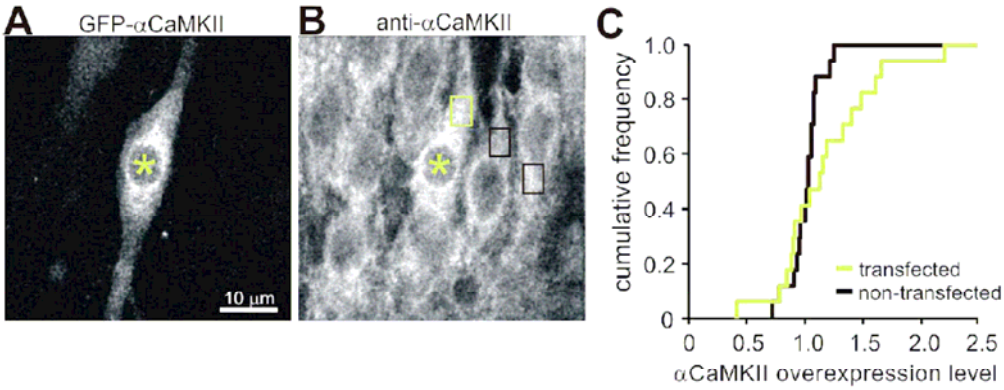

Supplementary figure 3.2. ***Estimating overexpression level of αCaMKII.***

A, *Fixed hippocampal slice culture with single neuron expressing GFP-αCaMKII (single optical section, green color channel).* ***B,*** *Same optical section showing immunofluorescence signal of anti-αCaMKII (red color channel). Transfected cell (asterisk) shows slightly elevated αCaMKII level in this example.* ***C,*** *Cumulative distribution of αCaMKII overexpression. Green curve: Overexpression level was calculated by taking the ratio of total immunofluorescence in a cytoplasmic region (endogenous plus recombinant αCaMKII) between transfected and non-transfected neurons. Median overexpression level: 1.13, range: 0.4 - 2.2, n = 17 cell pairs. Black curve: Comparing non-transfected cells resulted in a more narrow distribution with median = 1.0.*

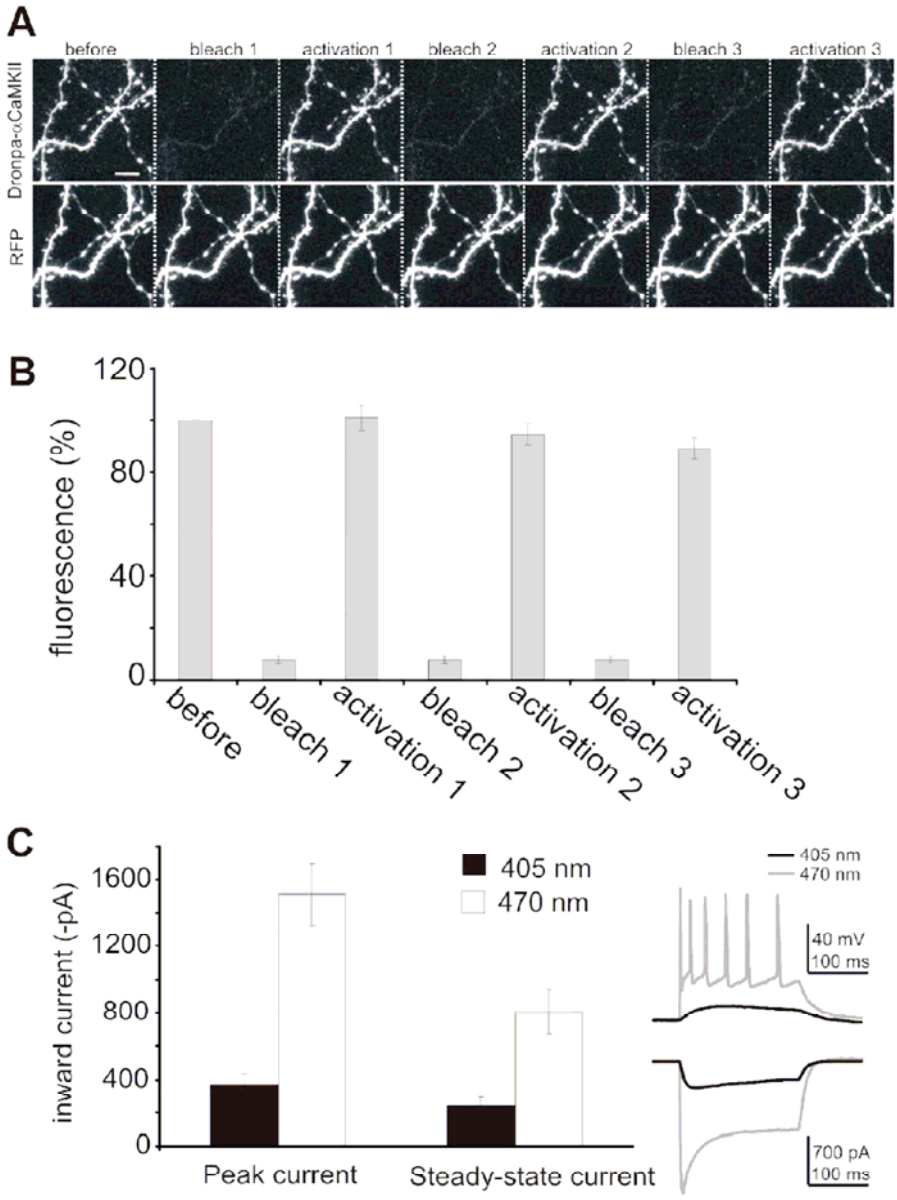

Supplementary figure 3.3. ***Reversible photoswitching of Dronpa-αCaMKII.***

A, *Simultaneous 2-photon imaging of Dronpa-αCaMKII and RFP. Dronpa-αCaMKII fluorescence slowly bleaches at 500 nm, but can be reactivated by UV illumination (405 nm). Scale bar: 6 µm.* ***B,*** *Quantification of Dronpa-αCaMKII fluorescence recovery after full bleaching (1st recovery: 101% ± 10%, 2nd recovery: 95% ± 9%, 3rd recovery: 89% ± 9%, n = 5 cells).* ***C,*** *Dronpa-reactivation (405 nm) caused small depolarizing current, but no spiking in ChR2-expressing cells (405 nm peak current: 373 pA ± 64 pA, steady state current: 244 pA ± 49 pA; 470 nm peak current: 1510 pA ± 182 pA, steady state current: 806 pA ± 136 pA, n = 5 cells).*

Discussion

Here we introduce a new, all-optical method to investigate synapse-specific changes during the induction of LTP. A combination of time-lapse two-photon imaging, two-photon glutamate uncaging and channelrhodopsin-2 stimulation enabled us to induce LTP without the need for intracellular recording, thus avoiding potential artifacts due to changes in the intracellular milieu. Moreover, our method permitted us to measure spine morphology and protein concentration before and after plasticity induction at the level of single synapses. We show that coincident activity leads to a lasting increase in volume of the stimulated spine, but not in neighboring spines on the same dendrite. Furthermore, we show that only in those spines that underwent lasting volume changes, αCaMKII concentration significantly increased. This concentration increase was not seen in spines that responded only with a transient swelling to the paired stimulation.

Advantages and limitations of the optical pairing protocol

Our CaMKII measurements highlight the advantages of the optical pairing protocol. An inherent limitation of non-invasive experiments, however, is the fact that direct information about the synaptic currents is lacking. To test the efficacy of our plasticity-inducing protocols, we therefore performed patch clamp recordings of CA1 pyramidal cells that were not used for imaging experiments (Fig. 3.1 E, Fig. 3.2 C, Fig. 3.5 D). Paired patch clamp recordings from CA3-CA1 connections provided an excellent model for single-synapse uncaging experiments: Excitatory postsynaptic currents from paired recordings (pEPSC = 24 pA ± 5 pA, n = 15 pairs) were of similar amplitude to spontaneous miniature EPSCs recorded in TTX (mEPSC = 18 pA ± 3 pA, n = 7 cells, data not shown), indicating that most CA3-CA1 connections were made by a single or very few synapses. Uncaging laser power was adjusted to give similar response amplitudes to paired recordings (uEPSC = 24 pA ± 3 pA, n = 23 cells). A second caveat of the optical pairing protocol is the danger of bleaching fluorescent proteins by the uncaging laser pulse. While soluble fluorescent proteins are constantly replenished from the dendritic reservoir, the fluorescence of bound proteins is lost irreversibly (Fig. 3.3 C). To circumvent this problem, we created a fusion protein of αCaMKII with the photoactivatable Dronpa-Green. This allowed us

to reactivate the fluorescence before each acquisition and thus prevent loss of signal from the bound fraction (Supp. Fig. 3.3).

Since we found solutions for the technical problems mentioned above, we could exploit the advantages of optical stimulation: Unlike chemical LTP and zero Mg^{2+} protocols (Fong et al., 2002; Otmakhov et al., 2004; Sharma et al., 2006), optical pairing does not lead to unspecific activation of the entire tissue. Therefore, activity-induced changes at individual synapses can be studied in an unperturbed environment. The spatial resolution is clearly superior to local perfusion approaches, which have been used previously to probe the input specificity of LTP and CaMKII translocation (Engert and Bonhoeffer, 1997; Thalhammer et al., 2006). The timing of pre- and postsynaptic activation can be controlled independently and with millisecond precision, which will allow for a more detailed investigation of spike-timing-dependent plasticity at identified synapses in the future. Unlike electrophysiological recordings, all-optical experiments are not limited in time. Most importantly, the intracellular milieu of the postsynaptic cell is not affected, such that even subtle changes in protein concentration can be detected.

Transient vs. persistent spine volume changes

In response to optical pairing, we observed a rapid volume increase in the stimulated spines (Fig. 3.2 E, Fig. 3.4 B). Among them, 55% were still significantly (> 30%) enlarged 30-40 min after stimulation. Interestingly, the variable morphological change was reflected in the variable amount of LTP that could be induced at individual CA3-CA1 connections (Fig. 3.1 E). A correlation between LTP induction and persistent increase in spine volume has been reported previously, using chemical LTP (Kopec et al., 2006) or repetitive glutamate uncaging under zero Mg^{2+} conditions (Matsuzaki et al., 2004). We did not find a correlation between the persistent volume change and the initial spine volume or the initial concentration of αCaMKII in the spine (Fig. 3.4), and conclude that there is no obvious way to predict the sensitivity of a spine to the pairing protocol from these parameters. Our results confirm that individual Schaffer collateral synapses can be more or less susceptible to potentiation (Petersen et al., 1998; Debanne et al., 1999).

Apart from the pairing protocol, tetanic stimulation is another classic stimulus paradigm for the induction of LTP. In our hands, tetanic synaptic stimulation induced a very similar volume response of the stimulated spines: A rapid, transient expansion, leading over to a persistent spine enlargement by a factor of 1.4 after 30-40 min (Fig. 3.5 E). Transient, but not persistent volume changes were reported in a previous study on acute mouse hippocampal slices after tetanic stimulation at 100 Hz (Lang et al., 2004). Tetanic stimulation leads to large Ca^{2+} transients in the entire dendrite that could trigger transient volume changes in spines that were not activated synaptically. Therefore, we restricted our analysis to spines that did receive direct synaptic input as verified by *post hoc* calcium imaging, which might explain the difference to the previous study. Our results complement a recent study on dissociated cells, in which spine shrinkage was reported following the induction of long-term depression (Zhou et al., 2004). Taken together, our results suggest that the simple equation 'big spine = big EPSP' holds true for the early phase of long-term plasticity. Since we only stimulated existing spines, our results are not incongruous with the formation of new spines reported after LTP induction (Engert and Bonhoeffer, 1999; Maletic-Savatic et al., 1999).

αCaMKII binding is specific to spines that received coincident activity

We show that translocation of αCaMKII to postsynaptic sites that has been reported after extracellular glutamate application or chemical LTP (Shen and Meyer, 1999; Otmakhov et al., 2004; Merrill et al., 2005; Thalhammer et al., 2006) is also observed following paired stimulation of individual synapses. Baseline levels of CaMKII were quite variable between individual spines (Fig. 3.3), but unlike following chemical LTP (Otmakhov et al., 2004), this variability did not predict the response of individual spines to paired stimulation (Fig. 3.4). A general concern with overexpression studies are potential differences in the distribution of endogenous and exogenous proteins. Here we used a non-viral, neuron-specific promoter, which resulted in surprisingly small changes in total protein concentration: Two weeks after transfection, total αCaMKII in transfected CA1 pyramidal cells was increased by only ~12% relative to neighboring untransfected cells (Supp. Fig. 3.2). This suggests that the distribution of fluorescently labeled αCaMKII was representative of endogenous αCaMKII in most transfected cells.

We used two different plasticity-inducing protocols in our study: Optical pairing of pre- and postsynaptic depolarization, and high frequency synaptic stimulation. Both stimulation protocols triggered very similar processes that were highly specific to the spines receiving excitatory input, namely a rapid expansion of the spine head, followed by a slow increase of total αCaMKII content. It should be noted that tetanic stimulation via bipolar electrode activates many axons simultaneously, leading to strong depolarization of the postsynaptic cell. Therefore, from the point of view of the stimulated synapse, both stimulation protocols fulfill the 'coincidence condition' necessary for NMDA receptor activation and induction of long-term plasticity. Given the time constant of αCaMKII diffusion measured in our FRAP experiments (τ = 12.5 s), αCaMKII increase in the stimulated spines was surprisingly slow. One potential explanation is an increased diffusional resistance of the spine neck that has been reported after paired stimulation (Bloodgood and Sabatini, 2005). Diffusion of large proteins like CaMKII might be significantly slowed down due to a burst of actin polymerization after paired stimulation. A second possibility would be the slow generation of additional binding sites for αCaMKII by a structural enlargement of the PSD in first 5-10 minutes following potentiation. In a previous study, where AMPA receptor density was optically measured in spines, a similar, delayed time course of GluR1 increase was reported, peaking 6 min after induction of chemical LTP (Kopec et al., 2006). The similar time course and the persistent, 2-fold increase in the bound fraction of CaMKII we report here is consistent with a structural role of CaMKII in anchoring glutamate receptors to the postsynaptic density (Hayashi et al., 2000; Lisman and Zhabotinsky, 2001). Recently, it has been demonstrated that LTP can be partially reversed by blocking CaMKII activity, providing further evidence for its role in the maintenance of synaptic strength (Sanhueza et al., 2007). In summary, the insertion of additional AMPA receptors, which is the accepted structural correlate of LTP at Schaffer collateral synapses (Matsuzaki et al., 2004), seems to be linked with a lasting increase in spine volume and binding of additional CaMKII molecules to postsynaptic sites. Here we show that these changes can be induced with single spine specificity, validating Hebb's postulate on the micrometer scale.

Materials and Methods

Plasmid construction. ChR2-YFP, a gift from Dr. K. Deisseroth, was modified by inserting a stop codon (TAG) after amino acid 309 by PCR and inserted into a synapsin-I (syn) promoter vector (Kugler et al., 2001) to ensure neuron-specific expression. The fragment of syn-ChR2-SV40-polyA was excised and inserted into a second expression vector containing syn-tdimer2, a dimeric red fluorescent protein (from Dr. R.Y. Tsien). GFP-αCaMKII (from Dr. T. Meyer) was subcloned into a separate syn promoter vector, and new αCaMKII fusions were made by replacing GFP with YFP or Dronpa-Green (MBL, Naka-ku Nagoya, Japan). Mutant αCaMKII (TTVA) was generated by site-directed mutagenesis (Thr^{305} → Val and Thr^{306} → Ala) using the QuickChange kit (Stratagene). All constructs were verified by DNA sequencing, amplified and purified using MaxiPrep Kits (Qiagen).

Slice culture and transfection. Organotypic hippocampal slices were prepared from Wistar rats at postnatal day 5 as described (Stoppini et al., 1991), in accordance with the animal care and use guidelines of the Veterinary Department Basel-Stadt. After 7 days in vitro, cultures were transfected with syn-ChR2-syn-tdimer2 in combination with syn-αCaMKII fused to YFP or Dronpa-Green, using a Helios Gene Gun (BioRad). All experiments were performed 2-3 weeks after transfection. Retinal (1 μM, Sigma) was added to the culture medium, but not to the recording solution.

Electrophysiology. Hippocampal slice cultures were placed in the recording chamber of the microscope and superfused with artificial cerebrospinal fluid (ACSF) containing (in mM): 119 NaCl, 2.5 KCl, 4 $CaCl_2$, 4 $MgCl_2$, 26.2 $NaHCO_3$, 1 NaH_2PO_4, 11 glucose. The solution was gassed with 95% O_2, 5% CO_2, pH was adjusted to 7.2. Single and dual whole-cell recordings were performed using Axopatch 200B and MultiClamp 700B amplifiers (Axon Instruments). Recording pipettes (4.5 - 5.5 MΩ) were filled with intracellular solution containing (in mM): 135 K-gluconate, 10 HEPES, 4 $MgCl_2$, 4 Na_2-ATP, 0.4 Na_2-GTP, 10 Na_2-phosphocreatine, 3 ascorbate, pH was adjusted to 7.2. LTP of unitary EPSCs was induced by repeatedly pairing (20 times, 0.1 Hz) presynaptic stimulation (2 nA, 5 ms) with a postsynaptic burst of 4-9 action potentials induced by blue light stimulation (200 ms). For uncaging experiments, MNI-caged-L-glutamate (Tocris) was bath

applied at 5 mM in ACSF containing (in mM): 125 NaCl, 2.5 KCl, 2 $CaCl_2$, 2 $MgCl_2$, 26.2 $NaHCO_3$, 1 NaH_2PO_4, 11 glucose, 0.03 D-serine, 0.005 2-chloroadenosine. LTP of uncaging-evoked EPSCs was induced by repeatedly pairing (20 times, 0.07 Hz) uncaging of glutamate with postsynaptic blue light stimulation (200 ms). For tetanic stimulation experiments, bipolar electrodes (FHC Inc., ME) were placed in *stratum radiatum* ~200 μm lateral to the recording site, and 10 μM bicuculline and 4 μM 2-chloroadenosine were added to the ACSF to facilitate LTP induction and avoid recurrent excitation. All recordings were performed at 30-32^{o}C.

Light stimulation, 2-photon imaging, 2-photon uncaging. The 2-photon imaging and uncaging setup was based on a Olympus BX51WI microscope equipped with a LUMFL 60× 1.1 NA objective, controlled by a free software package (Pologruto et al., 2003) written in Matlab (The MathWorks). Two ultrafast IR lasers (Chameleon-XR, Coherent; Mai Tai HP, Spectra-Physics) controlled by electro-optic modulators (350-80, Conoptics) were combined by a polarizing beamsplitting cube (Thorlabs) for simultaneous imaging (930 nm) and uncaging (725 nm). A blue LED (470 nm, Cairn Research Ltd.) was coupled into the epifluorescence pathway to deliver light pulses for ChR2 activation. Two PMTs (R3896, Hamamatsu) below a 1.4 NA oil immersion condenser were used to detect red and green emission. During the blue light pulse, they were protected by a VS25 shutter (Vincent Associates). Glutamate uncaging was achieved using a 0.5 ms pulse of 725 nm light. Laser intensity was adjusted to mimic the amplitude of unitary EPSCs. To combine the blue light used for stimulation with the IR lasers, we used a 470/40 bandpass and 720DCXR dichroic mirror (Chroma).

Image analysis. Off-line analysis was performed using custom routines written in Matlab. We used the ratio of green/red fluorescence (*G*/*R*, or *Y*/*R* in case of YFP-αCaMKII) as a measure of αCaMKII concentration. To display ratio images, we used a hue/saturation/brightness color model, where hue was determined by the *G*/*R* ratio of every pixel (using a rainbow color table), and brightness was set by the intensity in the red (volume) channel. For quantitative analysis, we calculated the *G*/*R* ratio in a region of interest after subtraction of background fluorescence and optical crosstalk. To compensate for differences in the relative expression levels of the two constructs

in different cells, we normalized the *G*/*R* ratio in the spine by the *G*/*R* ratio in the dendrite to get the spine/dendrite (*S*/*D*) ratio

$$S/D = \frac{G_{spine}/R_{spine}}{G_{dendrite}/R_{dendrite}} = \frac{[CaMKII]_{spine}}{[CaMKII]_{dendrite}} \qquad \text{(Eq. 1)}$$

To calculate the bound fraction from the S/D ratio, we assumed that the concentration difference between spine and dendrite was due to bound CaMKII in the spine:

$$[CaMKII]_{spine,bound} = [CaMKII]_{spine} - [CaMKII]_{dendrite} \qquad \text{(Eq. 2)}$$

$$[CaMKII]_{spine,bound} = [CaMKII]_{spine} - \frac{[CaMKII]_{spine}}{S/D} \qquad \text{(Eq. 1 in 2)}$$

or, expressed as a fraction of total $[CaMKII]_{spine}$

$$[CaMKII]_{spine,bound} = 1 - \frac{1}{S/D} \qquad \text{(Eq. 3)}$$

Average values are given as mean ± SEM if not indicated otherwise. Significance was defined as $p < 0.05$ and determined using Student's *t* test (two-tailed).

Immunofluorescence. Slices with cells expressing GFP-αCaMKII were fixed in 4% paraformaldehyde for 10 min at room temperature (RT), washed three times with PBS and incubated with PBS containing 0.5% Triton X-100 at 4°C overnight. The fixed slices were incubated in blocking solution (20% horse serum, 50 mM NH_4Cl in PBS) at RT for 4 h, washed again, incubated with anti-αCaMKII antibody (MAB 3119, Chemicon) at 2 μg/ml in PBS (1% horse serum) overnight at 4°C, and washed again. Next, the slices were incubated in Alexa Fluor 594 goat anti-mouse IgG1 secondary antibody (Invitrogen) at 2 μg/ml for 3 h at RT, and washed again. The fixed slices were mounted in Aquatex media (Merck) and imaged using a two-photon laser-scanning microscope. GFP-αCaMKII expressing cells were readily identified by their green fluorescence (930 nm excitation, Supplemental fig. 1 A). αCaMKII overexpression was quantified by dividing the αCaMKII immunofluorescence intensity of a GFP-αCaMKII expressing cell by the immunofluorescence of neighboring untransfected cells (810 nm excitation).

Spine volume measurements. To determine absolute spine volume, we measured the integrated fluorescence intensity of the spine in the red channel, which is proportional to its cytoplasmic volume. For each cell, a calibration measurement was taken by

focusing the laser into the proximal apical dendrite, a cellular compartment large enough to contain the entire point-spread function (PSF) of our microscope, to get the maximum fluorescence intensity (f_{max}). The attenuation of the laser was corrected by a single exponential attenuation function:

$$f(z) = f_{max} \times e^{a \cdot (z - z_{max})} \qquad (1)$$

were a = -0.0057 μm^{-1} is the attenuation coefficient, z_{max} is the depth of the proximal apical dendrite and z is the depth of the spine. To measure the absolute volume of a spine (V_{spine}), we first calculated the Gaussian intensity distribution a hypothetical PSF-sized object would produce if imaged at the same zoom factor and the same depth as the spine (f_{PSF}). The integrated intensity of f_{PSF} (sum of all pixel values within a region of interest, $\iint f_{PSF}$) was then compared to the integrated intensity of the spine image in a maximum intensity z-projection ($\iint f_{spine}$). The volume of the spine is related to the spine intensity as follows:

$$V_{spine} = \iint f_{spine} \times V_{PSF} / \iint f_{PSF} \qquad (2)$$

The volume of the PFS (V_{PSF} = 0.30 μm^3) was determined using fluorescent beads (0.1 μm, Molecular Probes).

Chapter 4. All-optical identification of functional synaptic contacts in intact brain tissue

Yan-Ping Zhang, Nunu Mchedlishvili, Thomas G. Oertner

Abstract:

Dendritic spines are tiny protrusions where most glutamatergic synapses are made. Electron microscopy (EM) has the ability to resolve functional synaptic contacts, but cannot examine the same set of synapse before and after stimulation. Here we present an all-optical method to identify closely associated presynaptic varicosities and postsynaptic spines *in situ* and verify putative synaptic contacts without the need for EM reconstruction. To control glutamate release and postsynaptic depolarization non-invasively, we expressed a light-sensitive cation channel (Channelrhodopsin-2) both pre- and post-synaptically. Our strategy to validate functional synapses was to monitor the fluorescence changes of a genetically encoded Ca^{2+} indicator (GCaMP2) postsynaptically. We show that morphologically associated axons and spines are not necessary functional physical synaptic contacts. Functional calcium imaging is needed to validate the visually identified synapses. GCaMP2 is able to detect Ca^{2+} influx through NMDA receptors following synaptic stimulation. Therefore, the combination of ChR2 stimulation and two-photon calcium imaging is ideal for investigating synaptic plasticity at the level of single synapses.

Introduction

Most glutamatergic synapses are made on the heads of dendritic spines (Nimchinsky et al., 2002). Spines show a great diversity in shape and size. A neuron can have up to 100,000 spines, each generally forming a single synapse. Since most synapses are beyond the range of normal light microscopy, it is the electron microscopy that has the ability to resolve the structure of synapses with unprecedented detail (Shepherd and Harris, 1998). The anatomical basis of the synaptic contact consists of the presynaptic element, located on a varicosity or terminal of an axon, and the postsynaptic density, mainly located on a spine head. Pre- and postsynatpic elements are separated by a gap of about 10 nm, the synaptic cleft. Transmitters bridge this gap

by diffusing from release sites on the presynaptic side to receptors on the postsynaptic side.

Interestingly, there are increasing evidences of structural changes of both presynaptic varicosity and postsynaptic spines in response to neuronal activity (Umeda et al., 2005; De Paola et al., 2006; Holtmaat et al., 2006; Knott et al., 2006; Majewska et al., 2006). Varicosities of the pyramidal cell axons in the hippocampus exhibited rapid structural changes, including protrusive activity and remodelling associated with transport of membrane organelles (Nikonenko et al., 2003). EM studies of the neuropil were used to make population comparisons of the structure of dendritic spines across developmental or plasticity states. During development, clear changes in the density, shape and size of the dendritic spines of hippocampal pyramidal neurons were revealed (Harris et al., 1992). However, in terms of detecting changes that accompany stimulus-induced synaptic plasticity, EM may have the limitation to examine the same set of spines before and after the induction protocol.

Here we have developed an all-optical method to identify closely associated presynaptic varicosities and postsynaptic spines *in situ* using two-photon laser scanning microscopy. By monitoring the fluorescence changes of a genetically encoded Ca^{2+} indicator (GCaMP2) (Lee et al., 2006; Tallini et al., 2006; Diez-Garcia et al., 2007) in the dendritic spines, we could verify putative synaptic contacts without the need for EM reconstruction. We took the advantage of a newly identified light-gated cation channel, ChR2, that can control neuronal activity with millisecond precision (Boyden et al., 2005), to stimulate visually identified synaptic contacts precisely and uninvasively. The combination of two-photon calcium imaging, two-photon time-lapse imaging and Channelrhodopsin-2 stimulation offers the great potential to visualize individual synapses as they undergo LTP.

Results

Visualization of presynaptic and postsynaptic components in hippocampal slice cultures

To visualize synaptic contacts in the CA1 region of the hippocampus, we transfected CA1 and CA3 pyramidal neurons in hippocampal organotypic slice cultures with two

different fluorescent probes using particle-mediated gene transfer (Fig 4.1). For the observation of dendritic morphology, we expressed CFP in a small number of pyramidal neurons (Fig 4.1B). In turn, CA3 cells were transfected with a red-labeled light-gated cation channel, ChR2 (Fig 4.1A). We obtained multiple optical sections with spacing of 0.5-1 μm using a high NA objective lens and simultaneous activation of two fluorescent probes using two-photon laser microscopy (930nm). We could successfully visualize CFP-positive dendrites and ChR2-RFP positive axons in CA1 area (Fig 4.2). Since the synapses between the Schaffer collateral and commissural axons and the apical dendrites of CA1 pyramidal cells are formed between dendritic spines and axonal varicosities, we restricted our analysis of putative synaptic contacts to the contact sites between axonal varicosities and dendritic spines. We used our custom written program (ContactChecker) to identify close association of axons and spines. Rotation of reconstructed 3D images of the axon-spine pairs also confirmed the association of two structures (Fig 4.2C).

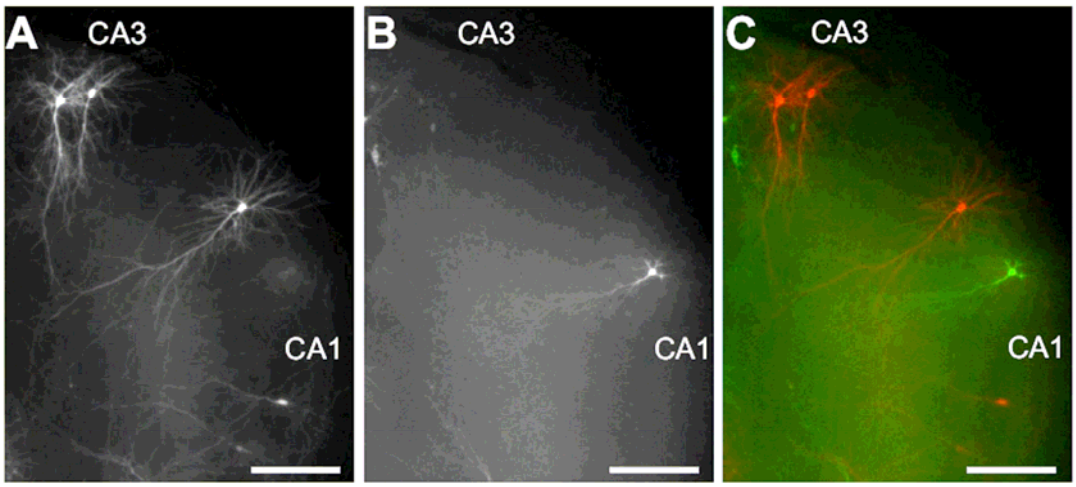

Figure 4.1. ***Visualization of CA3 and CA1 pyramidal cells with multiple fluorescent probes in hippocampal slice cultures.***

A. *ChR2-RFP expression in CA3 hippocampal neurons in slice culture 21 d in vitro at day 14 after transfection.* ***B.*** *CFP expression in a CA1 neuron in the same culture.* ***C.*** *Overlay of the hippocampal slice culture. Scale bar: (A-C) 500 μm.*

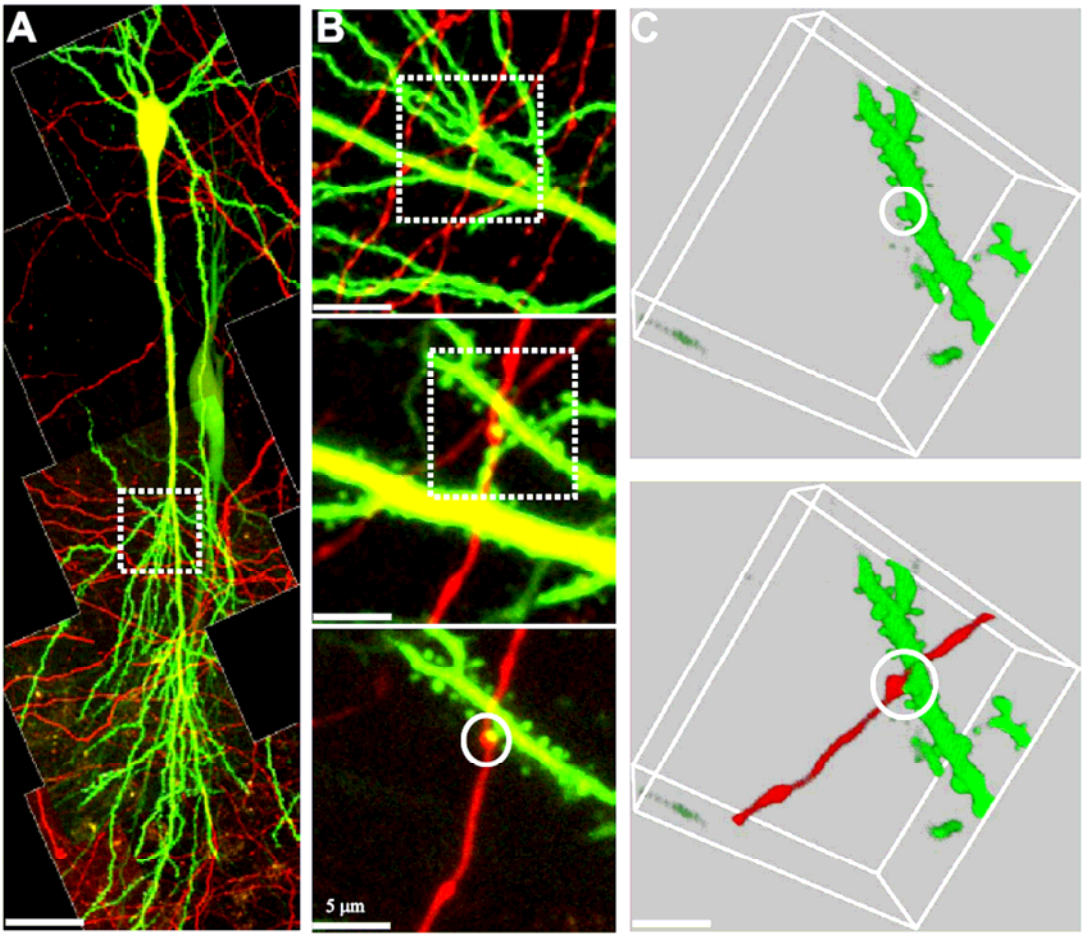

Figure 4.2. ***Detection of putative synaptic contacts between axonal varicosities and dendritic spines using two-photon microscopy.***

A*. Two-photon laser microscopic imaging of ChR2-RFP positive axons and CFP positive CA1 cells. Scale bar: 50 µm.* ***B.*** *Zoomed images of the region indicated in A, showing one contact site (white circle). Scale bar: upper 20 µm; middle 10 µm; lower 5 µm.* ***C.*** *Rotation of reconstructed 3D images of the same contact site shown in B, confirming the close association of the varicosity and the spine. Scale bar: 5 µm.*

Verification of functional synaptic contacts

We have previously shown that ChR2-expressing axonal terminal provide a highly reliable and precisely timed source of glutamate, and two-photon calcium imaging can be used to verify putative synaptic contacts without the need for electron microscopic reconstruction. N-Methyl-D-aspartate (NMDA) receptors activated by presynaptic glutamate release trigger calcium transients in dendritic spines, which can be readily detected by two-photon microscopy (Oertner et al., 2002; Yasuda et al., 2004). We set out to check all visually identified points of contact between the dendrite of CFP expressing CA1 cell and ChR2-positive axons. For postsynaptic responses, CFP

positive cells were loaded with calcium sensitive dye X-Rhod-5F through a patch-clamp electrode and imaged using two-photon excitation at 870 nm. When the postsynaptic cell was voltage-clamped at +40 mV, light stimulation (10 ms) did evoke detectable calcium influx in 5/19 spines (Fig 4.3). Similar results were previously reported when verifying visually identified synapses (Zhang and Oertner, 2007). We conclude that morphologically associated axons and spines are not necessary functional synaptic contacts. Postsynaptic calcium imaging is needed to validate the presence of functional synapses.

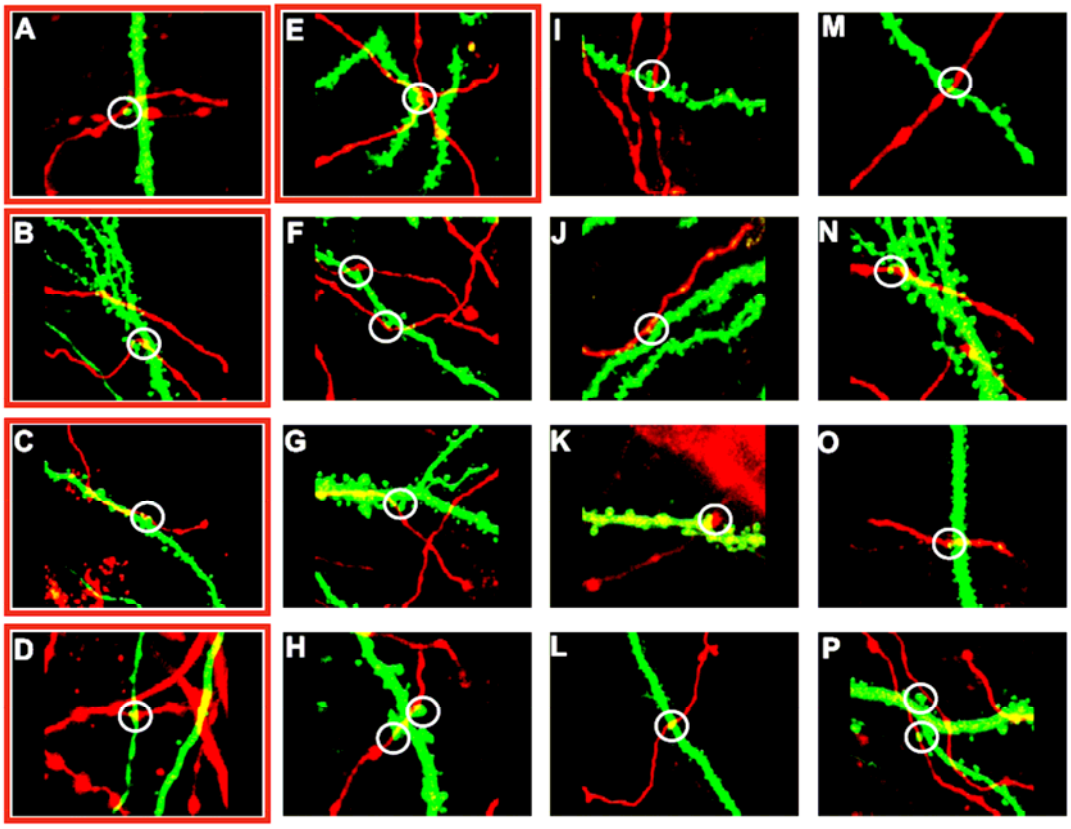

Figure 4.3. ***Verification of functional synaptic contacts.***

A-P. *All putative synaptic contacts tested by two-photon calcium imaging (white circles).* ***A-E.*** *Functional synaptic contacts, displayed detectable calcium influx after light stimulation (10 ms).* ***F-P.*** *Non-functional synaptic contacts.*

Characterization of a genetically encoded Ca^{2+} indicator, GCaMP2

Despite the successful use of synthetic Ca^{2+} indicators, they have significant limitations. They have to be introduced into neurons by a patch pipette or bulk loading of membrane permeable AM-ester derivatives. It is tedious to load cells especially

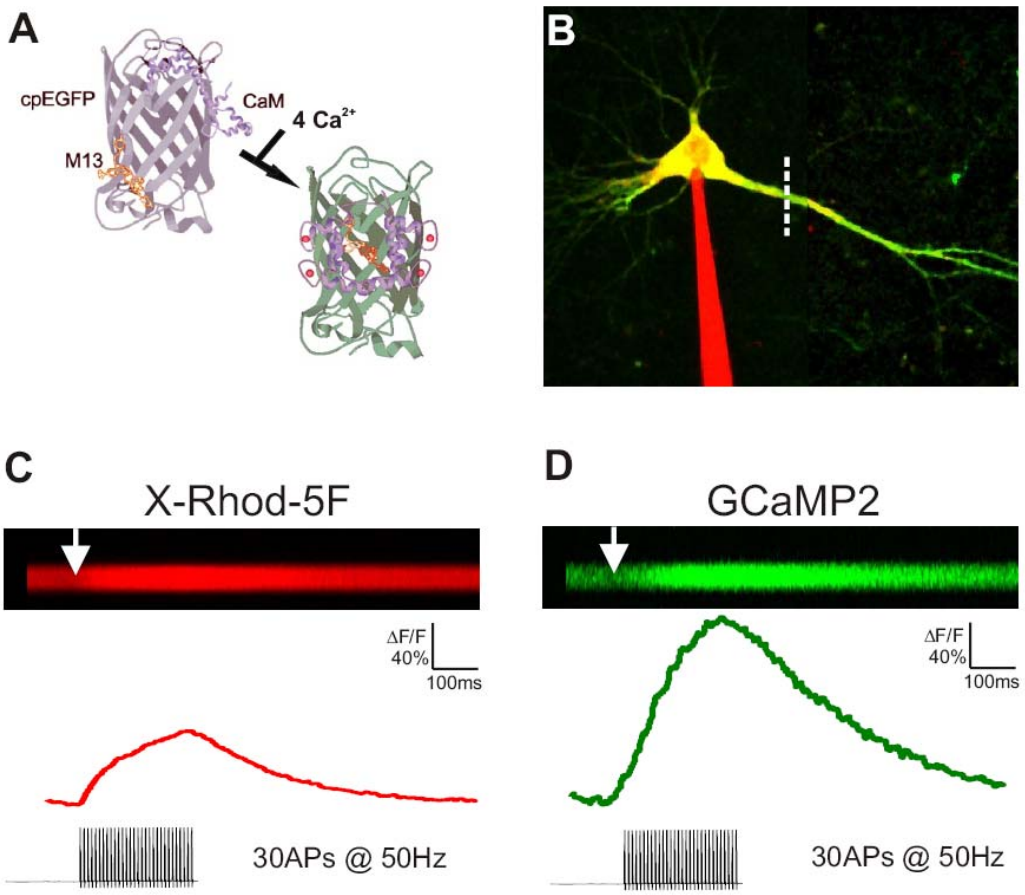

Figure 4.4. ***Dual-color imaging of AP-evoked fluorescence responses in GCaMP2 expressing CA1 cells.***

A*. Molecular topology of GCaMP2. GCaMP2 is based on cpGFP, containing CaM in the cpGFP barrel and the CaM-binding peptide M13. Binding of* Ca^{2+} *cause changes in GFP fluorescence.* ***B.*** *CA1 pyramidal neuron expressing GCaMP2 (green) and patched with a pipette filled with 150 μM X-Rhod-5F (red). The yellow region indicates overlapping green and red fluorescence. Dashed white line: location of line scan.* ***C, D.*** *Red and green fluorescence changes evoked by a train of 30 APs at 50 Hz. Fluorescence was averaged across the spatial extent of the dendrite to produce the fluorescence response (red and green traces, bottom) used for subsequent analysis. White arrow: onset of the stimulation.*

after long-term imaging. Moreover, unnecessary background fluorescence can be introduced due to the spill over of the dye. Here we set out to use a genetically encoded Ca^{2+} indicator, GCaMP2 that is based on circular permutation of GFP (cpGFP) (Baird et al., 1999; Nagai et al., 2001; Nakai et al., 2001). Ca^{2+} -dependent fluorescence of GCaMP2 arises from the interaction between Ca^{2+} / calmodulin at the C terminal of cpGFP and an N-terminal myosin light chain kinase (MLCK) fragment. GCaMP2 has been reported to have markedly improved brightness and thermal stability. We analyzed the property of GCaMP2 in hippocampal neurons and compared fluorescence responses of GCaMP2 and a red synthetic Ca^{2+} indicator, X-Rhod-5F, in response to back-propagating action potentials (bAPs) (Pologruto et al., 2004) (Fig 4.4). Under our experimental conditions, fluorescent changes in response

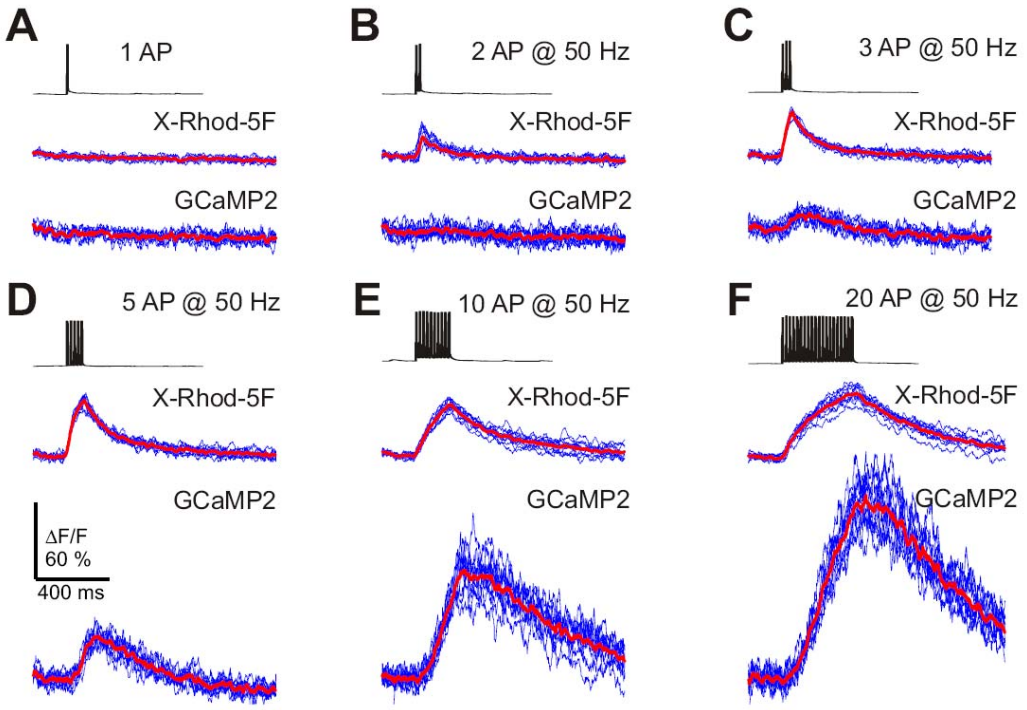

Figure 4.5. ***Fluorescence responses to APs for X-Rhod-5F and GCaMP2.***

A. *Single AP-evoked fluorescence transients for X-Rhod-5F (middle) and GCaMP2 (bottom). Red trace: averaged trace; blue traces: 10 individual trials from the same cell. The scale bar applies to all traces.* ***B-F.*** *Responses to trains of APs at 50 Hz for X-Rhod-5F (middle) and GCaMP2 (bottom).*

to a single bAP were not detectable both by X-Rhod-5F and GCaMP2. In response to two bAPs (at 50 Hz), X-Rhod-5F produced robust, rapid onset fluorescence changes. GCaMP2 began to show clear fluorescent responses, with signal to noise ratio above 2, only when three or more bAPs were given (Fig 4.5). Despite the non-linear

response to very low Ca^{2+} concentrations, GCaMP2 had a very large dynamic range. The maximal fluorescence change ($(\Delta F/F)_{max}$) required intense trains (> 40 APs at 50 Hz).

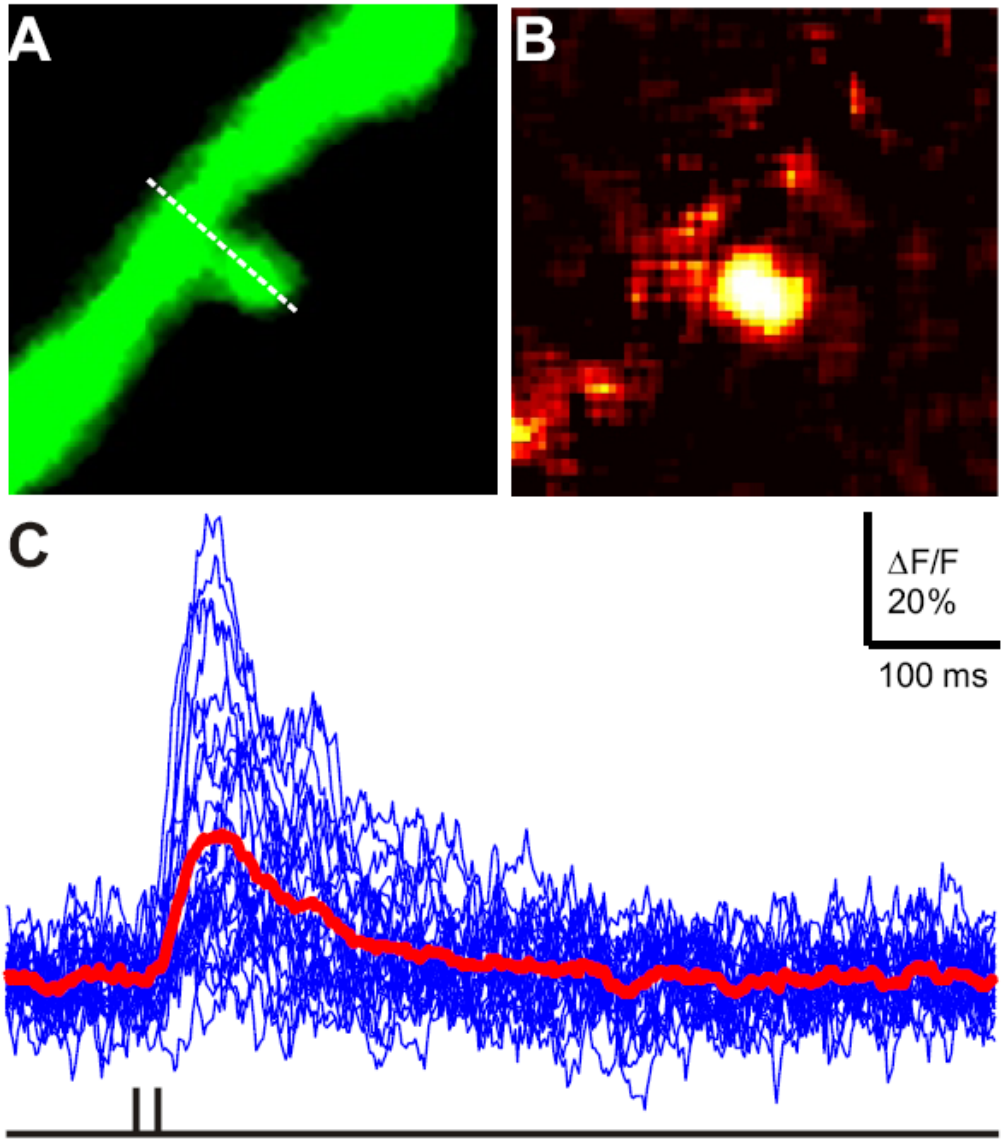

Figure 4.6. ***Monitoring synaptic transmission with GCaMP2.***

A-B. *Localized Ca^{2+} transient in a dendritic spine of a GCaMP2 expressing cell in responses to a paired stimuli (two presynaptic action potentials, paired with two postsynaptic action potentials, at 50 Hz). Dashed white line: location of line scan. GCaMP2 signal before stimulation (A). GCaMP2 signal change upon stimulation is displayed in hot color (B).* ***C.*** *Fourteen consecutive trials of spine calcium transients (blue traces) and averaged trace (red). Black line below indicates the onset of the paired stimuli.*

Monitoring synaptic transmission with a genetically encoded Ca^{2+} indicator

Activation of a single synapse leads to very small postsynaptic calcium transients, since the majority of NMDARs are blocked by Mg^{2+}. It has been shown that coincident activity , i.e. pairing of presynaptic activity with bAPs, results in supralinear Ca^{2+} transients in single spines (Nevian and Sakmann, 2004). Backpropagating APs relieved the Mg^{2+} block from NMDARs, which were activated by bound glutamate, thus maximized Ca^{2+} influx through the NMDA receptors during synaptic transmission. Thus, we used two paired stimuli (at 50 Hz) to look for active spines (i.e. those responding with a Ca^{2+} transient to stimulation). Indeed, active spines could be detected by GCaMP2, recognized by a clear, localized increase in fluorescence in the spine after stimulation (Fig 4.6). In the vicinity of the active spine no other active spines were observed. The Ca^{2+} transients evoked by either two APs or extracellular synaptic stimulation only were under the detection limit of GCaMP2. These results suggest that GCaMP2 is sensitive to the supralinear summation of Ca^{2+} signals in spines evoked during pairing of synaptic stimulation and backpropagating APs. Given the detected signal is restricted to the active synaptic contact, GCaMP2 is suitable to validate functional synapses between morphologically associated axons and spines.

All-optical identification of functional synaptic contacts

To control glutamate release and postsynaptic depolarization non-invasively, we expressed a light-sensitive cation channel (Channelrhodopsin-2) both pre- and post-synaptically. We constructed a convenient two-promoter vector for neuron-specific co-expression of unlabeled ChR2 and GCaMP2 (Fig 4.7 A). Two weeks after transfection, cells were tested with light stimulation. As a standard test stimulus, we used 200 ms blue light pulses, which triggered train of APs (5.4 ± 0.5 spikes, n = 21 cells). In response to blue light stimulation, GCaMP2 produced robust signals at the apical dendrite (Fig 4.7 B). Responses amplitudes vary between cells to cell, indicating that different numbers of spike were induced by 200 ms light (Fig 4.7 C). Knowing that the postsynaptic cell could be spiked by light, we went on to identify potential points of contact between the dendrite of ChR2/GCaMP2 expressing CA1

pyramidal cells and ChR2-RFP positive axons. The program, ContactChecker, reported morphologically associated axons and spines unbiasly. We then manually

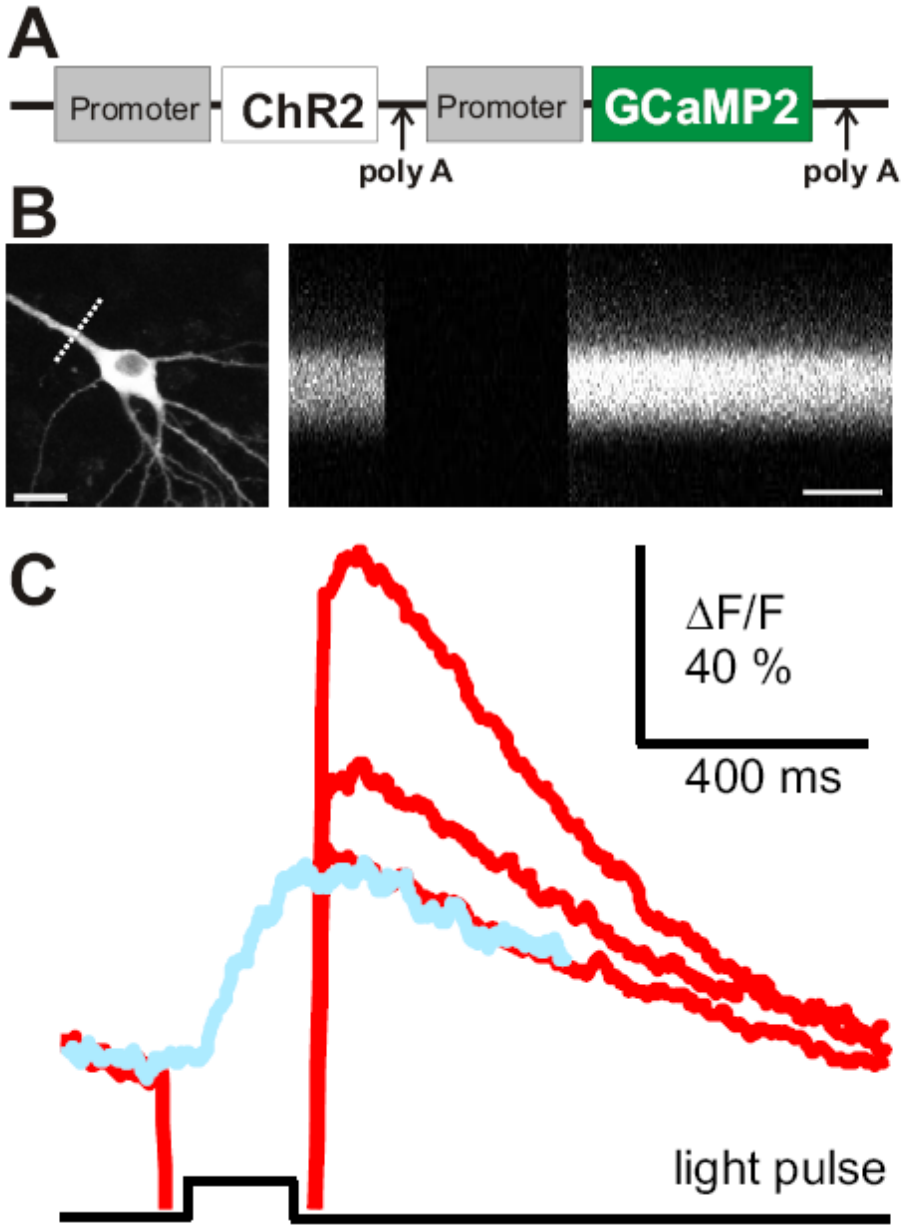

Figure 4.7. ***Remote control of postsynaptic depolarization.***

A. *Schematic drawing of the dual promoter vector expressing ChR2 and GCaMP2. Promoter denotes synapsin-1 promoter, poly A denotes SV40 poly A sequence.* ***B.*** *CA1 pyramidal cell in organotypic slice culture expressing ChR2 and GCaMP2. Dashed white line: location of line scan. Right: line scan across the apical dendrite (dashed white line in B, left) after 200 ms light stimulation.* ***C.*** *Averaged GCaMP2 fluorescence changes in three cells in response to 200 ms light stimulation (red traces). Light blue trace: averaged GCaMP2 fluorescence change in response to 5 APs at 50 Hz. Black line below indicates the onset of the light stimulation.*

verified each of these putative contacts by monitoring fluorescence changes of GCaMP2 in the spines (Fig 4.8). To trigger pre- and post coincident stimuli, we used two 10 ms pulses of blue light (at 50 Hz), which provides a precisely timed source of glutamate and a highly reliable depolarization at the postsynaptic cell. Testing 20 putative contacts, we found 2 functional synapses. The synaptic Ca^{2+} signal was highly localized in the spines. Failures in the transient rise in Ca^{2+} upon paired light stimulation were observed only infrequently. Once an active spine was found almost every stimulus evoked a transient rise in Ca^{2+}, consisting with our previous finding that release probability at ChR2-positive terminal is increased. Since the visually identified synapses are unperturbed, activity induced changes can to be studied with no time limitation.

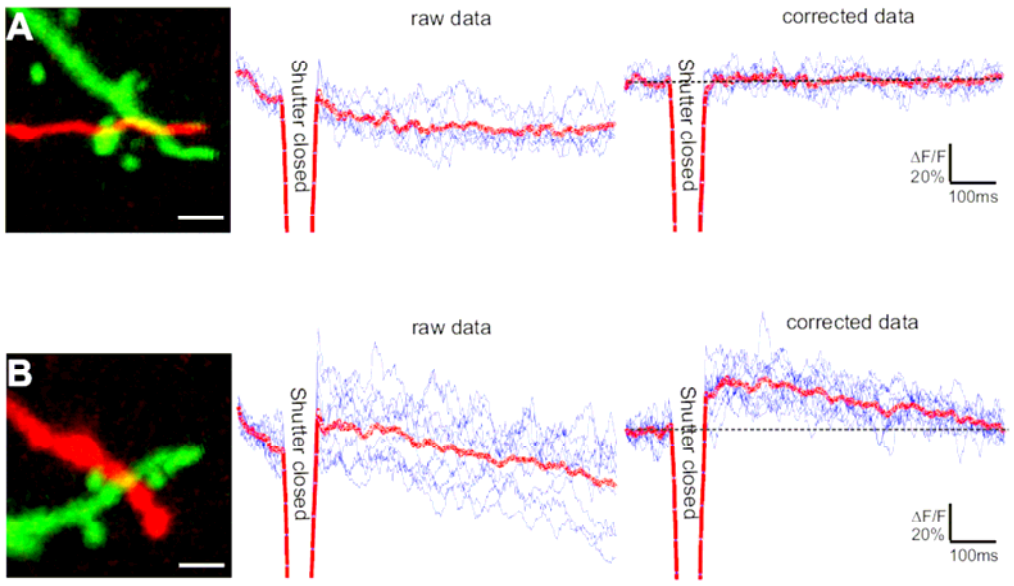

Figure 4.8. ***All-optical identification of functional synaptic contacts.***

A, C. *Two-photon laser microscopic imaging of two putative contacts between ChR2-RFP positive axons and ChR2/GAMP2 dendritic segments.* ***B.*** *GCaMP2 fluorescence changes tested on the putative contact in (A). Left: raw data. Right: bleach corrected data. No calcium signal was detected after light stimulation, indicating no functional synapse.* ***D.*** *GCaMP2 fluorescence changes tested on the putative contact in (C). Left: raw data. Right: bleach corrected data. Clear calcium signal was detected after light stimulation, indicating a functional synapse. Consecutive trials in blue and averaged trace in red.*

Discussion

Here we have introduced an all-optical method to identify closely associated presynaptic varicosities and postsynaptic spines *in situ* and verify putative synaptic contacts without the need for EM reconstruction. GCaMP2 was able to detect Ca^{2+} influx through NMDA receptors following paired synaptic stimulation. To control glutamate release and postsynaptic depolarization non-invasively, we expressed a light-sensitive cation channel (Channelrhodopsin-2) both pre- and post-synaptically. Functional synaptic contacts could therefore be verified precisely and uninvasively, making this all-optical method ideal for investigating synaptic plasticity at the level of single synapses.

In this study, we showed that morphologically associated axons and spines are not necessarily functional physical synaptic contacts. Using function calcium imaging using X-Rhod-5F or GCaMP2, we only found 7/39 functional physical synaptic contacts. Since the postsynaptic cell was depolarized during calcium imaging, even silent synapses that lack postsynaptic AMPA receptors should be revealed. Consist with our previous finding that release probability at ChR2-positive terminal is increased (Zhang and Oertner, 2007), once an active spine was found almost every stimulus evoked a transient rise in Ca^{2+}. Since individual axons were stimulated, our method will not produce false positives, i.e. postsynaptic Ca^{2+} signals in the absence of a functional synapses. Spill-over of glutamate can be safely excluded due to the wide spacing of axonal boutons (~10 μm) (Harris and Sultan, 1995).

However, it is possible that we failed to detect functional synapses in some cases (false negatives). There are two possibilities: failure of firing in the axon, or failure of deporlization in the postsynaptic cell. A key requirement for NMDAR-mediated Ca^{2+} influx is sufficient depolarization of the postsynaptic membrane. In our case, it depends on light intensity and expression level of ChR2 in the postsynaptic cell. As a positive control for postsynaptic depolarization, we monitored GCaMP2 fluorescence changes in the apical dendrite in response to a 200 ms light pulse (Fig 4.7). In our study, we only used strongly ChR2 expressing cells. Such a light pulse triggers a burst of APs, accompanied by a calcium influx that is readily detected by GCaMP2 (Fig 4.7). The second possibility, failure of AP in the axon, we cannot exclude at this

point. But the combination of ChR2 and GCaMP2 in presynaptic cell may offer a convenient tool to test the spikes in the axonal terminals.

The potential result of false negatives was with standing. This is the first technique that enables the observation of identified active synapses over extentially unlimited time periods. One possible effect of overexpressing GCaMP2 in the neurons should be kept in mind while interpreting the results. GCaMP2 is an exogenous calcium buffer protein. Changes in calcium concentrations could affect synaptic plasticity (Neveu and Zucker, 1996). There is now much evidence to suggest that when neuronal activity strays from a normal physiological range, synaptic gain can be altered to regain normal activity (reviewed by Burrone and Murthy, 2003). In fact, there appears to be multiple ways to alter synaptic gain in the direction of homeostasis, including changes in pre- and postsynaptic properties, and in the number of synapses (Burrone et al., 2002; Desai et al., 2002; Heynen et al., 2003; Hartman et al., 2006). It remains to be determined if these changes occur in GCaMP2 overexpressing cells. In summary, the method presented here enables to verify functional synaptic contacts in the intact tissue. Since the visually identified synapses are unpertured, activity induced changes should be possible to be studied with no time limitation.

Materials and Methods

Plasmid construction. The red labeled ChR2 construct used in this study have been previously described. The twol-promoter vector containing ChR2 and GCaMP2 was constructed as follows: ChR2-YFP, a gift from Dr. K. Deisseroth, was modified by inserting a stop codon (TAG) after amino acid 309 by PCR and inserted into a neuron-specific expression vector (synapsin-1 promoter vector). The fragment of syn1-ChR2-SV40-polyA was then excised and inserted into a second expression vector containing syn1-GCaMP2, a genetically encoded Ca^{2+} indicator (from Dr. Junichi Nakai). The encoding sequence of cyan fluorescent protein (CFP, from Dr. Oliver Griesbeck) was subcloned into synapsin-1 promoter vector. All constructs were verified by DNA sequencing, amplified and purified using MaxiPrep Kits (Qiagen).

Slice culture and transfection. Organotypic hippocampal slices were prepared from Wistar rats at postnatal day 5 as described (Stoppini et al., 1991), in accordance with the animal care and use guidelines of the Veterinary Department Basel-Stadt. After 7 days in vitro, cultures were double transfected with syn1-ChR2-syn1-GCaMP2 and syn1-ChR2-RFP or syn1-CFP and syn1-ChR2-RFP, using a Helios Gene Gun (BioRad). All experiments were performed 2-3 weeks after transfection. Retinal (1 μM, Sigma) was added to the culture medium, but not to the recording solution.

Electrophysiology. Hippocampal slice cultures were placed in the recording chamber of the microscope and superfused with artificial cerebrospinal fluid (ACSF) containing (in mM): 119 NaCl, 2.5 KCl, 4 $CaCl_2$, 4 $MgCl_2$, 26.2 $NaHCO_3$, 1 NaH_2PO_4, 11 glucose. The solution was gassed with 95% O_2, 5% CO_2, pH was adjusted to 7.2. Single whole-cell recordings were performed using an Axopatch 200B amplifier (Axon Instruments). The recording pipettes (4.5 - 5.5 MΩ) were filled with intracellular solution containing (in mM): 135 K-gluconate, 10 HEPES, 4 $MgCl_2$, 4 Na_2-ATP, 0.4 Na_2-GTP, 10 Na_2-phosphocreatine, 3 ascorbate, 0.15 X-Rhod-5F, pH was adjusted to 7.2. For voltage clamp experiments, intracellular K^+ was replaced by Cs^+. Synaptic responses were evoked using either blue light (470nm, 10ms) or monopolar electrodes in ~10 μm lateral to the imaging dendrite. All recordings were performed at 30°C.

Light stimulation and 2-photon imaging. The 2-photon imaging and light stimulation setup was based on a Olympus BX51WI microscope equipped with a LUMFL 60× 1.1 NA objective, controlled by a free software package (Pologruto et al., 2003) written in Matlab (The MathWorks). An ultrafast IR laser (Chameleon-XR, Coherent) controlled by electro-optic modulators (350-80, Conoptics) was used for imaging. A blue LED (470 nm, Cairn Research Ltd.) was coupled into the epifluorescence pathway to deliver light pulses for ChR2 activation. Two PMTs (R3896, Hamamatsu) below a 1.4 NA oil immersion condenser were used to detect red and green emission. During the blue light pulse, they were protected by a VS25 shutter (Vincent Associates). To combine the blue light used for stimulation with the IR laser, we used a 470/40 bandpass and 725DCXR dichoic mirror (Chroma).

Synapse Checker. Putative synaptic contacts were automatically identified using a program (ContactChecker) written in Matlab. The detection of green and red fluorescence in the same voxel indicates a putative synaptic contact. Green and red signal were multiplied pixel by pixel after median filtering, subtraction of background fluorescence and optical crosstalk. The resulting 3D dataset (R&G) was smoothed using a Gaussian kernel. The xyz coordinates of local maxima, indicating points of contact, were listed in descending order. The resulting list of potential synapses was then sequentially tested at high magnification for postsynaptic calcium signals.

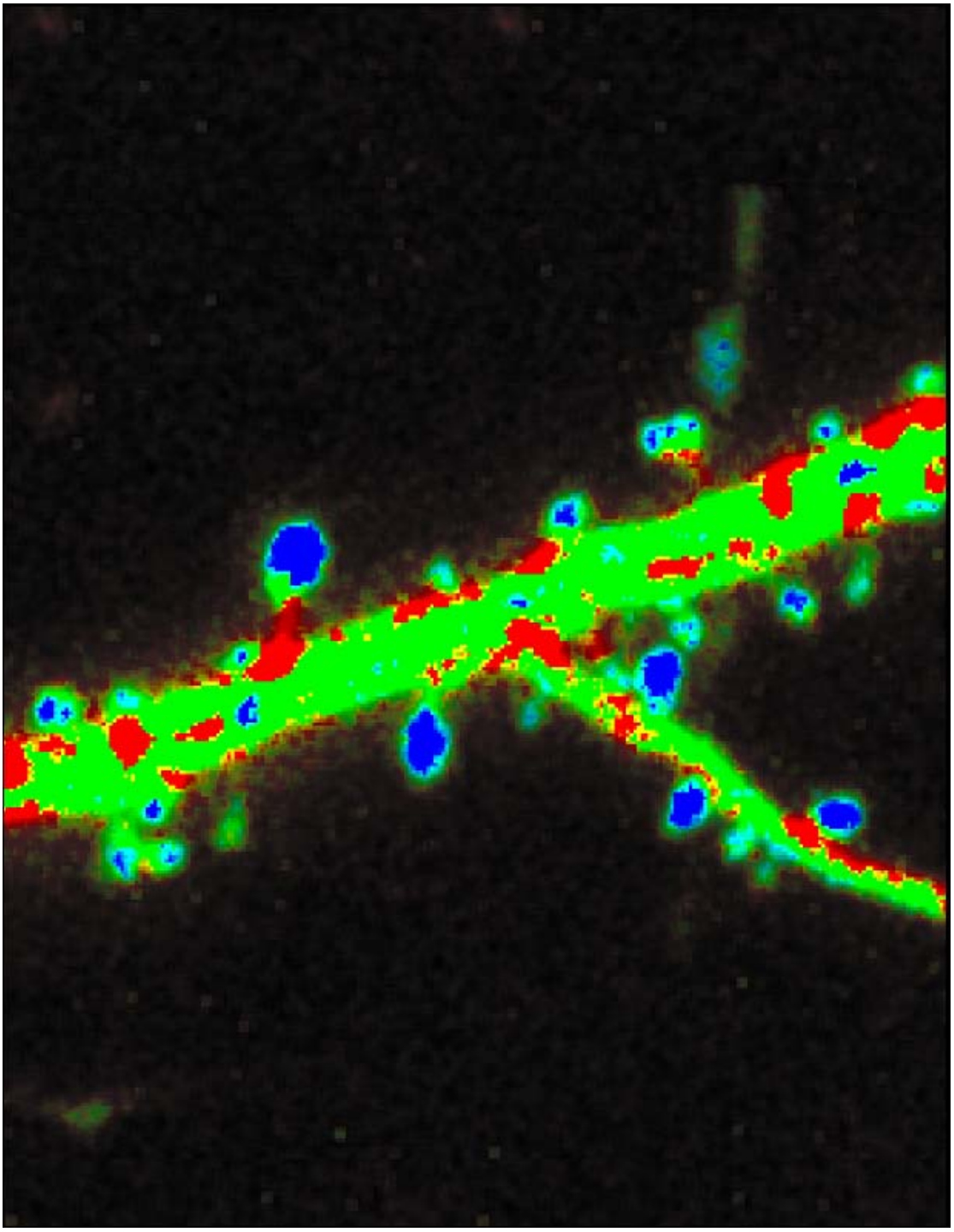

Chapter 5. Differential Compartmentalization and Distinct Functions of $GABA_B$ Receptor Variants

Réjan Vigot[1], Samuel Barbieri[1] , Hans Bräuner-Osborne[1, 2], Rostislav Turecek[1, 3], Ryuichi Shigemoto[4, 5], Yan-Ping Zhang[6], Rafael Luján[4, 5, 7], Laura H. Jacobson[8], Barbara Biermann[1], Jean-Marc Fritschy[9], Claire-Marie Vacher[1], Matthias Müller[8], Gilles Sansig[8], Nicole Guetg[1], John F. Cryan[8, 12], Klemens Kaupmann[8], Martin Gassmann[1], Thomas G. Oertner[6] and Bernhard Bettler[1]

1. Department of Clinical-Biological Sciences, Institute of Physiology, Pharmazentrum, University of Basel, CH-4056 Basel, Switzerland

2. Department of Medicinal Chemistry, Danish University of Pharmaceutical Sciences, DK-2100 Copenhagen, Denmark

3. Institute of Experimental Medicine, Academy of Sciences, 142 20 Prague, Czech Republic

4. Division of Cerebral Structure, National Institute for Physiological Sciences, Myodaiji, Okazaki 444-8585, Japan

5. CREST, Japan Science and Technology Corporation, Kawaguchi 332-0012, Japan

6. Friedrich Miescher Institute, CH-4058 Basel, Switzerland

7. Department Ciencias Médicas, Facultad de Medicina-CRIB, Universidad de Castilla-La Mancha, 02006 Albacete, Spain

8. Novartis Institutes for BioMedical Research, Novartis Pharma AG, CH-4002 Basel, Switzerland

9. Institute of Pharmacology and Toxicology, University of Zurich, CH-8057 Zurich, Switzerland

Neuron. 2006 May 18:50 (4):581-601

Summary

$GABA_B$ receptors are the G protein-coupled receptors for the main inhibitory neurotransmitter in the brain, γ-aminobutyric acid (GABA). Molecular diversity in the $GABA_B$ system arises from the $GABA_{B1a}$ and $GABA_{B1b}$ subunit isoforms that solely differ in their ectodomains by a pair of sushi repeats that is unique to $GABA_{B1a}$. Using a combined genetic, physiological, and morphological approach, we now demonstrate that $GABA_{B1}$ isoforms localize to distinct synaptic sites and convey separate functions

in vivo. At hippocampal CA3-to-CA1 synapses, $GABA_{B1a}$ assembles heteroreceptors inhibiting glutamate release, while predominantly $GABA_{B1b}$ mediates postsynaptic inhibition. Electron microscopy reveals a synaptic distribution of $GABA_{B1}$ isoforms that agrees with the observed functional differences. Transfected CA3 neurons selectively express $GABA_{B1a}$ in distal axons, suggesting that the sushi repeats, a conserved protein interaction motif, specify heteroreceptor localization. The constitutive absence of $GABA_{B1a}$ but not $GABA_{B1b}$ results in impaired synaptic plasticity and hippocampus-dependent memory, emphasizing molecular differences in synaptic $GABA_B$ functions.

Introduction

$GABA_B$ receptors are considered promising drug targets for the treatment of neurological and mental health disorders (Bettler et al., 2004; Cryan and Kaupmann, 2005). Presynaptic $GABA_B$ receptors are subdivided into auto- and heteroreceptors that control the release of GABA and other neurotransmitters, respectively. They restrict neurotransmitter release either by inhibiting voltage-sensitive Ca^{2+} channels or through a direct modulation of synaptic vesicle priming (Mintz and Bean, 1993; Poncer et al., 1997; Sakaba and Neher, 2003). Postsynaptic $GABA_B$ receptors induce slow inhibitory potentials by gating Kir3-type K^+ channels (Luscher et al., 1997). Considerable evidence has accumulated over the years, using a variety of preparations and techniques, to support the notion that multiple subtypes of $GABA_B$ receptors exist (Bonanno and Raiteri, 1993; Gemignani et al., 1994; Cunningham and Enna, 1996; Deisz et al., 1997; Mohler and Fritschy, 1999; Pozza et al., 1999; Yamada et al., 1999; Bowery et al., 2002; Lei and McBain, 2003). The predicted receptor heterogeneity is not readily supported by molecular studies (Bettler et al., 2004). $GABA_B$ receptors are heterodimers composed of $GABA_{B1}$ and $GABA_{B2}$ subunits, which are both required for normal receptor functioning (Marshall et al., 1999; Mohler and Fritschy, 1999). Accordingly, mice lacking $GABA_{B1}$ (referred to as $1^{-/-}$ mice) or $GABA_{B2}$ subunits show a complete absence of typical $GABA_B$ responses (Prosser et al., 2001; Schuler et al., 2001; Gassmann et al., 2004). The only firmly established molecular diversity in the $GABA_B$ system arises from the $GABA_{B1a}$ and $GABA_{B1b}$ subunit isoforms (Kaupmann et al., 1997). However, no unique pharmacological or functional properties could be assigned to $GABA_{B1a}$ or $GABA_{B1b}$. Most, if not all neurons

coexpress $GABA_{B1a}$ and $GABA_{B1b}$, which are generated by differential promoter usage from the $GABA_{B1}$ gene (Bischoff et al., 1999; Steiger et al., 2004). $GABA_{B1a}$ and $GABA_{B1b}$ expression levels vary during development and across individual cells, suggestive of a functional specialization. Structurally, the isoforms differ in their N-terminal ectodomain by a pair of sushi repeats that is present in $GABA_{B1a}$ but not in $GABA_{B1b}$ (Blein et al., 2004). Sushi repeats, also known as complement control protein modules, or short consensus repeats, are found in other G protein-coupled receptors as well (Grace et al., 2004) and mediate protein interactions in a wide variety of adhesion proteins (Lehtinen et al., 2004). The presence of sushi repeats in $GABA_{B1a}$, together with the absence of functional or pharmacological differences in vitro, suggested the existence of auxiliary proteins that modify receptor activity, pharmacology, and localization (Marshall et al., 1999; Mohler and Fritschy, 1999), precedence for which is found with other G protein-coupled receptors (McLatchie et al., 1998). So far, the lack of selective reagents has not allowed addressing the individual contributions of $GABA_{B1a}$ and $GABA_{B1b}$ to native $GABA_B$ functions. In the light of the proposed heterogeneity of native $GABA_B$ receptors, it therefore remains a key question whether $GABA_{B1}$ isoforms exhibit pharmacological and/or functional differences in vivo. Here, we have taken a genetic approach to dissociate the native functions of $GABA_{B1a}$ and $GABA_{B1b}$.

Results

Generation of Mice Selectively Expressing $GABA_{B1a}$ or $GABA_{B1b}$ Subunits

To selectively prevent translation of the $GABA_{B1a}$ and $GABA_{B1b}$ proteins, we converted their initiation codons in the $GABA_{B1}$ gene into stop codons (Figure 5.1). Balb/c gene targeting constructs with mutated initiation codons (Figure 5.1A) were electroporated into Balb/c embryonic stem cells (Dinkel et al., 1999) and homologous recombination events diagnosed with short-arm PCR and Southern blots (data not shown). Targeted embryonic stem cells were injected into C57BL/6 blastocysts. Founder mice were crossed with Balb/c mice expressing Cre-recombinase under control of the cytomegalus virus promoter to excise the neomycin cassette. Pups born from these matings were scored for Cre-mediated loss of the neomycin cassette and bred to homozygosity. Consequently, all mutant mice were on a pure inbred Balb/c

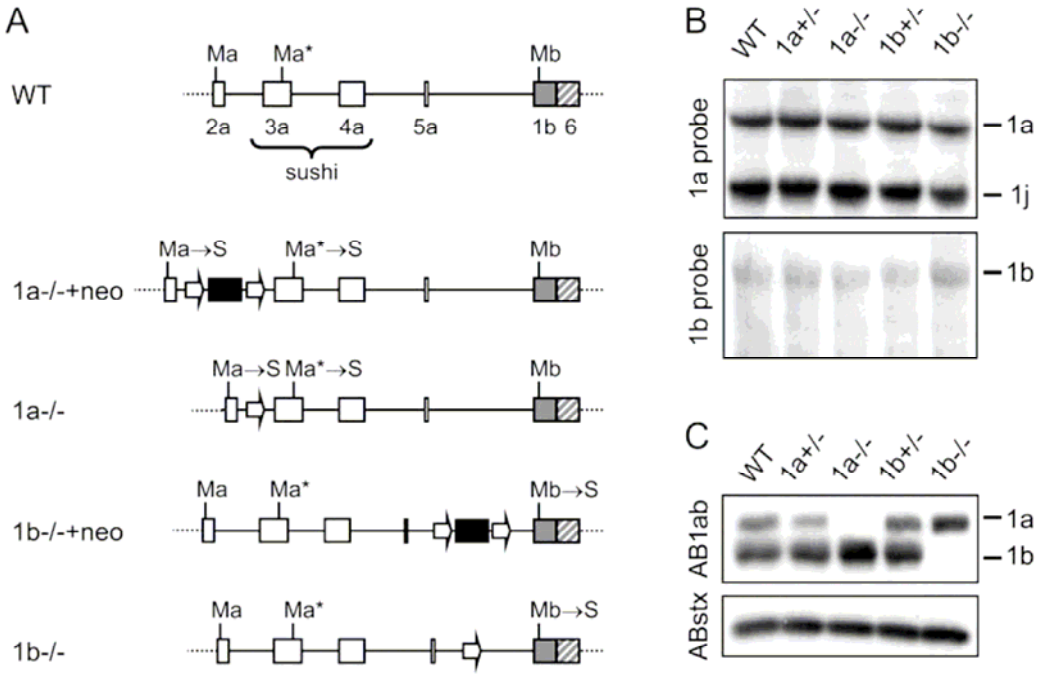

Figure 5.1. ***Generation of $1a^{-/-}$ and $1b^{-/-}$ Mice.***

(A) *5' region of wild-type (WT) (Martin et al., 2001) and mutated $GABA_{B1}$ alleles. Exons encoding the N terminus of $GABA_{B1a}$ are represented by white boxes and specify the signal peptide (exon 2a), a pair of sushi repeats of 75 amino acids each (exons 3a, 4a), and a linker of six amino acids (exon 5a). The exon specifying the N terminus of $GABA_{B1b}$ is represented by a gray box. All exons downstream of exon 1b are shared between the two isoforms (only exon 6 is shown; hatched box). Start codons for $GABA_{B1a}$ (Ma) and $GABA_{B1b}$ (Mb) transcripts were converted into stop codons (S) using a knockin approach. A putative alternative start site (Ma*) in $GABA_{B1a}$ transcripts was mutated in addition. The floxed neomycin cassette (black bar) for selection of transfected embryonic stemcells was introduced in the introns between exons 2a/3a ($1a^{-/-}$ neo) or exons 5a/1b ($1b^{-/-}$ neo). A loxP site (arrow) is left behind after Cremediated excision of the neomycin cassette ($1a^{-/-}$, $1b^{-/-}$).* ***(B)*** *Northern blot analysis of $GABA_{B1a}$ and $GABA_{B1b}$ mRNA expression in the brain of WT, heterozygous (+/-), and homozygous (-/-) knockout mice. The 1a hybridization probe (1aprobe) corresponds to nucleotides 1–405 of the $GABA_{B1a}$ cDNA (Kaupmann et al., 1997) and detects $GABA_{B1a}$ as well as a truncated $GABA_{B1j}$ transcript (M.G., unpublished data) of ~ 1.6 kb (upper panel). The 1b probe corresponds to nucleotides 16–259 of the $GABA_{B1b}$ cDNA (Kaupmann et al., 1997) and detects 1b transcripts (lower panel).* ***(C)*** *Immunoblot analysis of total brain lysates using antibodies recognizing thecommonCterminus of$GABA_{B1a}$ and $GABA_{B1b}$ (AB1ab) (Gassmann et al., 2004). Anti-syntaxin (ABstx) antibodies control for sample loading.*

genetic background, which was maintained throughout the experiments. Homozygous mice with mutations in the $GABA_{B1a}$ (referred to as $1a^{-/-}$ mice) or $GABA_{B1b}$ ($1^{b-/-}$ mice) initiation codon were viable, reproduced normally, and exhibited no overt phenotypic abnormalities. Mutant mice showed normal levels of $GABA_{B1a}$ and $GABA_{B1b}$ mRNA, indicating that the genetic manipulations do not influence mRNA

expression or stability (Figure 5.1B). Immunoblot analysis revealed the total absence of $GABA_{B1a}$ and $GABA_{B1b}$ protein in $1a^{-/-}$ and $1b^{-/-}$ mice, respectively, confirming that mutation of the initiation codons prevents translation of the individual subunits (Figure 5.1C). $GABA_{B1a}$ and $GABA_{B1b}$ proteins appeared upregulated in total brain extracts of knockout mice (Figure 5.1C), possibly because of increased availability of complementary $GABA_{B2}$ protein, which is required for cross-stabilization (Gassmann et al., 2004). We analyzed whether $GABA_B$ protein is also upregulated in the CA1 region of the hippocampus, where the electrophysiological and morphological studies described below were carried out. Similar to those seen in total brain extracts, $GABA_{B1a}$ and $GABA_{B1b}$ protein levels in CA1 extracts were increased in the $1b^{-/-}$ (129% of wild-type) and $1a^{-/-}$ mice (115% of wild-type), respectively.

Immunohistochemical, Pharmacological, and Biochemical Characterization of $1a^{-/-}$ and $1b^{-/-}$ Mice

Immunohistochemistry in the CA1 and CA3 region of the hippocampus revealed completely overlapping expression patterns for the $GABA_{B1a}$ and $GABA_{B1b}$ proteins (Figure 5.2), consistent with an ubiquitous expression of the two proteins in brain neurons (Bischoff et al., 1999). The regional immunostaining in $1a^{-/-}$ and wild-type mice was similar, while the staining in $1b^{-/-}$ mice was more diffuse and lacked distinct laminar boundaries. Immunohistochemistry therefore suggests differences in the relative abundance of the two isoform proteins at different subcellular sites. For example, intense immunoreactivity is evident in CA3 stratum lucidum of $1b^{-/-}$ mice, which may hint at a preferential expression of $GABA_{B1a}$ protein at presynaptic sites (arrowhead in Figure 5.2). The immunostainings obtained with antibodies directed at the $GABA_{B1}$ and $GABA_{B2}$ proteins are similar in the different strains of mice, suggesting that most of the $GABA_{B2}$ and $GABA_{B1}$ protein assembles into heterodimeric receptors. To compare the pharmacology of $GABA_{B1a}$ and $GABA_{B1b}$ in native tissue, we analyzed the inhibition of [^{125}I]CGP64213 antagonist binding (Kaupmann et al., 1997) by GABA and L-baclofen in cortical membranes (Figure 5.3A). In agreement with recombinant data (Kaupmann et al., 1998), the inhibition curves for wild-type, $1a^{-/-}$, and $1b^{-/-}$ mice were almost identical (IC_{50} values for

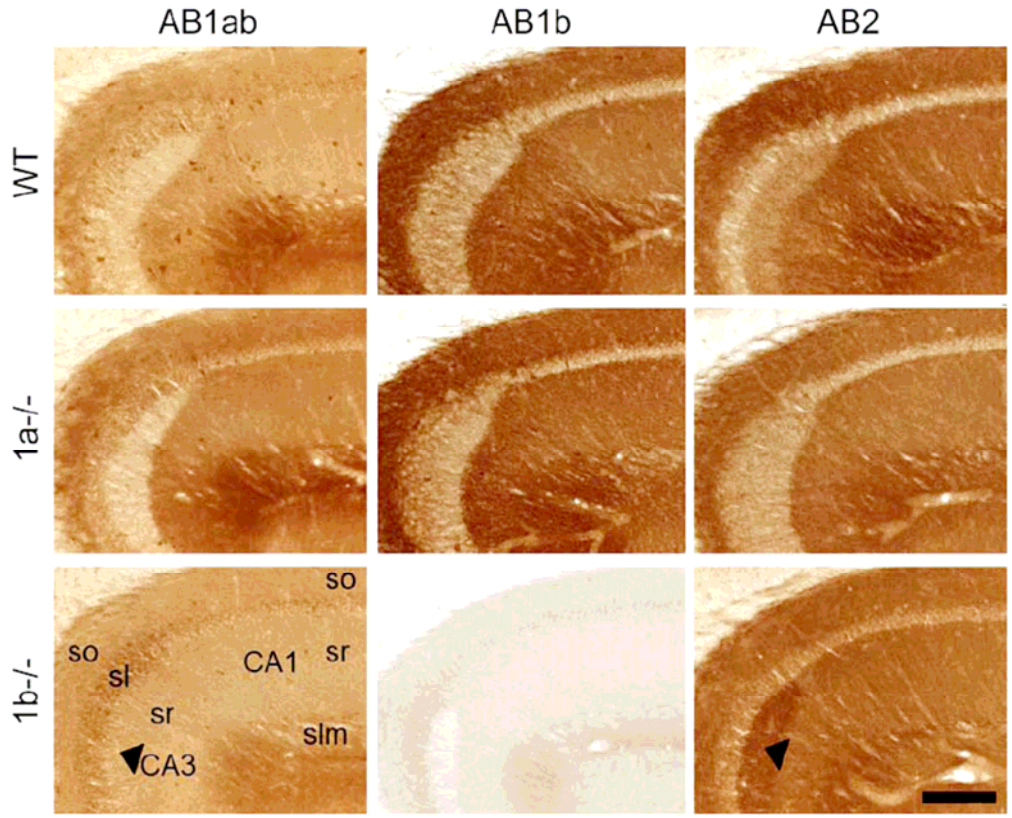

Figure 5.2. ***Distribution of $GABA_{B1a}$ and $GABA_{B1b}$ Protein in the Hippocampus of $1a^{-/-}$ and $1b^{-/-}$ mice.***

Immunohistochemistry in the CA1/CA3 region using antibodies specific for $GABA_{B1}$ (AB1ab, recognizing an epitope shared by $GABA_{B1a}$ and $GABA_{B1b}$), $GABA_{B1b}$ (AB1b), and $GABA_{B2}$ (AB2). No $GABA_{B1a}$-specific antibody suitable for immunohistochemistry is available. The expression pattern of $GABA_{B1a}$ protein is revealed in $1b^{-/-}$ mice stained with AB1ab. No specific immunostaining is observed with AB1b in $1b^{-/-}$ mice, demonstrating the specificity of this antibody for $GABA_{B1b}$ protein. No specific immunostaining was obtained in control experiments with AB1ab/AB1b and AB2 antibodies in mice devoid of $GABA_{B1}$ and $GABA_{B2}$ subunits, respectively (Fritschy et al., 2004). Abbreviations: so, stratum oriens; sl, stratum lucidum; sr, stratum radiatum; slm, stratum lacunosum- moleculare. Scale bar, 200 μm. The WT mouse was a littermate of the $1a^{-/-}$ mouse.

wild-type, $1a^{-/-}$, and $1b^{-/-}$ mice in μM are as follows: GABA: 0.7 ± 0.2, 0.4 ± 0.2, 0.6 ± 0.2; baclofen: 1.2 ± 0.3, 0.8 ± 0.3, 0.9 ± 0.3; n = 3 per genotype). [^{3}H]baclofen binding in $1a^{-/-}$ and $1b^{-/-}$ cortical membranes was similarly reduced compared to wild-type membranes (Figure 5.3B), in agreement with the relative abundance of the two isoform proteins in the cortex (Kaupmann et al., 1997). To determine functional $GABA_B$ receptor levels, we measured GTPγ[^{35}S] binding, which assesses the activation of Gαi/o-type G proteins, the main effectors of $GABA_B$ receptors (Figure

5.3C). Cortical membranes of $1a^{-/-}$ and $1b^{-/-}$ mice showed 52% ± 4% and 28% ± 8% of the maximal GTPγ[^{35}S] binding seen with wild-type mice. The sum of the

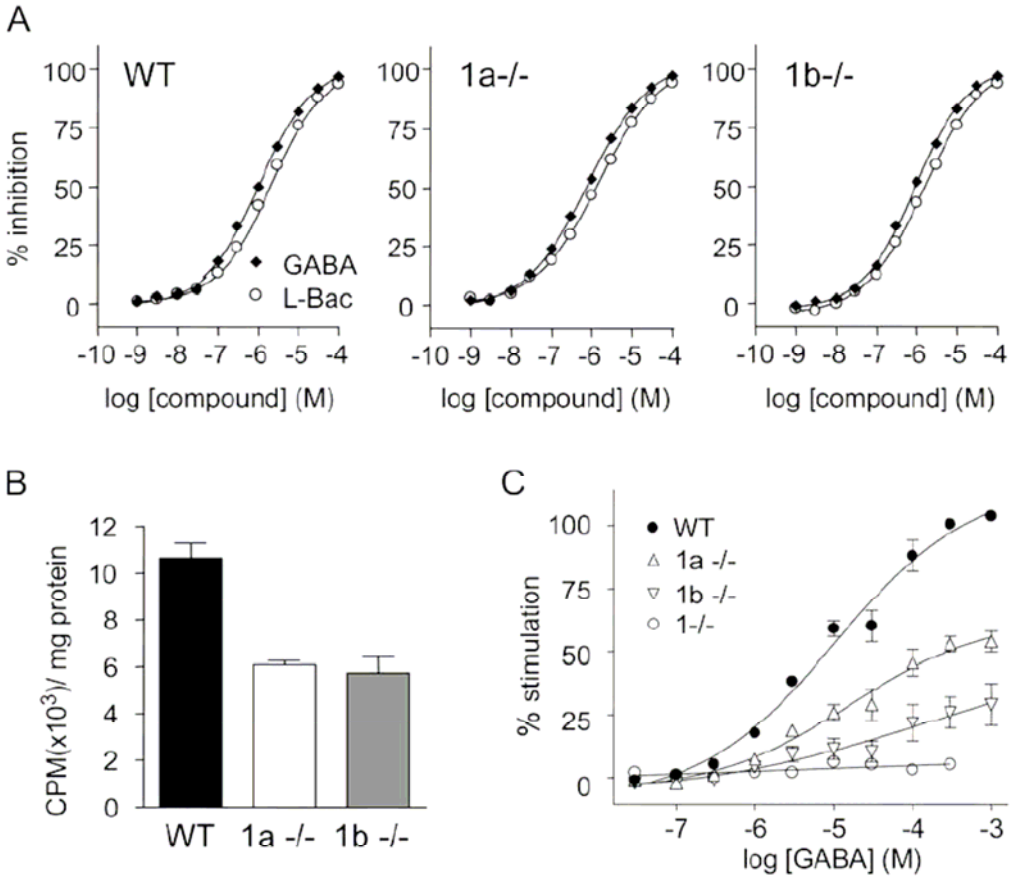

Figure 5.3. ***Pharmacological and Biochemical Analysis of Brain Membranes from Wild- Type, $1a^{-/-}$, and $1b^{-/-}$ Mice.***

(A) *Inhibition of [^{125}I]CGP64213 $GABA_B$ antagonist binding to cortical membranes by the agonists GABA and L-baclofen (L-Bac). The curves were fitted using nonlinear regression (Graph Pad PRISM program, Graph Pad software Inc., San Diego). Error bars (±SEM) are smaller than the symbols.* ***(B)*** *Binding of [^{3}H]baclofen to cortical membranes of $1a^{-/-}$ and $1b^{-/-}$ mice was 57% ± 2% and 50% ± 7%, respectively, of the binding to WT membranes (±SEM of two independent experiments performed in triplicate).* ***(C)*** *GABA-stimulated GTP_γ [^{35}S] binding in cortical membranes. Data points are mean (±SEM) values calculated from five (WT) and four ($1a^{-/-}$, $1b^{-/-}$, $1^{-/-}$) mice.*

maximal GTPγ[^{35}S] responses in knockout membranes is therefore 20% lower than expected. This suggests the absence of a compensatory upregulation of functional receptor levels, despite the upregulation of $GABA_{B1}$ isoforms seen at the protein level (Figure 5.1C). Presumably, most of the extra $GABA_{B1}$ isoform protein is retained intracellularly and does not participate in functional responses.

Distinct Contributions of $GABA_{B1a}$ and $GABA_{B1b}$ to Pre- and Postsynaptic GABAB Functions

Using whole-cell patch-clamp recording in slice preparations, we examined whether wild-type and knockout mice differ in their hippocampal $GABA_B$ responses. We first checked for the presence of heteroreceptors on excitatory terminals. Stimulation of the Schaffer collateral-commissural fibers induces excitatory postsynaptic currents (EPSCs) in CA1 pyramidal neurons, which are reduced by blocking glutamate release through activation of $GABA_B$ heteroreceptors (Schuler et al., 2001). Baclofen, a $GABA_B$ agonist, was effective in reducing the EPSC amplitude in wild-type and $1b^{-/-}$ mice but not in $1a^{-/-}$ mice (Figures 5.4A and 5.4B). As a control, adenosine inhibited glutamate release in all three genotypes. This indicates that $1a^{-/-}$ mice, in contrast to $1b^{-/-}$ mice, lack $GABA_B$ heteroreceptors on Schaffer collateral terminals. Small residual heteroreceptor activity in $1a^{-/-}$ mice suggests that minute amounts of $GABA_B$ receptors assembled with $GABA_{B1b}$ are localized at glutamatergic terminals. We next looked for the presence of autoreceptors on GABAergic terminals and recorded inhibitory postsynaptic currents (IPSCs) in the presence of the ionotropic glutamate receptor antagonist kynurenate. Baclofen reduced the amplitude of IPSCs in CA1 pyramidal neurons of all genotypes, suggesting that both $GABA_{B1a}$ and $GABA_{B1b}$ can efficiently participate in autoreceptor function (Figures 5.4C and 5.4D). Postsynaptic $GABA_B$ receptors induce a late IPSC by activating Kir3-type K^+ channels (Luscher et al., 1997). At a holding potential of −50 mV and in physiological extracellular $[K^+]$, baclofen elicited similar outward currents in CA1 pyramidal cells of $1a^{-/-}$ and wild-type mice (Figures 5.4E and 5.4F). However, in CA1 pyramidal cells of $1b^{-/-}$ mice, the baclofen-induced outward current was reduced by ~60% compared to wild-type or $1a^{-/-}$ mice. This indicates that predominantly $GABA_{B1b}$ mediates postsynaptic inhibition. As a control, adenosine receptors, which converge on the same Kir3 channels (Luscher et al., 1997), induced similar outward currents in all genotypes. It is formally possible that the upregulation of $GABA_{B1a}$ protein observed in the $1b^{-/-}$ mice (Figure 5.1C) compensates to some extent for the missing $GABA_{B1b}$ protein. We consider this unlikely because functional receptor levels in the $1b^{-/-}$ mice are lower than expected (Figure 5.3C). Moreover, GFP-tagged $GABA_{B1a}$ protein clearly distributes to the dendritic

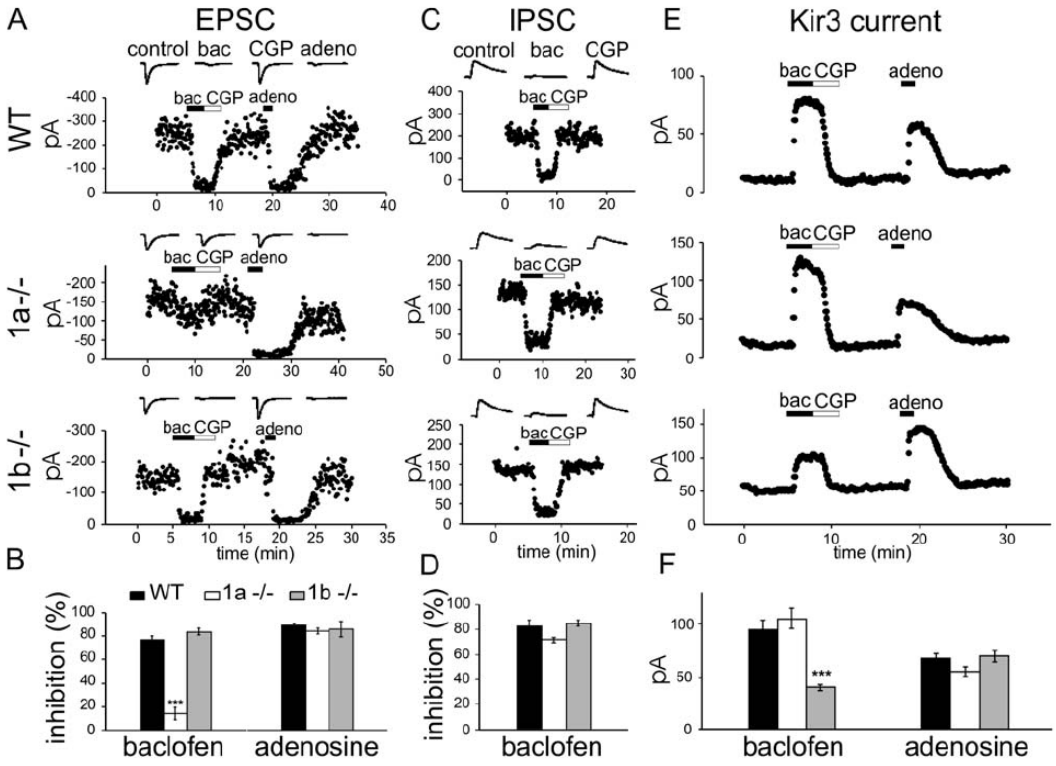

Figure 5.4. ***GABA$_B$ Responses in Wild-Type, 1a$^{-/-}$, and 1b$^{-/-}$ CA1 Pyramidal Neurons***

(A and B) *Peak amplitudes and representative traces (A) and summary histogram (B) of monosynaptic EPSC inhibition by baclofen and adenosine. Baclofen (50 μM) depresses the amplitude of EPSCs in WT (76.5% ± 3.1% inhibition; n = 8) and 1b$^{-/-}$ (83.4% ± 2.9% inhibition; n = 5) but not in 1a$^{-/-}$(15.9% ± 5.3% inhibition; n = 13; p < 0.001, ANOVA/Scheffe post hoc test) mice. Adenosine (100 μM) depresses EPSCs in all genotypes (WT: 89.1% ± 1.6% inhibition, n = 6; 1a$^{-/-}$: 85.3% ± 1.8% inhibition, n = 13; 1b$^{-/-}$: 85.6% ± 6.6% inhibition, n = 4).* ***(C and D)*** *Peak amplitudes and representative traces (C) and summary histogram (D) of IPSC inhibition by baclofen. Baclofen significantly depresses the IPSC amplitude in all genotypes (WT: 82.7% ± 4.8% inhibition, n = 12; 1a$^{-/-}$: 71.8% ± 2.3% inhibition, n = 9; 1b$^{-/-}$ mice: 85.7% ± 2.4% inhibition, n = 7).* ***(E and F)*** *Representative changes in the holding current of CA1 neurons following application of baclofen and adenosine (E) and summary histogram of the amplitude of baclofen- and adenosine-induced K$^+$ currents (F). The amplitude of the outward K$^+$ current induced by baclofen application is similar in 1a$^{-/-}$(99.3 ± 8.8 pA; n = 14) and WT (89.8 ± 7.7 pA; n = 16) neurons. In 1b$^{-/-}$ cells, the amplitude of the baclofen-induced current is strongly reduced (37.4 ± 2.7 pA; n = 10; p < 0.001, ANOVA/Scheffe post hoc test). Control adenosine-induced K$^+$ currents are similar in all genotypes. (Vclamp:-50 mV, TTX 1 μM, ***p < 0.001, ANOVA/Scheffe post hoc test). All baclofen-induced responses (inhibition of PSCs and activation of K$^+$ currents) were fully blocked by the GABA$_B$ antagonist CGP54626 (1 μM). Values are expressed as mean ± SEM.*

compartment of CA1 neurons when expressed in organotypic slice culture (Figure 5.6A). Likely, therefore, both $GABA_{B1a}$- and $GABA_{B1b}$-containing receptors address Kir3 channels under normal conditions.

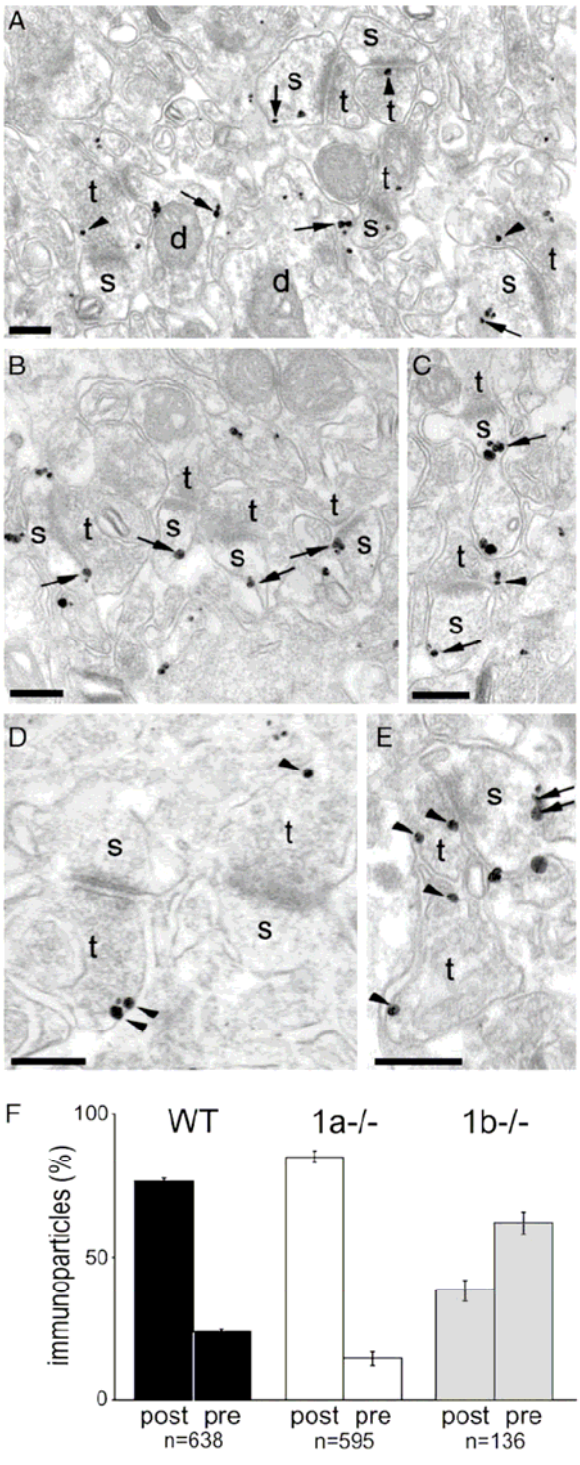

Figure 5.5. ***Preembedding Electron Micrographs Showing $GABA_{B1}$ Immunogold Labeling at Asymmetrical, i.e. Glutamatergic, Synapses in CA1 Stratum Radiatum***

(A) *Pre- and postsynaptic immunogold labeling in WT mice.* ***(B and C)*** *Predominant postsynaptic (B) and rare presynaptic (C) labelling (arrowhead) in $1a^{-/-}$ mice.* ***(D and E)*** *Predominant presynaptic (D) and less frequent postsynaptic (E) labeling in $1b^{-/-}$ mice.* ***(F)*** *Percentage of pre- and postsynaptic immunogold particles in WT, $1a^{-/-}$, and $1b^{-/-}$ mice (presynaptic: WT, 24% ± 1%; $1a^{-/-}$, 14% ± 3%; $1b^{-/-}$, 62% ± 4%; n = 3 for each genotype; mean ± SEM). Immunogold labeling was less frequent in $1b^{-/-}$ compared to $1a^{-/-}$ mice, which is reflected in the number of immunogold particles that were analyzed. Arrow: examples of immunogold particles in spines and dendritic shafts; arrowhead: examples of immunogold particles in presynaptic terminals. t, terminal; s, spine; d, dendrite; scale bars, 200 nm.*

Distinct Subcellular Compartmentalization of the GABAB1a and GABAB1b Proteins

The lack of suitable antibodies thus far prevented studying the distribution of $GABA_{B1}$ isoforms using electron microscopy. We now used the $1a^{-/-}$ and $1b^{-/-}$ mice

to determine the subcellular localization of $GABA_{B1b}$ and $GABA_{B1a}$ protein, respectively. Preembedding immunogold labeling experiments in the CA1 stratum radiatum of wild-type mice confirmed that $GABA_{B1}$ protein is present in pre- and postsynaptic elements (Figure 5.5A), as reported for rat brain (Kulik et al., 2003). In $1a^{-/-}$ mice, $GABA_{B1b}$ was mostly found in spines opposite glutamate release sites (Figures 5.5B and 5.5C). In $1b^{-/-}$ mice, $GABA_{B1a}$ predominantly localized to glutamatergic terminals (Figures 5.5D and 5.5E). Quantitative analysis of $GABA_{B1}$ labeling showed that the ratio of pre- to postsynaptic immunoparticles in wild-type, $1a^{-/-}$, and $1b^{-/-}$ mice was 0.31, 0.17, and 1.61, respectively (Figure 5.5F). Thus, the electron microscopy data support the electrophysiological data (Figure 5.4) and confirm that $GABA_{B1a}$ preferentially localizes to glutamatergic terminals. Consistent with residual heteroreceptor activity (Figures 5.4A and 5.4B), some presynaptic immunogold labeling persisted at glutamatergic $1a^{-/-}$ synapses.

Selective Localization of $GABA_{B1a}$ to Axons and $GABA_{B1b}$ to Dendritic Spines in Transfected Hippocampal Neurons

We analyzed whether GFP-tagged $GABA_{B1a}$ and $GABA_{B1b}$ proteins exhibit a distinct subcellular distribution when expressed in hippocampal neurons. For these experiments, we transfected organotypic hippocampal slice cultures, which preserve the basic CA3-CA1 connectivity, with expression vectors coding for $GABA_{B1a}$-GFP or $GABA_{B1b}$-GFP. We coexpressed a freely diffusible red fluorescent protein (RFP), tdimer2, to normalize the green fluorescence to the red fluorescence. Both $GABA_{B1a}$-GFP and $GABA_{B1b}$-GFP proteins were robustly expressed in the dendrites of transfected CA1 pyramidal neurons (Figures 5.6A, 5.6B, and 5.6D). $GABA_{B1b}$-GFP was expressed in the majority of dendritic spines, while $GABA_{B1a}$-GFP was largely excluded from this location. This agrees with the electron microscopy data showing a preferential association of the $GABA_{B1b}$ protein with spines opposite to glutamate release sites (Figures 5.5B and 5.5C), a location where Kir3 channels are highly coclustered with $GABA_B$ receptors (Kulik et al., 2006). This may explain why predominantly $GABA_{B1b}$ mediates the activation of Kir3 currents

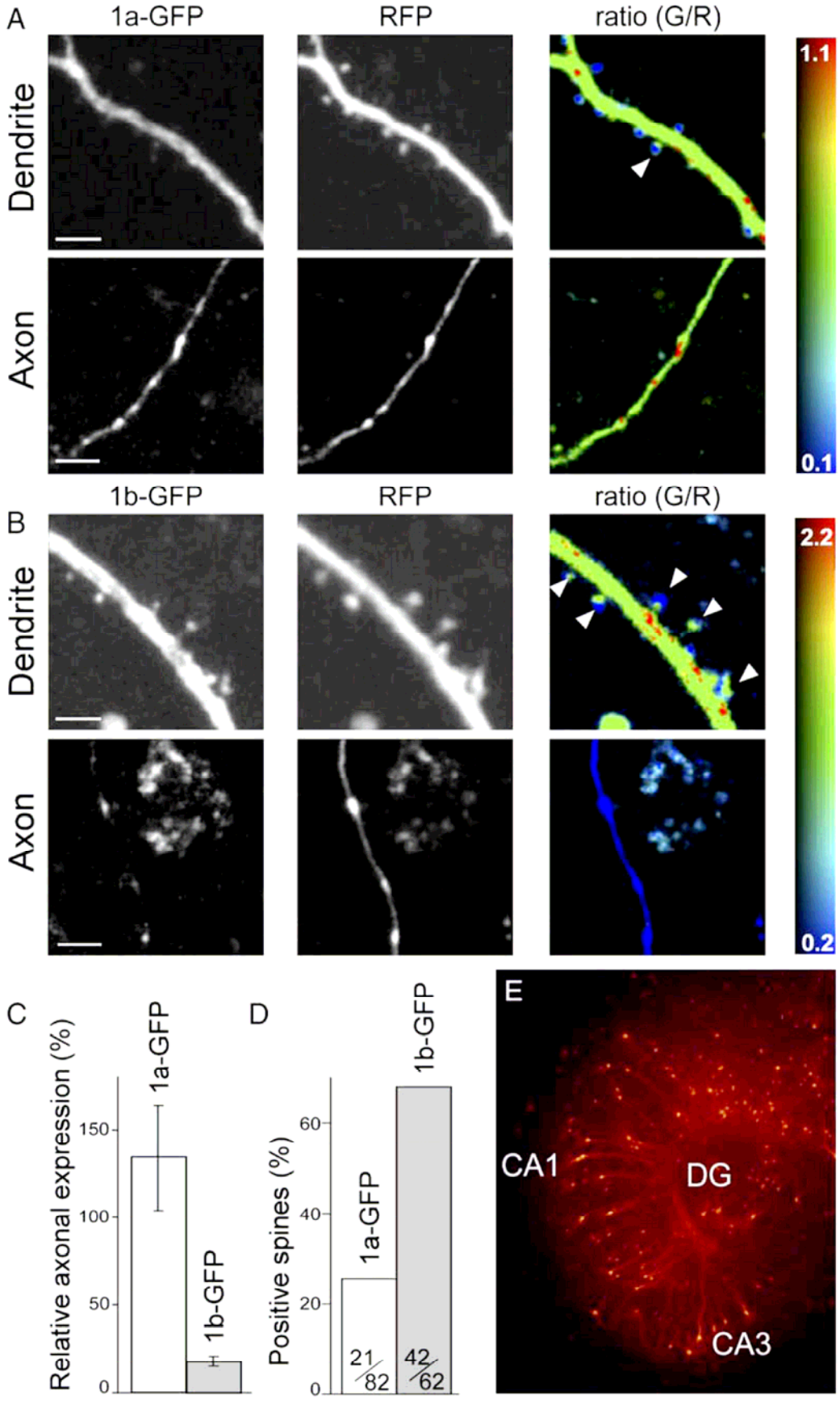

Figure 5.6. ***Expression of GFP-TaggedGABA$_{B1a}$ and GABA$_{B1b}$ Subunits in Organotypic Slice***

Culture

(A and B) *Maximum intensity projections of dendrites and axons in the CA1 region of the hippocampus expressing $GABA_{B1a}$-GFP (A) or $GABA_{B1b}$-GFP (B) in combination with the freely diffusible tdimer2 RFP are shown. The ratio of green-to-red fluorescence (G/R) is coded in rainbow colors. Scale bar, 5 μm.* ***(C)*** *Predominantly $GABA_{B1a}$-GFP protein is expressed in axons. The axonal expression level of $GABA_{B1a}$ and $GABA_{B1b}$ was normalized to the dendritic expression level ($GABA_{B1a}$: 133.84% ± 29.53%, n = 9; $GABA_{B1b}$: 18.01% ± 2.80%, n = 5; mean ± SEM).* ***(D)*** *$GABA_{B1b}$-GFP was expressed in the majority of dendritic spines, while $GABA_{B1a}$- GFP was excluded from most spines (spines positive for $GABA_{B1a}$-GFP: 21 of 82; spines positive for $GABA_{B1b}$-GFP: 42 of 62). Examples of positive spines are indicated by white arrowheads in the G/R ratio images in (A) and (B).* ***(E)*** *Example of an organotypic hippocampal slice culture 7 days after cotransfection of $GABA_{B1b}$-GFP and tdimer2 expression vectors.*

(Figures 5.4E and 5.4F). The data further indicate an almost exclusive association of the $GABA_{B1a}$-GFP protein with distal axons (Figure 5.6), again in agreement with the electrophysiological (Figures 5.4A and 5.4B) and morphological data (Figures 5.5D and 5.5E).

Impaired Synaptic Plasticity in $1a^{-/-}$ Mice

Activation of postsynaptic $GABA_B$ receptors was shown to restrict long-term potentiation (LTP), whereas activation of autoreceptors promotes LTP (Davies et al., 1991; Davies and Collingridge, 1996). A role for $GABA_B$ heteroreceptors in synaptic plasticity is not known. We therefore addressed whether the genetic loss of heteroreceptors in $1a^{-/-}$ mice affects LTP at CA3-to-CA1 synapses. In wild-type CA1 neurons, the pairing protocol induced a marked potentiation of the EPSC amplitude (268.9% ± 58.3%; n = 7) (Figures 5.7A and 5.7B). No LTP developed when NMDA receptors were antagonized (CPP + 7-Cl-kynurenic acid) or when the cell under recording was kept at −70 mV (Figure 5.7B). $1^{-/-}$ mice, which completely lack functional $GABA_B$ receptors (Schuler et al., 2001), did not exhibit notable LTP (9.4% ± 20.3%; n = 5), nor did $1a^{-/-}$ mice (−8.9% ± 9.3%; n = 9) (Figures 5.7A and 5.7B). In contrast, $1b^{-/-}$ mice exhibited normal LTP (228.7% ± 43.3%; n = 5). Wild-type neurons developed LTP even after acute pharmacological blockade of $GABA_B$ receptors with the antagonist CGP54626 (182.8% ± 54%; n = 6), showing that acute blockade of $GABA_B$ receptors does not prevent the induction of LTP. Adaptive changes (see below) due to the constitutive absence of heteroreceptors are therefore expected to underlie the lack of LTP in $1a^{-/-}$ neurons (Figure 5.7B).

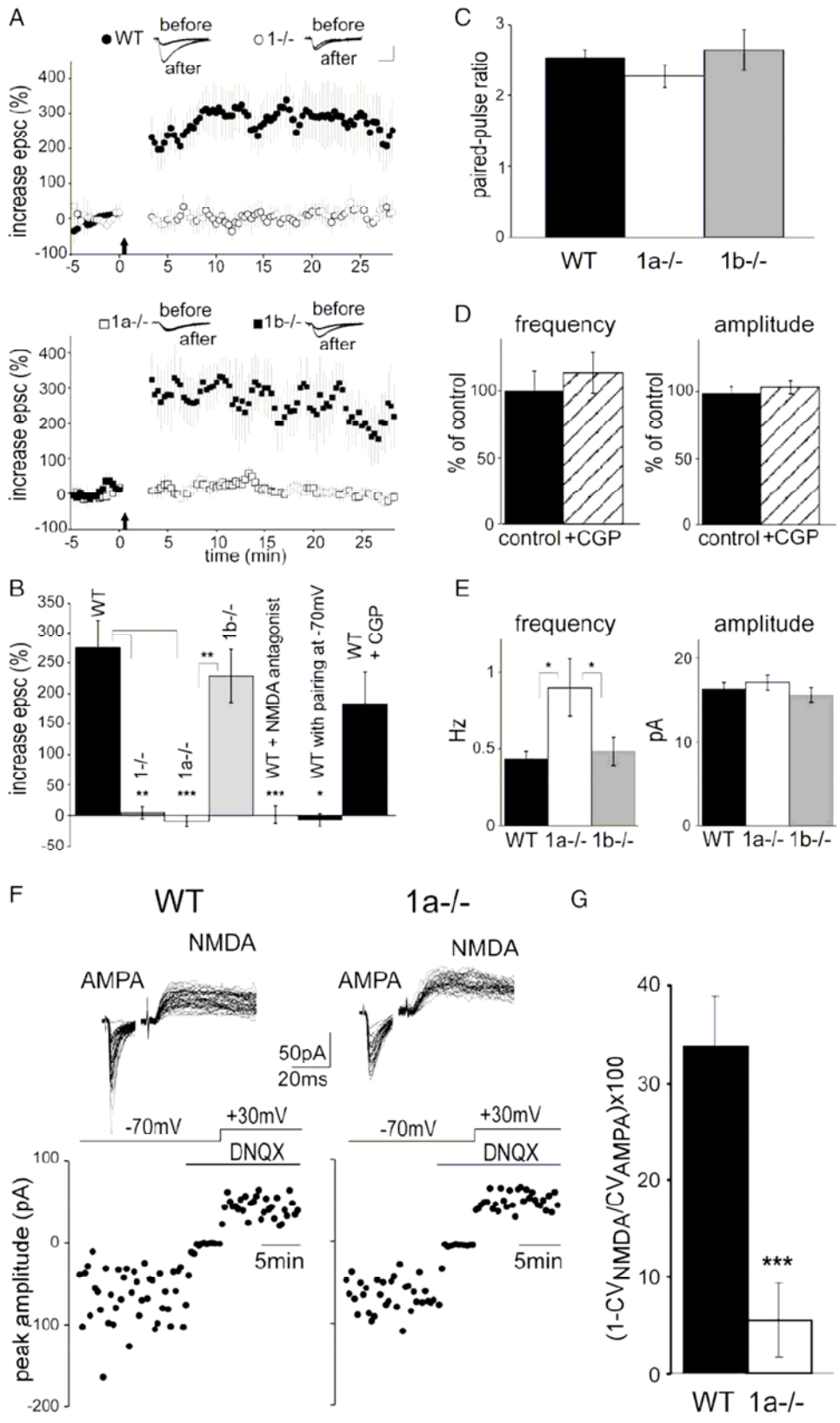

Figure 5.7. ***Lack of LTP and Reduction in the Proportion of Silent Synapses in 1a$^{-/-}$ Mice***

(A) *The pairing protocol fails to induce LTP in 1$^{-/-}$ and 1a$^{-/-}$ mice but induces a clear potentiation of the EPSC amplitude in WT and 1b$^{-/-}$ mice. Averages of the maximal EPSC amplitudes (±SEM) are shown.*

Figure 5.7. Continues

Pairing induction is indicated with an arrow. (Insets) Mean of 10 to 15 successive EPSCs recorded before and after pairing. Scale, 20 ms, 50 pA. ***(B)*** *Summary histogram of LTP experiments. The percent increase in EPSC amplitude after pairing is shown. Values for EPSC potentiation were assessed 25 min after induction. No LTP is induced in WT mice in the presenceof NMDA antagonists (5 μM R-CPP + 10 μM 7-Cl-kynurenate; WT + NMDA antagonist; $p < 0.001$ compared to WT, Student's t test) and in the absence of paradigm-associated depolarization (WT with pairing at -70 mV; $p < 0.05$ compared to WT, Student's t test). LTP is not significantly impaired in the presence of 1 mMCGP54626 (WT +CGP). The ANOVA/Scheffe post hoc test was used for the comparison of genotypes. For clarity, only the statistical significance between the genotypes linked by the brackets are shown (*$p < 0.05$; **$p < 0.01$; ***$p < 0.001$).* ***(C)*** *The pairedpulse ratio of EPSCs at CA3-to-CA1 synapses in WT (2.54 ± 0.11; n = 15), $1a^{-/-}$ (2.27 ± 0.16; n = 15) and $1b^{-/-}$ (2.64 ± 0.28; n = 8) mice was similar.* ***(D)*** *The $GABA_B$ antagonist CGP54626 (1 μM) did not alter mEPSC frequency (increase of 13.6% ± 15.3% versus control; n = 11) or amplitude (increase of 4.3% ± 5.1%; n = 11) inWTmice.* ***(E)*** *The frequency of mEPSCs was increased in $1a^{-/-}$ mice (WT: 0.44 ± 0.05 Hz, n = 11; $1a^{-/-}$: 0.90 ± 0.14 Hz, n = 15; $1b^{-/-}$: 0.49 ± 0.09 Hz, n = 8; $p < 0.05$, Student's t test). In contrast, the mEPSC amplitude did not differ between WT(16.39 ± 0.79 pA; n = 11), $1a^{-/-}$ (17.12 ± 0.78 pA; n = 18), and $1b^{-/-}$ (15.68 ± 0.88 pA; n = 8) mice.* ***(F)*** *Raw traces of AMPA and NMDA receptor-mediated EPSCs components (top). The protocol used to determine the CV_{AMPA} and CV_{NMDA} is outlined. At -70 mV, NMDA receptors are blocked byMg^{2+} ions, and the EPSCs are primarily mediated by AMPA receptors. NMDA receptor-mediated EPSCs were recorded in the same cell at +30 mV in the presence of 10 μM DNQX, a non-NMDA receptor antagonist.* ***(G)*** *The variability of the AMPA compared to the NMDA EPSC component (calculated as $[1-(CV_{NMDA}/CV_{AMPA})]\times100$) is significantly smaller in $1a^{-/-}$ than in WT mice (WT: 34.0 ± 5.0, n = 12; $1a^{-/-}$2: 5.6 ± 3.9, n = 10; $p < 0.01$, Student's t test), suggestive of a decreased proportion of silent synapses. WT mice were littermates of $1a^{-/-}$ mice. Data are represented as mean ± SEM.*

Synaptic Modifications in $1a^{-/-}$ Mice

The amplitude ratio of evoked EPSCs in response to paired-pulse stimulation was similar in wild-type, $1a^{-/-}$, and $1b^{-/-}$ CA1 pyramidal neurons (Figure 5.7C). A change in the paired-pulse ratio is generally believed to reflect an underlying change in the presynaptic probability of release. The absence of differences in the paired-pulse ratio between the three genotypes therefore provides no evidence for a change in the release probability in $1a^{-/-}$ mice. Moreover, these results indicate that the paired-pulse protocol does not result in the activation of $GABA_B$ heteroreceptors in wild-type neurons, nor do heteroreceptors appear to be tonically activated by ambient GABA, in agreement with earlier studies (Morrisett et al., 1991; Scanziani, 2000). CGP54626 had no effect on the miniature EPSC (mEPSC) frequency or amplitude in wild-type CA1 neurons, further supporting that ambient GABA does not tonically activate heteroreceptors under baseline conditions (Figure 5.7D). The frequency of spontaneous mEPSCs was significantly increased in $1a^{-/-}$ mice, while the mEPSC

amplitude remained similar as in wild-type or $1b^{-/-}$ mice (Figure 5.7E). The observed increase in the baseline mEPSC frequency in $1a^{-/-}$ mice would normally argue for an increase in the probability of glutamate release. However, since CA3-to-CA1 synapses in $1a^{-/-}$ mice exhibit no change in the paired-pulse ratio and heteroreceptors remain inactive under baseline conditions, we favor that the increase in mEPSC frequency is indicative of an increased number of functional synapses. An increase in mEPSC frequency, with a concomitant modest increase in mEPSC amplitude, has been observed in cultured hippocampal neurons as a consequence of the unmasking of "silent" synapses (Liao et al., 1999). The insertion of AMPA receptors into synapses that only contain NMDA receptors is expected to result in a decrease in the coefficient of variation (CV) of the AMPA receptor-mediated component of the EPSC (CV_{AMPA}), with no change in the CV of the NMDA component (CV_{NMDA}) (Kullmann, 1994). We measured the variability of the AMPA and NMDA receptor-mediated EPSC amplitudes recorded in the same cells at −70 mV and +30 mV, respectively (Figure 5.7F). We found that the CV_{AMPA} was significantly higher for the wild-type (0.37 ± 0.04; n = 12) than for the $1a^{-/-}$ mice (0.24 ± 0.03; n = 10; $p < 0.02$), while the CV_{NMDA} for wild-type (0.23 ± 0.02; n = 12) and $1a^{-/-}$ mice (0.22 ± 0.03; n = 10) was similar. Comparison of the CV_{AMPA} and CV_{NMDA} between $1a^{-/-}$ and wild-type mice is therefore consistent with a decreased proportion of silent synapses in $1a^{-/-}$ mice (Figure 5.7G).

Impaired Object Recognition in $1a^{-/-}$ Mice

Changes in hippocampal LTP accompany certain alterations in cognitive function (Barnes et al., 1994). We used an object recognition task that depends on hippocampal function (Broadbent et al., 2004) to analyze whether impaired presynaptic heteroreceptor inhibition and lack of LTP in $1a^{-/-}$ mice is paralleled by memory deficits. The task relies upon the tendency of rodents to attend to a novel object more than to a familiar one. For each mouse, we scored the number of stretch attend postures (SAP, defined as head and shoulders extended toward the object) in response to a PVC disc presented at times 10 min and 24 hr following initial presentation at time 0, as well as to a novel PVC cone at 24 hr + 10 min. Wild-type and $1b^{-/-}$ mice, in contrast to $1a^{-/-}$ mice, showed a significantly reduced number of SAPs toward the

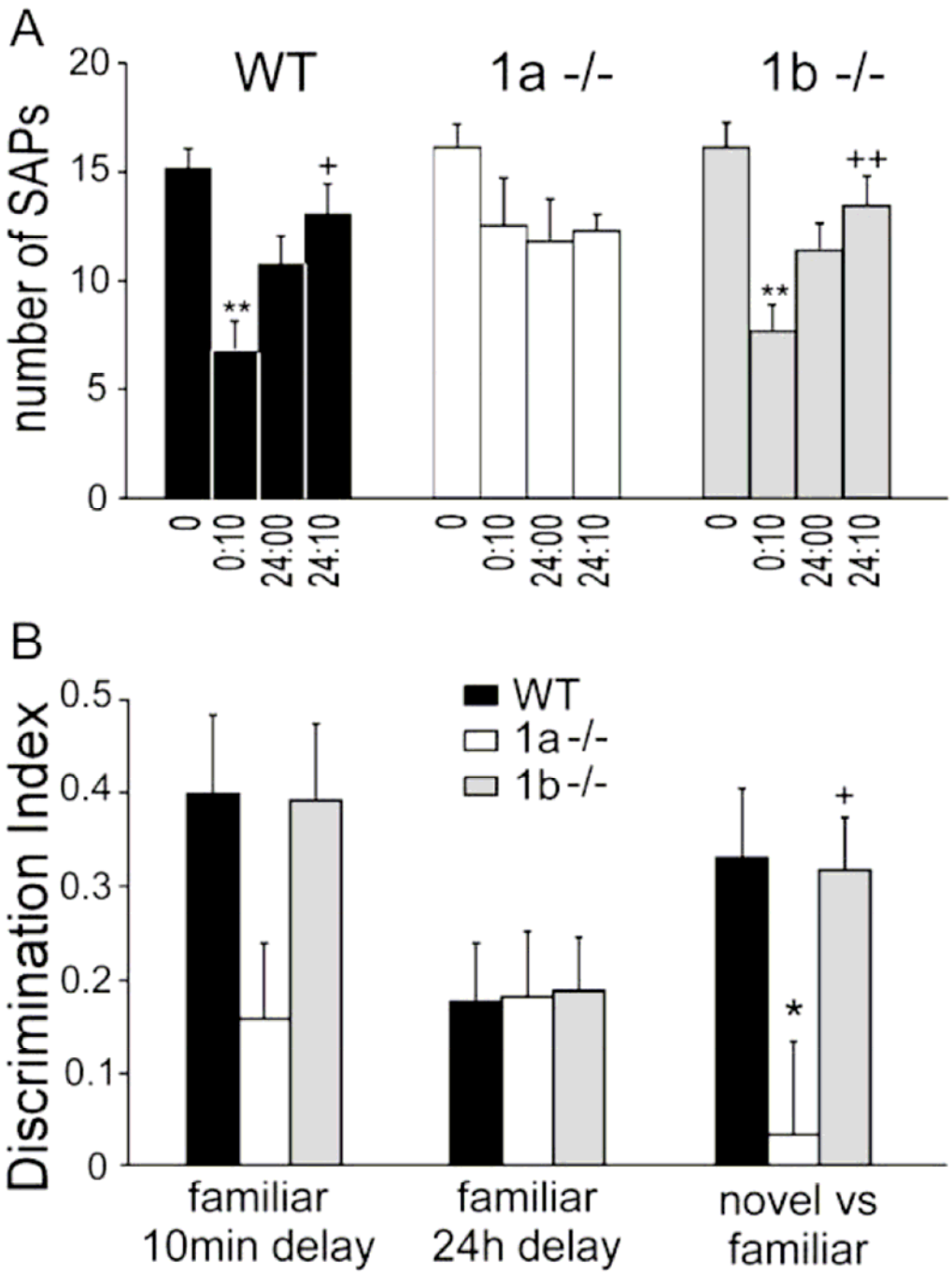

Figure 5.8. ***Impaired Object Recognition in 1a$^{-/-}$ Mice***

(A) *Data represent the number of SAPs (mean ± SEM) to a PVC disc presented at time 0 min (0), 10 min (0:10), and 24 hr (24:00), and to a novel PVC cone at 24 hr + 10 min (24:10). **p < 0.01 versus 0 min; +p < 0.05 versus 10 min; ++p < 0.01 versus 10 min. 1a$^{-/-}$ mice do not discriminate between familiar and novel objects (χ^2 = 5.824, 3 df, p = 0.121), in contrast to WT (χ^2 = 13.80, 3 df, p = 0.003) and 1b$^{-/-}$2 mice (χ^2 = 23.016, 3 df, p < 0.001). This deficit of 1a$^{-/-}$ mice was also evident in a separate cohort of mice (data not shown).* ***(B)*** *Discrimination indices (DIs; mean ± SEM) in the object recognition test for WT, 1a$^{-/-}$, and 1b$^{-/-}$ mice. Time points for calculating Dis were chosen to reflect the*

Figure 5.8. Continues

*following: short-term memory of a familiar object (familiar 10 min delay), long-term memory of a familiar object (familiar 24 hr delay), and short-term discriminative memory between a novel and familiar object (novel versus familiar). The mean DI for discrimination of a familiar object after 10 min delay appeared to be lower in $1a^{-/-}$ mice but failed to meet statistical significance [DI: $F(2, 26) = 2.006$; $p = 0.149$]. However, the decrease in the mean DI for discrimination of a novel versus a familiar object is significantly lower in $1a^{-/-}$ mice than in $1b^{-/-}$ or WT mice [$F(2, 26) = 4.404$; $p = 0.023$]. After a delay of 24 hr, the three genotypes similarly demonstrated a lack of familiarity with the previously presented disc [DI: $F(2, 26) = 0.001$; $p = 0.999$]. *$p = 0.05$ versus WT; +$p < 0.05$ versus $1a^{-/-}$).*

familiar object (time 10 min) and subsequently an increased number of SAPs toward the novel versus familiar object (time 24 hr + 10 min) (Figure 5.8A). Calculation of discrimination indices (DIs) showed that $1a^{-/-}$ mice did not discriminate between familiar or novel objects (Figure 5.8B). Therefore, in $1a^{-/-}$ mice, the lack of LTP is correlated with an impairment of nonspatial hippocampal memory formation. The effects on synaptic plasticity and memory formation in $1a^{-/-}$ mice emphasize that the $GABA_{B1b}$ protein cannot compensate for the loss of $GABA_{B1a}$ protein.

Discussion

The objective of this study was to determine if $GABA_{B1a}$ and $GABA_{B1b}$ exhibit functional or pharmacological differences in vivo. Our experiments with genetically modified mice indicate that, at CA3-to-CA1 synapses, $GABA_{B1a}$ assembles heteroreceptors inhibiting glutamate release, while predominantly $GABA_{B1b}$ mediates postsynaptic inhibition (Figure 5.4). This functional specialization relates, at least in part, to a distinct subcellular distribution of the $GABA_{B1}$ isoforms (Figure 5.5). Autoreceptor function is unaltered in the $1a^{-/-}$ and $1b^{-/-}$ mice (Figures 5.4C and 5.4D). Possibly, both $GABA_{B1a}$ and $GABA_{B1b}$ are present at GABAergic terminals impinging onto CA1 pyramidal neurons. However, since our recordings from the CA1 pyramidal soma cannot distinguish IPSCs from different types of GABAergic neurons, it is equally possible that some GABAergic terminals express $GABA_{B1a}$ and others express $GABA_{B1b}$. In general, the extent of subcellular segregation of $GABA_{B1a}$ and $GABA_{B1b}$ may vary according to brain regions and cell types. For example, GABAergic neurons impinging onto cortical layer 5 pyramidal neurons express $GABA_{B1a}$ but not $GABA_{B1b}$ at their terminals (Perez-Garci et al., 2006). The distribution of $GABA_{B1a}$ and $GABA_{B1b}$ may also vary within the dendritic compartment. This is suggested by the organotypic slice culture experiments showing that $GABA_{B1a}$-GFP is mostly excluded from dendritic spines, while $GABA_{B1b}$-GFP is expressed in most spines (Figure 5.6).

No significant pharmacological differences were found in radioligand binding experiments with cortical membranes from $1b^{-/-}$ and $1a^{-/-}$ mice (Figure 5.3). This confirms that $GABA_B$ isoforms display a similar binding pharmacology in vivo, as already suggested by earlier experiments with the photoaffinity antagonist [^{125}I]CGP71872 (Malitschek et al., 1998). Of note, receptors assembled from $GABA_{B1a}$ or $GABA_{B1b}$ may still display pharmacological differences in functional assays, depending on the local effector system and/or the receptor reserve. This may also be the reason why the data obtained in a functional assay (GTPγ[^{35}S] binding) and in ^{3}[H]baclofen binding show differences in the relative contribution to the total binding (Figures 5.3B and 5.3C). Depending on the subcellular localization, $GABA_{B1a}$ and $GABA_{B1b}$ may also be exposed to different concentrations of ambient GABA. Tonic activation of $GABA_B$ auto- but not heteroreceptors could, for example, account

for different potencies of baclofen in inhibiting release at excitatory and inhibitory terminals (Scanziani, 2000; Lei and McBain, 2003). Moreover, $GABA_{B1a}$ and $GABA_{B1b}$ may exhibit distinct desensitization properties depending on their localization and exposure to cyclic AMP-dependent protein kinase (Couve et al., 2002). These factors may have contributed to pharmacological differences between pre- and postsynaptic receptors reported in the past (Pozza et al., 1999; Lei and McBain, 2003). However, they likely do not explain differences in the rank order of drug potencies at native $GABA_B$ receptors, which have been reported as well (Cunningham and Enna, 1996; Bonanno et al., 1997).

An interesting question is how the functional segregation between the $GABA_{B1a}$ and $GABA_{B1b}$ isoforms is achieved. In principle, receptor compartmentalization could involve mechanisms such as mRNA trafficking, protein targeting, or protein retention (Horton and Ehlers, 2003; Sampo et al., 2003). We addressed the mechanism underlying the differential compartmentalization by expressing GFP-tagged $GABA_{B1a}$ or $GABA_{B1b}$ proteins in hippocampal neurons in organotypic slice cultures. The data show an almost exclusive association of the $GABA_{B1a}$-GFP protein with the axons of transfected CA3 neurons (Figure 5.6). We therefore favor protein targeting or retention as the reason for $GABA_{B1a}$ compartmentalization, in which case the information for segregation is probably carried by the extracellular pair of sushi repeats, the only region of sequence divergence between $GABA_{B1a}$ and $GABA_{B1b}$. Interestingly, the two sushi repeats in $GABA_{B1a}$ have strikingly different structural properties (Blein et al., 2004). This led to the proposal that they participate in protein interactions with multiple partners, which could generate additional heterogeneity in the $GABA_B$ receptor system.

An open question remains why LTP at CA3-to-CA1 synapses is impaired in $1a^{-/-}$ mice. Since autoreceptor and postsynaptic $GABA_B$ functions are preserved in $1a^{-/-}$ mice (Figure 5.4), the impairment of LTP must relate to the constitutive absence of heteroreceptors. Heteroreceptors do not appear to be activated by ambient or released GABA under baseline conditions (Figures 5.7C and 5.7D), as already suggested in earlier experiments (Morrisett et al., 1991; Scanziani, 2000). Presumably, heteroreceptors are only activated during periods of intense neuronal activity, when GABA released from interneurons spills over to the glutamatergic terminals.

Uncontrolled release of glutamate during such periods is likely to trigger adaptive changes (Burrone and Murthy, 2003). For example, excess released glutamate may spill over to synapses at which glutamate release has not occurred (Scimemi et al., 2004), which could convert silent synapses to a functional state (Isaac et al., 1995; Liao et al., 1995). The observed increase in the mEPSC frequency in $1a^{-/-}$ mice (Figure 5.7E) could reflect such an increase in the rate of activation of previously silent synapses (Liao et al., 1999). We addressed this possibility and compared the CVs of AMPA and NMDA receptor-mediated EPSCs in wild-type and $1a^{-/-}$ mice. The CV_{AMPA} was significantly reduced in $1a^{-/-}$ mice, while the CV_{NMDA} was unaffected by genotype, consistent with a decreased number of silent synapses in $1a^{-/-}$ mice (Kullmann, 1994). Since silent synapses provide an ideal substrate for LTP (Kullmann, 1994; Isaac et al., 1995; Liao et al., 1995; Durand et al., 1996; Malinow and Malenka, 2002), the observed impairment of LTP in $1a^{-/-}$ mice could be explained by the decrease in the proportion of silent synapses. A plausible physiological role for heteroreceptors could therefore be to limit the loss of silent synapses and to ensure that plasticity processes are maintained in the dynamic range. However, the constitutive absence of heteroreceptors in $1a^{-/-}$ mice may have allowed time for other compensatory adaptations. For example, disinhibition of adenylate cyclase activity (Pineda et al., 2004), transcriptional (West et al., 2002) and/or morphological changes (Luthi et al., 2001) may contribute to the impairment of LTP and hippocampus-dependent memory. Importantly, however, the LTP and behavioral data reinforce that $GABA_{B1a}$ and $GABA_{B1b}$ convey separate functions in vivo.

In summary, our combined physiological, morphological, and behavioral analysis of $1a^{-/-}$ and $1b^{-/-}$ mice clearly establishes that $GABA_{B1a}$ and $GABA_{B1b}$ are differentially compartmentalized and fulfill distinct functions. We hypothesize that interactions with the sushi repeats are responsible for retaining $GABA_{B1a}$ at its specific location. From a pharmaceutical perspective, the existence of functionally distinct receptor subtypes opens up new opportunities for therapeutic interference.

Experimental Procedures

Generation and Pharmacological and Biochemical Characterization of $1a^{-/-}$ and $1b^{-/-}$ Mice

Knockin mice were generated as outlined in Figure 5.1. All animal experiments were subjected to institutional review and conducted in accordance with Swiss guidelines and approved by the veterinary Office of Basel-Stadt. [^{125}I]CGP64213 was synthesized at Novartis and labeled to a specific radioactivity of >2000 Ci/mmol (ANAWA, Wangen, Switzerland). The probes used for Northern blot analysis, the [^{125}I]CGP64213 displacement experiments, immunoblot, and GTPγ[^{35}S] analysis were as described (Bischoff et al., 1999, Gassmann et al., 2004 and Kaupmann et al., 1997). Since we did not observe significant differences in any of our assays between wild-type littermates derived from $1a^{+/-}$ or $1b^{+/-}$ heterozygous breeding pairs, the data from wild-type mice were pooled.

Electrophysiology

Standard procedures were used to prepare 300 μm thick parasagittal hippocampal slices from P18–P28 mice. Slices were incubated for 45 min at 35°C in an interface chamber containing saline (124 mM NaCl, 2.7 mM KCl, 1.3 mM MgCl2, 2 mM $CaCl_2$, 1.24 mM NaH_2PO_4, 26 mM $NaHCO_3$, 18 mM glucose, 2.25 mM ascorbate) equilibrated with 95% O_2/5% CO_2. Slices were then kept at room temperature for at least 45 min before starting recordings at 30°C–32°C. Whole-cell patch-clamp recordings were performed from the somata of CA1 pyramidal neurons to measure holding currents and synaptic responses; neurons were visualized using infrared and differential interference contrast optics. Drugs, applied by superfusion into the recording chamber, were kept as aliquots, and solutions were freshly prepared on the day of the experiment. K^+ currents induced by baclofen (50 μM) or adenosine (100 μM) were elicited at −50 mV in the presence of TTX (1 μM). Patch electrodes (~5 MΩ) were filled with a solution containing the following: 140 mM K-gluconate, 5 mM HEPES, 2 mM $MgCl_2$, 1.1 mM EGTA, 2 mM Na_2ATP, 5 mM phosphocreatine, 0.6 mM Tris-GTP, at pH 7.25 with KOH and 285 mOsm). EPSCs and IPSCs were elicited by voltage pulses (100 μs, 2–5 V stimuli) or by current pulses (100 μs, 0.1–

0.3 mA stimuli) delivered through a bipolar Pt-Ir electrode (25 μm in diameter) placed in the stratum radiatum at a distance of 150–200 μm from the soma of the recorded cell. The recording electrode was filled with a solution containing the following: 140 mM Cs-gluconate, 10 mM HEPES, 10 mM phosphocreatine, 5 mM QX-314, 4 mM Mg-ATP, 0.3 mM Na-GTP, at pH 7.25 with CsOH and 285 mOsm. EPSCs were measured at −70 mV in the presence of 100 μM picrotoxin. In some cells, stimuli were delivered in pairs (interpulse interval 70 ms) (Palmer et al., 2004), and the paired-pulse ratio (PPR) was calculated as the ratio of the 2nd EPSC amplitude/1st EPSC amplitude. IPSCs were measured at 0 mV in the presence of 2 mM kynurenic acid. For the LTP experiments, the baseline stimulus frequency was set to 0.05 Hz to minimize "rundown" of the EPSC amplitudes (Gasparini et al., 2000; Xiao et al., 2004). Cells were voltage clamped at −70 mV during baseline and recovery periods. LTP was induced by depolarizing the cell to 0 mV while delivering 40 stimuli at 0.5 Hz at baseline stimulus intensity (pairing paradigm) (Palmer et al., 2004). When the potentiation of EPSC amplitudes lasted for >30 min, we considered this as LTP. mEPSCs were recorded at −70 mV in the presence of 0.5 μM TTX and 10 μM bicuculline. Detection and analysis of mEPSCs were done using the MiniAnalysis software (Synaptosoft, Decatur, GA). For analysis of the CV_{AMPA} (Kullmann, 1994), AMPA receptor-mediated EPSCs were recorded in the presence of 100 μM picrotoxin and 5 μM bicuculline while neurons were clamped at −70 mV (0.05 Hz stimulation). Following 15–20 min recording, non-NMDA glutamate receptors were blocked with 10 μM DNQX, and the holding voltage was changed to +30 mV. For analysis of the CV_{NMDA}, NMDA receptor-mediated EPSCs were recorded for >10 min and, as a control, eventually blocked by adding CPP (5 μM) and 7-chlorokynurenate (10 μM) to the superfusion. CV_{AMPA} and CV_{NMDA} were calculated as SD/mean of AMPA and NMDA receptor-mediated EPSC peak amplitudes, respectively. Data were obtained with an Axopatch 200B (Axon Instruments, Union City, CA), filtered at 2 kHz and digitized at 10 kHz, and acquired and analyzed with pClamp9 (Axon Instruments, Union City, CA). Values are expressed as mean ± SEM. The experimenter was blind to the genotype of the mice.

Immunohistochemistry and Preembedding Electron Microscopy

Hippocampal sections were treated for light and electron microscopy immunolabeling as described (Kulik et al., 2002; Gassmann et al., 2004). For ultrastructural analysis, only immunogold particles inside the plasma membrane (closer than 30 nm) of morphologically identifiable terminals (with presynaptic active zone or clear vesicles) and dendrites/spines were counted. Unassigned particles represent background labeling and labeling in axonal fibers (Kulik et al., 2002)). The immunogold particle density in $1^{-/-}$ mice, which completely lack $GABA_{B1}$ protein (Schuler et al., 2001), was 7% of that seen in wild-type mice. The presynaptic percentage of particles allocated to the plasma membrane in $1^{-/-}$ mice was 52%, thus showing that background labeling equally distributes over pre- and postsynaptic membranes. Only asymmetrical (glutamatergic) synapses were analyzed. An ultrastructural analysis of GABAergic (symmetrical) synapses in $1a^{-/-}$ and $1b^{-/-}$ mice was impossible due to infrequent $GABA_{B1}$ immunogold labeling (Kulik et al., 2002; Kulik et al., 2003). The experimenter was aware of the genotype of the mice.

Transfection of Organotypic Slice Cultures and Two-Photon Laser Scanning Microscopy

Organotypic hippocampal slices were prepared from Wistar rats at postnatal day 5 as described (Stoppini et al., 1991). After 7 days in vitro, cultures were biolistically transfected with a Helios Gene Gun (Bio-Rad, CA) with $GABA_{B1a}$-GFP or $GABA_{B1b}$-GFP expression vectors in combination with a tdimer2 expression vector (gift from R. Tsien). Expression of $GABA_{B1a}$-GFP and $GABA_{B1b}$-GFP was under control of the neuron-specific synapsin-1 promoter (gift from K. Svoboda) for 7–8 days. For imaging, we used a custom-built two-photon laser scanning microscope based on a BX51WI microscope (Olympus, Japan) and a pulsed Ti:Sapphire laser (Chameleon XR, Coherent, Scotland) tuned to $\lambda = 870$ nm, controlled by an open source software package (ScanImage) written in Matlab (Pologruto et al., 2003). Fluorescence was detected in epifluorescence (LUMPlan W-IR2 60 × 0.9 NA, Olympus) and transfluorescence mode (achromatic aplanatic condenser, 1.4 NA, Olympus) using four photomultiplier tubes (R2896, Hamamatsu, Japan). We used 725DCXR dichroic mirrors and E700SP blocking filters to reflect emitted photons into a secondary beamsplitter, containing a 560DCXR dichroic, 525/50 (green) and 610/75 (red) band-pass filters (AHF Analysentechnik AG, Tübingen, Germany). The slice was placed

into a perfusion chamber and superfused continuously (2 ml/min) with ACSF (119 mM NaCl, 2.5 mM KCl, 4 mM $CaCl_2$, 4 mM $MgCl_2$, 26.2 mM $NaHCO_3$, 1 mM NaH_2PO_4, 11 mM glucose, gassed with 95% O_2 and 5% CO_2 at room temperature). Stacks of images (256 × 256 pixels) from secondary dendritic branches and thin axons were obtained from transfected CA3 and CA1 pyramidal neurons (Z step: 0.5 μm). Maximum intensity projections of green and red stacks were constructed. For the ratio images, we used a hue/saturation/brightness model, where hue was determined by the green/red ratio (using a rainbow color table), and the intensity in the red channel was used to set the brightness. For quantitative analysis, we calculated the green-to-red ratio in a region of interest (dendrite or axon) after subtracting the background fluorescence. To compensate for differences in laser power and expression level, we normalized the ratio in the axon by the average dendritic ratio. Spines were identified by anatomy from tdimer2 images. $GABA_{B1a}$-GFP- and $GABA_{B1b}$-GFP-positive spines were defined as having intensity in the green channel at least three standard deviations above background.

Object Recognition Test

The test was designed according to the principles of Ennaceur and Delacour (1988), which rely upon the natural tendency of rodents to attend to a novel object more than a familiar one. Male wild-type (n = 7), $1a^{-/-}$ (n = 8), and $1b^{-/-}$ (n = 13) single-housed mice, aged 21 (± 0.7) weeks, were used. Mice were habituated overnight (17–21 hr) to a novel enclosure [22 × 37 × 15 (h)cm], with not, vert, similar2 cm sawdust and standard food and water provided ad libitum until testing began. All sessions were recorded on video while the experimenter was out of the testing room. The number of SAPs for each mouse in each 3 min period was scored by a trained observer blinded to the animals' genotypes. All videos were scored twice by the same observer, and duplicate SAP scores were averaged within animal and time point. The intrascorer correlation (Pearson Product Moment correlation) was 0.91. A DI, the difference in SAP numbers at a pair of time points divided by the total number of SAPs at those time points, was calculated for each animal (Figure 8B). DIs reflect (1) short-term memory of a familiar object ([Number of SAPs at Time 0 min − Number of SAPs at Time 10 min]/[Total number of SAPs at both time points]); (2) long-term memory of a familiar object ([Number of SAPs at Time 0 min − Number of SAPs at Time 24

hr]/[Total number of SAPs at both time points]); and (3) short-term discriminative memory between a novel and a familiar object ([Number of SAPs at Time 24 hr + 10 min − Number of SAPs at Time 10 min]/[Total number of SAPs at both time points]). A DI of 1 reflects perfect discrimination, while a DI of 0 indicates complete loss of discrimination. SAP data were analyzed within a given genotype for the factor “Time” using the nonparametric Friedman repeated measures ANOVA on ranks test followed by Dunn's method for post hoc analysis. DIs were analyzed within a given time for the factor “Genotype” using one-way ANOVA followed by Fisher's LSD post hoc analysis.

Reagents

Tetrodotoxin (TTX) was from Latoxan (Valence, France). (R)-CPP [3-((R)-2-carboxypiperazin-4-yl)-1-phosphonic acid] and 7-chlorokynurenic acid (7-chloro-4-hydroxyquinoline-2-carboxylic acid) were from Tocris Cookson Ltd. (Bristol, UK). Baclofen and CGP54626 were from Novartis Pharma AG (Basel, Switzerland). All other reagents were from Fluka/Sigma (Buchs, Switzerland).

Chapter 6. General discussion

This thesis was focused on the development and use of optical methods to study synaptic plasticity at the level of individual synapses. Two-photon excitation fluorescence microscopy allowed us to image individual spines in the highly scattering brain tissue with good contrast, high spatial resolution and temporal resolution. The use of a newly identified light sensitive channel, ChR2, made it possible to control neuronal activity non-invasively. Two-photon glutamate uncaging permitted the investigation of postsynaptic mechanisms with excellent spatial resolution. In the past four years, we have used various combination of these new optical techniques to study long-term potentiation at the single synapse level (Chapter 2-4). Furthermore, we have established methods to measure protein concentration at individual spines, which are far below the resolution limit of optical microscopy. We applied this method (two-photon ratiometry method) to measure the concentration of αCaMKII and $GABA_B$ receptor variants in small compartments (Chapter 3 and 5).

A. Technical challenges of combining ChR2 and two-photon imaging

In Chapter 2, we explored the possibility to combine the ChR2 stimulation technique with two-photon imaging. We compared ChR2 activation using single-photon and two-photon excitation (Chapter 2 supplementary figure 1.1). No direct activation of ChR2 was observed by two-photon imaging lasers. The reason is that the tiny focal volume of two-photon excitation makes it not possible to illuminate a large area of membrane. However, this made the combination of stimulating neurons with blue light and imaging Ca^{2+} transients or morphology at different positions along the neuron with two-photon excitation possible.

1. Blue light damages photomultiplier tubes (PMTs).

The first technical challenge is how to protect the sensitive photon detectors (PMTs). Our solution is to use a computer controlled shutter system. During the light pulse, PMTs were protected by a mechanical shutter (VS25, Uniblitz). The closing and opening signals were automatic generated with at least 5-10 ms safety margin before and after the light pulse.

2. Visualization of ChR2 expressing cells.

The second challenge is to visualize ChR2-positive neurons. GFP and YFP can be tagged to ChR2. But these two fluorescent proteins have similar excitation spectrum to ChR2. Therefore, red labeling is advantageous for visualizing ChR2-positive neurons without activating the channel: under 546-nm illumination, ChR2 absorption is only ~ 4% of the maximum (Nagel et al., 2003). In our study, we have two strategies: a ChR2-tdimer2RFP fusion protein (Chapter 2) and co-expression of ChR2 and tdimer2RFP using a two-promoter vector (Chapter 3). ChR2 fusion protein highlights the membrane of the cell, whereas co-expression of a freely diffusible protein is a good volume label. Since the two-promoter system expresses two genes of interest simultaneously at a constant ratio, ChR2 does not necessarily need to be labelled. Using DsRed filter sets, we could select cultures with a favorable expression pattern and target ChR2-positive cells for patch-clamp recordings.

3. Light source to generate short blue light pulses.

The third challenge is the choice of light source. The most convenient light source for a common fluorescent microscope is the Hg-lamp. Together with Uniblitz-shutters, we could generate blue light pulses as short as 5 ms (Chapter 2). This setup has two potential problems: the excessive heat from the Hg-lamp sometimes makes the shutter close improperly and the physical vibration caused by the shutter makes stable patch-clamp recordings difficult. Thus, the better light source is a blue light-emitting diode (LED). There is no vibration! The LED control signal input can be generated using computer with sub-millisecond precision. In Chapter 3 and 4, we have used blue LED (470 nm, Cairn Research Ltd.) for ChR2 stimulation. Using 1 ms light pulses, we could minimize the outlasting ChR2 conductance after action potential and reliably trigger action potentials up to 50 Hz. In the future, blue laser will be the method of choice to achieve precise focal illumination. The consequences owing to excessive activation of ChR2 can be avoided. In a recent study from Karel Svoboda's lab, the authors have shown that neurnons could be driven to spike when the laser was directed onto the descending axons, far from the soma and dendrites. The resulting action potential was indistinguishable with action potential evoked by current injections (Petreanu et al., 2007).

B. Optical LTP induction protocol.

The summary table:

Protocols	**Spine volume change**	**EPSCs change**
Presynaptic APs only	No change	No change
Postsynaptic burst by 200 ms light	No change	No change
Glutamate uncaging only	No change	No change
Pairing of uncaging laser pulse with postsynaptic burst without MNI-glutamate	No change	N/A
Pairing of uncaging or presynaptic AP with postsynaptic burst (5 mM MNI-glutamate)	69% of experiments showed a long-lasting change (> 30%)	71% of experiments showed a long-lasting change (> 50%)

Our results show that calcium influx during light-induced postsynaptic bursting in CA1 pyramidal cells is not sufficient to induce synaptic plasticity, but coincident activity of pre- and postsynaptic cell is necessary to trigger LTP at Schaffer collateral synapses. LTP and spine volume increase are closely related phenomena, which is consistent with others (Matsuzaki et al., 2001b; Matsuzaki et al., 2004; Tanaka et al., 2005).

Interestingly, the optical pairing protocol led to a lasting volume increase only in some stimulated spines, indicating that not every spine can be potentiated with the same induction protocol. The considerable heterogeneity in the induction of plasticity at individual Schaffer collateral synapses has been reported (Petersen et al., 1998; Debanne et al., 1999). What are the underlying mechanisms? It has been proposed by Kasai that large spines are “memory spines” and small spines are “learning spines” (Kasai et al., 2003). However, our data does not support this hypothesis, since the lasting volume expansion was indenpendent of the initial spine size. Given that there

is considerable variability of αCaMKII concentration between individual spines, we further investigated whether the initial concentration of αCaMKII in the spine has a predictive value for the sensitivity of LTP. The potentiated spines and non-potentiated spines showed a very similar initial αCaMKII concentration. Thus, we conclude that there is no obvious way to predict the sensitivity of a spine to the pairing protocol from these two parameters. Other molecular heterogeneity, such as the diversity in the component of ion channels, receptors, scaffolds and signal transducing proteins in individual synapses, remains to be investigated.

C. Measure protein concentrations at the level of single synapses.

In this thesis, we have established a novel method to measure protein concentrations before and after plasticity induction at the level of single synapses. We used αCaMKII as an example to show that fluorescence measurements in a single color channel are not sufficient to quantify protein concentration, not even relative to the dendrite. The reason is that the size of dendritic spines is smaller than the point spread function of the microscope. The fluorescence intensity of labeled αCaMKII in individual spines is determined by two unknown variables: the concentration of XPF-αCaMKII in the spine and the volume of that spine. Similar to the dual-color method for synaptic calcium imaging (Yasuda et al., 2004), we transfected cells with a fluorescence label αCaMKII (green or yellow) and a freely diffusible dimeric RFP as a marker of cytosolic volume. Since broad two-photon cross sections allow the simultaneous excitation of two or more fluorophores with vastly different emission wavelengths, we were able to compare the concentration of αCaMKII in compartments below the resolution limit of the microscope, by calculating the fluorescence intensity ratio between XPF-αCaMKII and RFP on a pixel-by-pixel basis (X/R). To pool spine data from cells with different relative expression levels of XPF-αCaMKII and RFP, we normalized the X/R ratio in the spine by X/R ratio in the dendrite (S/D ratio). The S/D ratio is a measure of αCaMKII enrichment in spines independent of spine volume. In Chapter 3, we compared the S/D ratio of cells expressing wild-type αCaMKII and a double mutant (TT305/6VA) where two inhibitory autophosphorylation sites were blocked. Indeed, cells transfected with mutant αCaMKII had higher enrichment in spines. Our data is consistent with the results from TT305/6VA mutant knock-in mice, where blocking inhibitory

phosphorylation increased CaMKII in the postsynaptic density (PSD) revealed by whole synaptic protein lysate (Elgersma et al., 2002).

The time-lapse ratiometry method further allowed us to investigate subtle changes in αCaMKII concentration on the level of individual synapses that underwent LTP (Chapter 3). We could estimate bound and soluble αCaMKII in the spines based on the S/D ratio and the volume of the spine (see Chapter 3 materials and Methods). Our data showed that both soluble and bound αCaMKII were increased after optical LTP induction. Our analysis revealed that in the spines that showed a persistent increase in volume, the absolute amount of bound αCaMKII in the spine had doubled 30-40 min after stimulation. αCaMKII accumulates specifically and exclusively at synapses that did experience coincident activity. For the first time, the physiological relevance of such translocation has been shown. Our results also provide a key piece of evidence for the function of αCaMKII as a memory molecule.

We have shown that the amount of bound αCaMKII increases after LTP. One important open question is: Does it stay in the active state for hours or even years, as proposed by Lisman (Lisman and McIntyre, 2001; Lisman and Zhabotinsky, 2001; Lisman et al., 2002)? Thus, a reporter of the activation of CaMKII should be used in combination with our optical pairing method. Approaches to optically monitor CaMKII activity have been investigated. The basic idea is using fluorescence resonance energy transfer (FRET) to detect conformational changes in CaMKII during the activation process (Takao et al., 2005). The FRET-based reporter has been used in neurons in response to glutamate and NMDA stimulation. Whether or not it is sensitive enough for individual synapses undergoing synaptic potentiation is still unknown. Based on the work of GCaMP2, I would like to propose another idea for CaMKII activity reporter (Fig 6.1). It can be constructed also based on circular permutation of GFP (cpGFP). Fluorescence of GFP can arise from the interaction between CaMKII at the C terminal of cpGFP and a special N-terminal fragment, i.e. from NMDA receptor, or another potent substrate of CaMKII. In basal conditions, CaMKII is kept inactive by an autoinhibitory domain that masks the catalytic core of the enzyme (Lisman et al., 2002). The binding of the Ca^{2+}/calmodulin complex induces a conformational change and relieves this

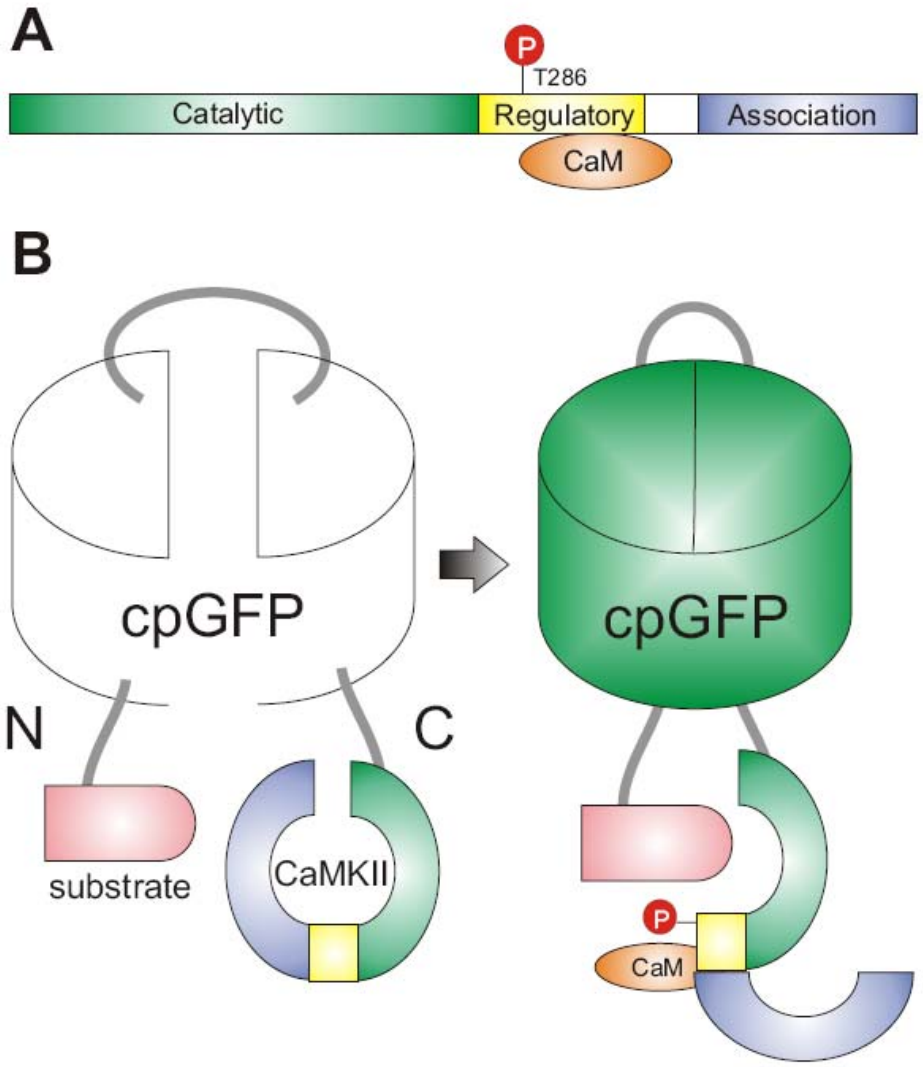

Figure 6.1. ***A cpGFP based CaMKII activity reporter.***

A. *The different functional domains in the primary structure of calcium/calmodulin-dependent protein kinase II (CaMKII).* ***B.*** *The report is based on a circular permuation of GFP (cpGFP) and contains CaMKII inserted at the C terminal to cpGFP barrel and potent substrate of CaMKII, e.g. NMDAR, inserted at the N terminal. Fluorescence of GFP arises from the interaction between CaMKII and its substrate. In basal conditions, CaMKII is kept inactive that masks the catalytic core of the enzyme. The binding of* Ca^{2+}*/calmodulin complex (CaM) induces a conformational change, thereby exposing the kinase domain to the substrate.*

interaction, thereby exposing the kinase domain to substrates. The reporter changes its fluorescence with the binding of CaMKII to its substrate in the same compartment as the enzyme. This single colour reporter might be advantageous to the FRET based reporter if using a two-photon microscope. Because the two-photon excitation

spectrum of donor and acceptor often overlaps, making quantitative measure of FRET more difficult.

D. LTP is input-specific at the level of single synapses

Although not explicitly stated in Hebb's postulate, it is generally assumed that Hebbian synaptic modifications are synapse (or input) specific — only synapses that had experienced concurrent pre- and postsynaptic activity are subject to synaptic modification. The extent to which LTP is synapse-specific influences a neuron's information processing and storage. For technical reasons, tests for 'input specificity' have resulted in controversial conclusions. Early experiments by stimulating two fairly distant pathways have shown that LTP was input specific (Andersen et al., 1977; Gustafsson et al., 1987). Engert and Bonhoeffer used a local perfusion technique, which allowed them to assess the synaptic specificity of LTP with a spatial resolution of ~30 μm (Engert and Bonhoeffer, 1997). Their results indicated that there was no input specificity at a distance of less than ~70 μm. Recently, two-photon glutamate uncaging has been used to investigate synaptic plasticity at the level of individual synapses (Matsuzaki et al., 2004; Bagal et al., 2005). Results from Matsuzaki *et al.* and us (in Chapter 3) indicate that individual synapses could follow Hebb's postulate for learning. Activity-induced changes were restricted to the stimulated spine, but not in neighboring spines on the same dendrite. The spatial resolution of local glutamate photolysis is clearly superior to the local perfusion approach. Even spines that are 2-10 μm away from the potentiated spine showed no change in volume and αCaMKII concentration.

E. Outlook

1.We have shown that pre- and postsynaptic activity can be controlled independently with millisecond precision by various optical stimulation techniques. Thus, it would be possible to optically investigate spike-timing-dependent plasticity at identified synapses in more detail. Since the intracellular milieus of the pre- and postsynaptic cells are not affected, plasticity experiments are not limited in time. Having undergone LTP, is this the end of the road for a synapse or is further potentiation possible or can it be reversed by depotentiation? In principle, the entire

life cycle of a synapse from formation to removal could be investigated using our optical methods.

2. Previous studies have suggested that synaptic plasticity can be influenced by prior neural activity. For example, previous stimuli may make it easier or harder to induce LTP. This kind of activity-dependent modulatory plasticity is termed "metaplasticity" (Abraham and Bear, 1996). The induction of metaplasticity does not change synaptic efficacy but affects synaptic physiology in such a way that subsequent attempts to induce synaptic plasticity will be modified. It will be of great interest to know the time scale and spatial scale of these modifications. Our optical approaches will allow us to investigate "metaplasticity" in more detail in the future, even tackle the question of which diffusing cytoplasmic factor is responsible for modifying synaptic properties.

3. We have shown that LTP is input-specific at the level of single synapses, indicating synapses may function as independent units of memory storage. However, it will be also interesting to know whether LTP induction at one set of synapses may subsequently influence the threshold for potentiation at nearby synapses. Our optical LTP induction method — pairing of two-photon glutamate uncaging with ChR2 stimulation postsynaptically, will be ideal to study the coupling between the recently potentiated synapse and nearby synapses.

4. Here, we have investigated αCaMKII accumulation at postsynaptic sites in response to optical LTP protocol. The next step is to using this optical LTP protocol to study other interesting molecules that are involed in LTP induction or expression. It will be of great interest to compare the specificity and dynamics of these molecules, such as PSD-95 or GluR1/2 receptors, with those of αCaMKII. These experiments might elucidate the temporal profile of LTP induction or expression at the molecular level.

Appendix

A. Generation of non-clumpy GFP and YFP fusion proteins using site-directed mutagenesis

Most *Aequorea*-derived GFPs and mutants of any color are in fact very weak dimers. They can be made truly monomeric simply by introducing the mutation A206K, generally without deleterious effects (Shaner et al., 2005). In our hands, mutation A206K in GFP and YFP indeed prevented forming intracellular aggregates of GFP-αCaMKII and YFP-αCaMKII (Appendix Fig 1A, B). It holds true for $GBAB_{B1a}$-GFP fusion protein (Appendix Fig 1C, D).

The generation of mutations is made based on the idea from the QuikChange site-directed mutagenesis Kit (Stratagene). The difference is that we ordered important enzymes from Promega instead of using the Kit, which of course is much cheaper. What you need are *Pfu* DNA polymerase, *DpnI* restriction enzyme and supercompetent bacteria.

The basic procedure utilizes a supercoiled double-stranded DNA vector with an insert of interest and two synthetic oligonucleotide primers containing the desired mutation. The oligonucleotide primers, each complementary to opposite strands of the vector, are extended during PCR by *Pfu* DNA polymerase. In corportation of oligonucleotide primers generates a mutated plasmid containing staggered nicks. Following PCR, the product is treated with Dpn I. The *Dpn* I endonuclease (target sequence: 5′-Gm6ATC-3′) is specific for methylated and hemimethylated DNA and is used to digest the parental DNA template and to select for mutation-containing synthesized DNA. DNA isolated from almost all *E. coli* strains is dam methylated and therefore susceptible to *Dpn* I digestion. The nicked vector DNA containing the desired mutations is then transformed into supercompetent cells (JM 109 or XL1-Blue). In our hands, more than 60% of colonies contain the desired mutation. It is important to start with small amount of starting DNA template (not more than 100 ng). The use of high fidelity DNA polymerase and the low number of thermal cycles (not more than 20 cycles) decrease potential for generating random mutations during the reaction. Both of the mutagenic primers must contain the desired mutation and anneal to the same sequence on opposite strands of the plasmid. Primers should be between 25 and 45 bases in

length, with a melting temperature (T_m) of ≥ 78 °C. The following formula is commonly used for estimating the T_m of primers:

$T_m = 81.5 + 0.41(\%GC)\ 675/N - \%$ mismatch

• *N* is the primer length in bases

• values for **%GC** and **% mismatch** are whole numbers

Examples (sense primers):

YFP WT: 5'- C CTG AGC TAC CAG TCC GCC CTG AGC AAA GAC CCC-3'

A206K: 5'- C CTG AGC TAC CAG TCC AAG CTG AGC AAA GAC CCC-3'

$T_m = 81.5 + 0.41 \times 100 + 20 / 34 - 675 / 34 - 100 \times 3 / 34 = 77\ ^oC$

GFP WT: 5'- C CTG AGC ACC CAG TCC GCC CTG AGC AAA GAC CCC-3'

A206K: 5'-C CTG AGC ACC CAG TCC AAG CTG AGC AAA GAC CCC-3'

$T_m = 81.5 + 0.41 \times 100 + 21 / 34 - 675 / 34 - 100 \times 3 / 34 = 78\ ^oC$

PCR reaction:

5 µl	10 × *Pfu* buffer
2 µl	*ds* DNA template (100ng in total)
1.7 µl	sense primer (10 µM)
1.7 µl	Anti-sense primer (10 µM)
1.6 µl	dNTPs mix
37 µl	H_2O
1 µl	*Pfu* DNA polymerase (2.5 U/µl)
50 µl	Total volume

PCR programme:

1:	95 °C	1 min
2:	95 °C	50 sec
3:	60 °C	50 sec
4:	72 °C	22 min
5:	Goto	2 for 17 cycles
6:	72 °C	30 min
7:	4 °C	forever

8: end

Dpn I reaction:

Transfer the PCR reaction to a 1.5 ml tube and add 1 μl of *Dpn* I.

Incubate the reaction at 37 ^{o}C ≥ 1 hour.

Transformation:

4 –5 μl *Dpn I* reaction + 100 μl JM 109 cell

Results:

The mutated sites should be confirmed by DNA sequencing.

In our hands, the successful rate of the mutagenesis is > 60%.

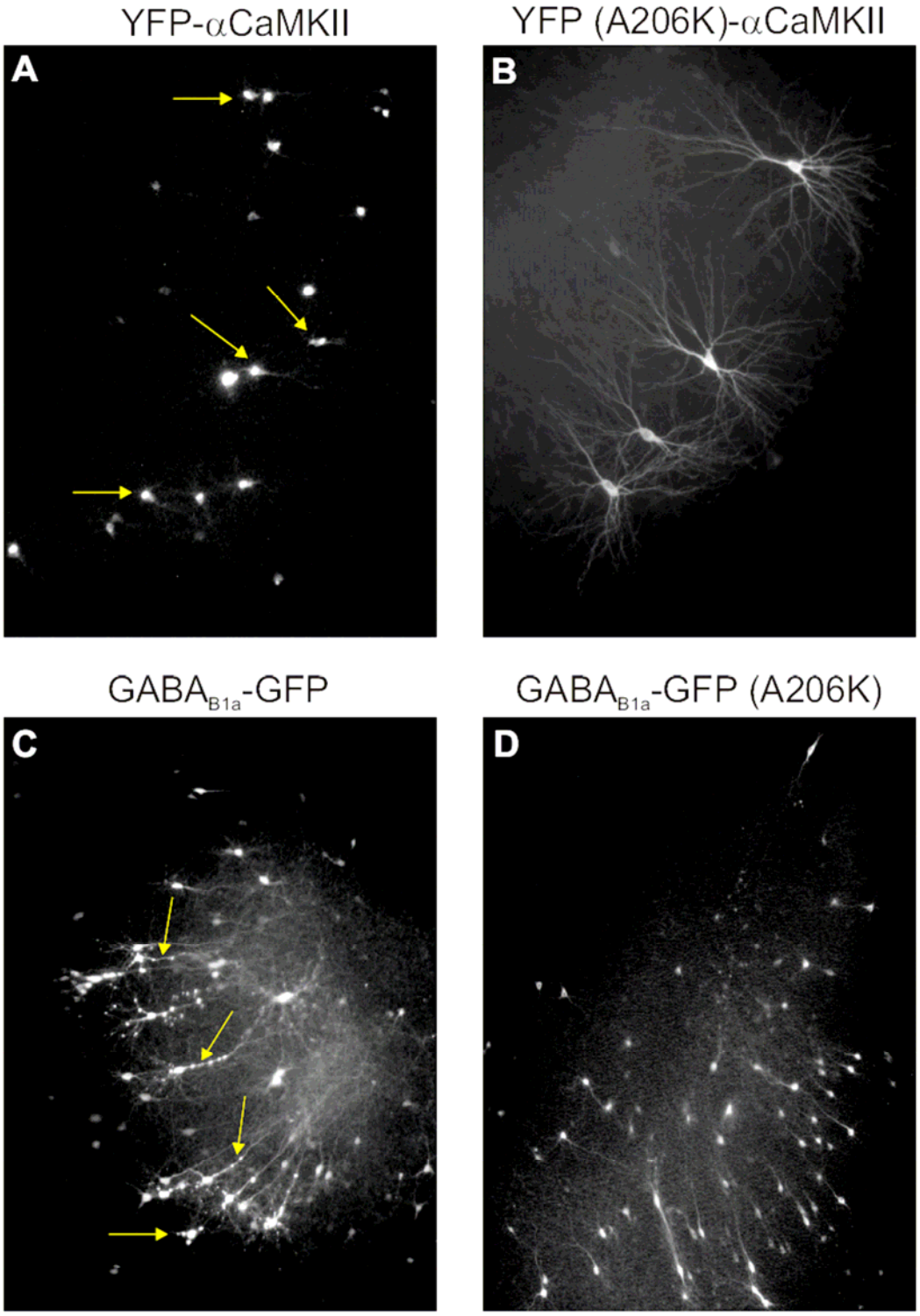

Appendix Figure 1. ***A206K Mutation in GFP and YFP prevents forming intracellular aggregates.***

A. *YFP-αCaMKII,* ***B****. YFP (A206K)-αCaMKII,* ***C****. GABA$_{B1a}$-GFP,* ***D****. GABA$_{B1a}$-GFP (A206K), were expressed in hippocampal neurons 14 days after transfection. As can be seen, GFP and YFP fusion proteins displayed a substantial amount of aggregates in the soma and dendrites (yellow arrows). No aggregates were observed after A206K mutation was introduced.*

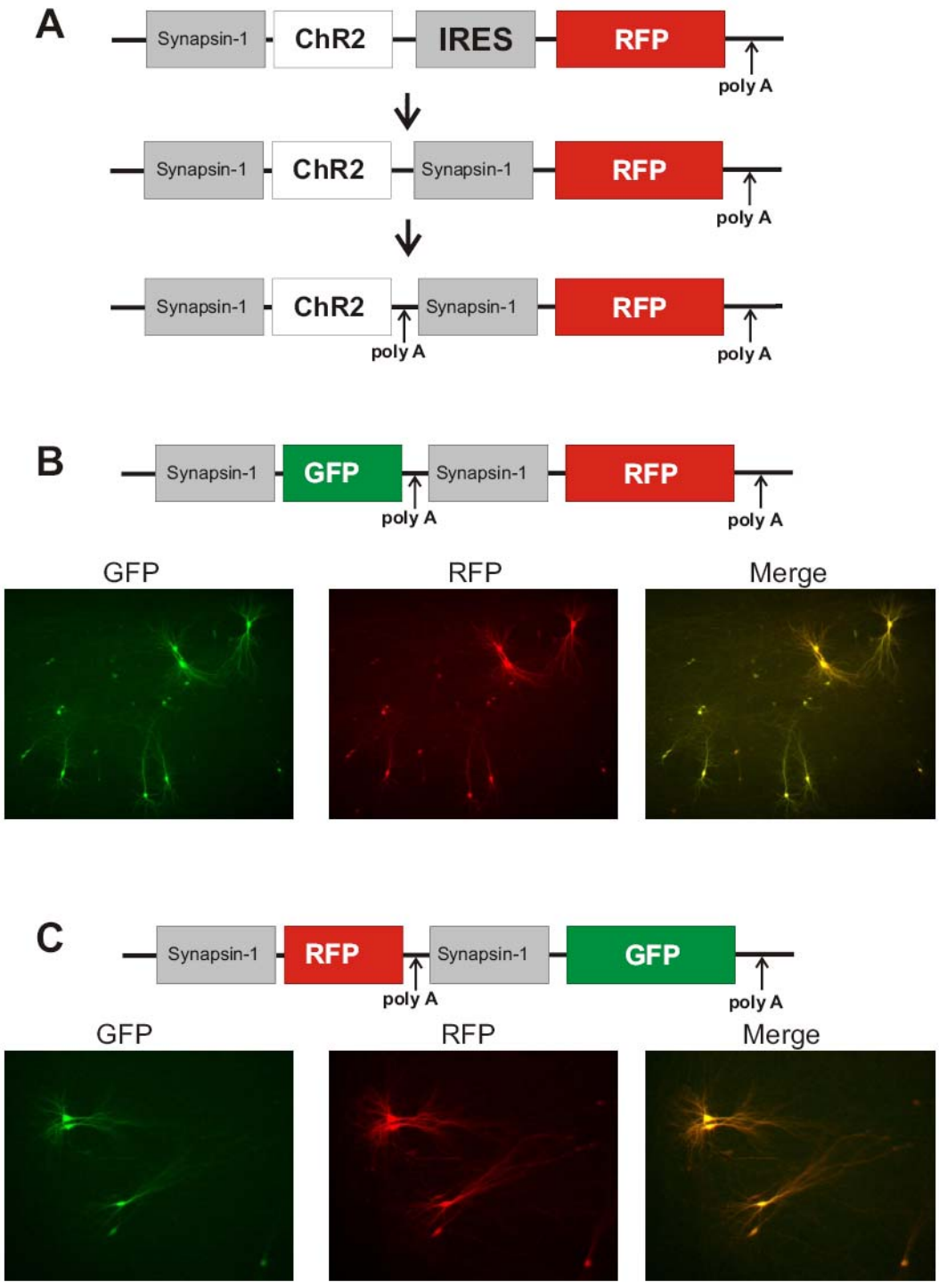

Appendix Figure 2. Generation and optimization of two-promoter vectors

A. *Three-step optimization of the two-promoter vector.* ***B, C.*** *Both GFP and RFP genes were highly expressed in cells regardless of the relative position. Note that constant expression ratio exists in all transfected cells.*

B. Generation and optimization of two-promoter vectors

Two methods for heterologous coexpression of proteins have been commonly used: the bicistronic vector and the dual-vector system. The bicistronic vector allows for the first gene of interest to be transcribed but in the absence of a termination signal. The transcription from the plasmid extends beyond the insert and another gene that is downstream gets transcribed as well. These transcripts are bicistronic (two coding regions). An internal ribosomal entry site (IRES) upstream of the second gene allows the translation of the second coding region independently of translation of the first one. In theory, the expression of the second gene could be comparable to that of the first gene. In practice, much less expression of the second gene compared with that of the first gene has been commonly observed. In the dual-vector system, two target genes are coexpressed from two different vectors. Dominance of one vector over the other in the copy number is the major problem.

In a first attempt to coexpress two proteins in a constant ratio, I made a bicistronic IRES vector containing unlabeled ChR2 and tdimerRFP under the control of synapsin-1 promoter. The expression of tdimer2RFP was below the detection limit in many cells, though ChR2 was expressed normally. Next, I tried to improve this vector simply by replacing the IRES sequence with a second synapsin-1 promoter. This idea came from a paper from Kim *et al.*, where they have successfully used a two-promoter system (two different promoters) to produce a large amount of protein in the bacteria expression system (Kim et al., 2004). This strategy partially worked, since the transfected cells were red and could be depolarized by blue light stimulation. However, none of the transfected cells could be spiked by light, only subthreshold depolarizations were recorded. Judging from the light induced responses, I concluded that ChR2 was weakly expressed in these cells, though RFP was highly expressed. Comparing with the vector containing the unlabeled ChR2 alone, the only difference was the lack of a SV 40 ploy A sequence after first gene in the two-promoter vector. Since poly A tails are known to function in mRNA stability, I inserted a SV 40 poly A sequence (about ~ 187bp) into the two-promoter vector (Appendix Fig 2A). As a result, 20 out of 21 RFP expressing cells showed strong depolarization and reliable burst of spikes by light. In a second step, I replaced the second gene (RFP) with a genetically encoded calcium indicator, GCaMP2. The resulting vector allowed me to optically screen light-spiking cells without even patching the cells (Fig 4.7).

In summary, the two-promoter vector containing two synapsin-1 promoter sequences, two SV 40 poly A sequences and two genes of interest is stably expressed in neurons. Both genes are highly expressed in the cell (Appendix Fig 2B). This vector was crucial for the all-optical synaptic stimulation experiments, where we had to co-express three different proteins in individual cells.

The SV 40 poly A sequence used in this study:
5'-GTCGACTTCGAGCAACTTGTTTATTGCAGCTTATAATGGTTACAAATAA
AGCAATAGCATCACAAATTTCACAAATAAAGCATTTTTTTCACTGCATTCT
AGTTGTGGTTTGTCCAAACTCATCAATGTATCTTATCATGTCTGGATCGTC
TAGCATCGAAGATCCTGCAGCCATCGATTAATTAAT –3'

C. Tdimer2RFP is advantageous for making a red label.

DsRed is a spontaneously red fluorescent protein cloned from the red coloration around the oral disk of a *Discosoma* species. Though oligomerization caused substantial trouble in the earlier days of red fluorescent proteins, there are now highly optimized monomers or tandem dimers available. I compared engineered DsRed (from CLONTECH, which has a decreased the oligomeric state), a monomeric red fluorescent protein (mRFP1) and a tandem dimer of DsRed with 12-residue linker (tdimer2RFP) both from Roger Tsien (Campbell et al., 2002). In our hands, tdimer2RFP has the best two-photon cross-section. When these three red proteins were used as freely diffusible volume makers, no aggregates were ever observed. DsRed-CaMKII and mRFP1-CaMKII fusion proteins, however, displayed a substantial amount of aggregates when expressed in hippocampal neurons (Appendix Fig 3A, D). The tandem dimer tdimer2RFP turned out to the best choice for red fusion proteins (Appendix Fig 3B, C, E). Although it is twice as big as the monomeric mRFP1, when fused with CaMKII no non-specific aggregates were observed. Using tdimer2RFP, we have successfully generated many bright, non-clumpy red fusion proteins, such as tdimer2RFP-CaMKII, CaMKII-tdimer2RFP, ChR2-tdimer2RFP, $GABA_{B1b}$-tdimer2RFP and membrane-targeted tdimer2RFP (MACKS-tdimer2RFP).

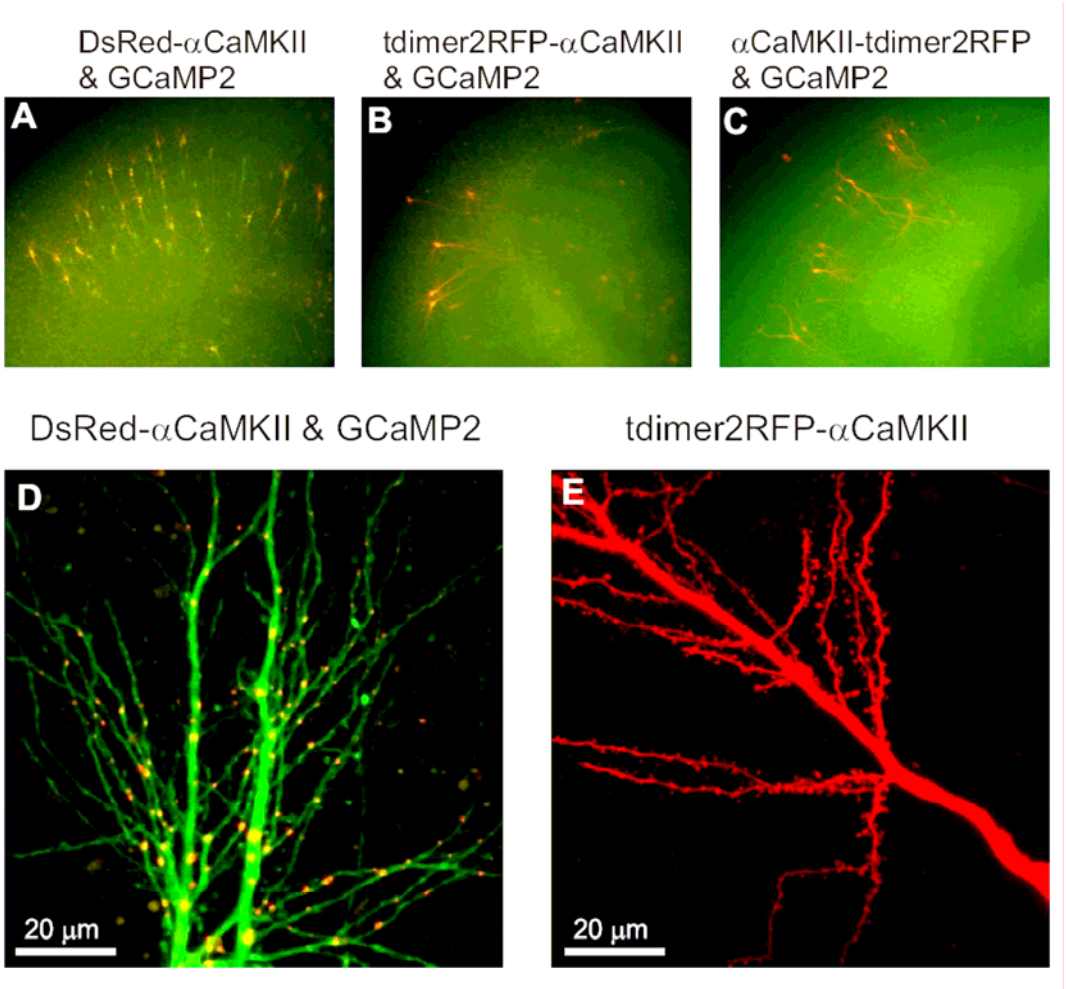

Appendix Figure 3. αCaMKII red fusion proteins.

A. *DsRed-αCaMKII and GCaMP2,* ***B.*** *tdimer2RFP-αCaMKII and GCaMP2,* ***C.*** *αCaMKII-tdimer2RFP and GCaMP2, co- expressed in CA1 hippocampal neurons in slice culture 7 days after transfection.* ***D.*** *A maximal projection image of dendrites from DsRed-αCaMKII and GCaMP2 co-expressed cells. As can be seen, DsRed-αCaMKII displayed a substantial amount of aggregates.* ***E.*** *A maximal projection image of dendrites from a tdimer2RFP-αCaMKII expressing cell. No aggregates were observed.*

D. Two-photon excitation spectrum of commonly used fluorophores

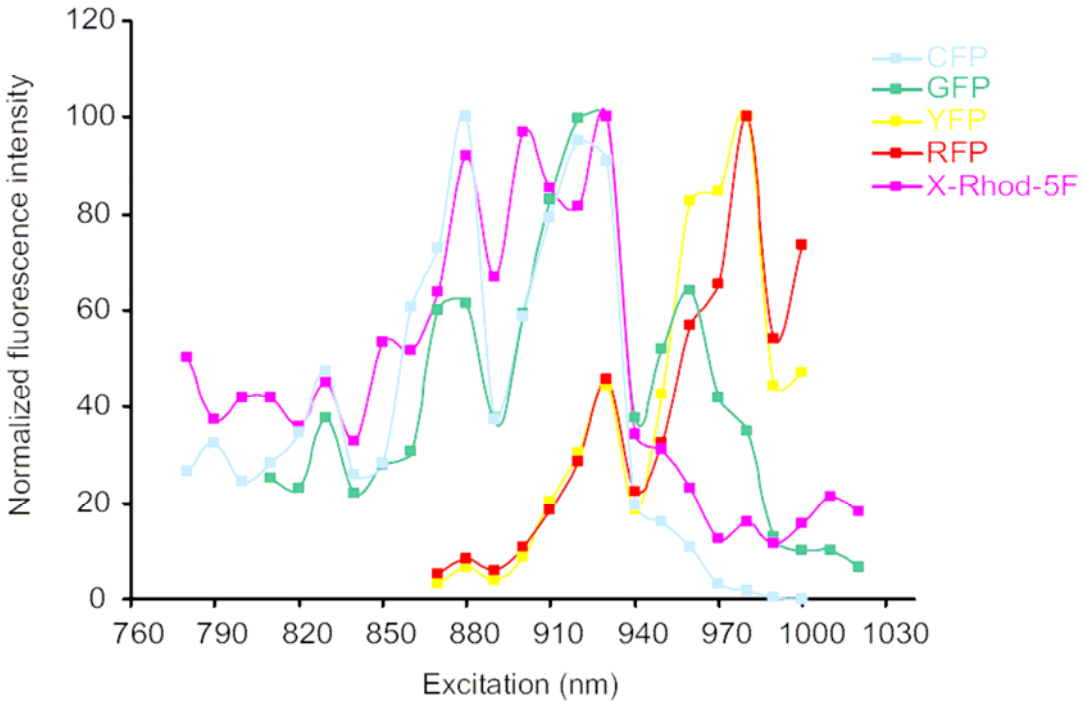

The figure shows the fluorescence excitation spectra for CFP, GFP, YFP, RFP (tdimer2) and X-Rhod-5F (a red calcium sensitive dye) measured at the apical dendrite of CA1 neurons. The laser power was measured by Si photodiode. The fluorescence intensity was normalized by laser power at different excitation wavelengths and the maximal intensity was then set to 100%.

References

Abraham WC, Bear MF (1996) Metaplasticity: the plasticity of synaptic plasticity. Trends in Neuroscience 19:126-130.

Andersen P, Sundberg SH, Sveen O, Wigstrom H (1977) Specific long-lasting potentiation of synaptic transmission in hippocampal slices. Nature 266:736-737.

Ando R, Mizuno H, Miyawaki A (2004) Regulated fast nucleocytoplasmic shuttling observed by reversible protein highlighting. Science 306:1370-1373.

Andrasfalvy BK, Smith MA, Borchardt T, Sprengel R, Magee JC (2003) Impaired regulation of synaptic strength in hippocampal neurons from GluR1-deficient mice. J Physiol 552:35-45.

Araya R, Jiang J, Eisenthal KB, Yuste R (2006) The spine neck filters membrane potentials. Proc Natl Acad Sci U S A 103:17961-17966.

Arenkiel BR, Peca J, Davison IG, Feliciano C, Deisseroth K, Augustine GJ, Ehlers MD, Feng G (2007) In vivo light-induced activation of neural circuitry in transgenic mice expressing channelrhodopsin-2. Neuron 54:205-218.

Bagal AA, Kao JP, Tang CM, Thompson SM (2005) Long-term potentiation of exogenous glutamate responses at single dendritic spines. Proc Natl Acad Sci U S A 102:14434-14439.

Baird GS, Zacharias DA, Tsien RY (1999) Circular permutation and receptor insertion within green fluorescent proteins. Proc Natl Acad Sci U S A 96:11241-11246.

Barnes CA, Jung MW, McNaughton BL, Korol DL, Andreasson K, Worley PF (1994) LTP saturation and spatial learning disruption: effects of task variables and saturation levels. J Neurosci 14:5793-5806.

Bennett MK, Erondu NE, Kennedy MB (1983) Purification and characterization of a calmodulin-dependent protein kinase that is highly concentrated in brain. J Biol Chem 258:12735-12744.

Bettler B, Kaupmann K, Mosbacher J, Gassmann M (2004) Molecular structure and physiological functions of GABA(B) receptors. Physiol Rev 84:835-867.

Bi G, Poo M (2001) Synaptic modification by correlated activity: Hebb's postulate revisited. Annu Rev Neurosci 24:139-166.

Bischoff S, Leonhard S, Reymann N, Schuler V, Shigemoto R, Kaupmann K, Bettler B (1999) Spatial distribution of GABA(B)R1 receptor mRNA and binding sites in the rat brain. J Comp Neurol 412:1-16.

Blein S, Ginham R, Uhrin D, Smith BO, Soares DC, Veltel S, McIlhinney RA, White JH, Barlow PN (2004) Structural analysis of the complement control protein (CCP) modules of GABA(B) receptor 1a: only one of the two CCP modules is compactly folded. J Biol Chem 279:48292-48306.

Bliss TV, Gardner-Medwin AR (1973) Long-lasting potentiation of synaptic transmission in the dentate area of the unanaestetized rabbit following stimulation of the perforant path. J Physiol 232:357-374.

Bliss TV, Lomo T (1973) Long-lasting potentiation of synaptic transmission in the dentate area of the anaesthetized rabbit following stimulation of the perforant path. J Physiol 232:331-356.

Bliss TV, Collingridge GL (1993) A synaptic model of memory: long-term potentiation in the hippocampus. Nature 361:31-39.

Bloodgood BL, Sabatini BL (2005) Neuronal activity regulates diffusion across the neck of dendritic spines. Science 310:866-869.

Bonanno G, Raiteri M (1993) Multiple GABAB receptors. Trends Pharmacol Sci 14:259-261.

Bonanno G, Fassio A, Schmid G, Severi P, Sala R, Raiteri M (1997) Pharmacologically distinct GABAB receptors that mediate inhibition of GABA and glutamate release in human neocortex. Br J Pharmacol 120:60-64.

Bowery NG, Bettler B, Froestl W, Gallagher JP, Marshall F, Raiteri M, Bonner TI, Enna SJ (2002) International Union of Pharmacology. XXXIII. Mammalian gamma-aminobutyric acid(B) receptors: structure and function. Pharmacol Rev 54:247-264.

Boyden ES, Zhang F, Bamberg E, Nagel G, Deisseroth K (2005) Millisecond-timescale, genetically targeted optical control of neural activity. Nat Neurosci 8:1263-1268.

Broadbent NJ, Squire LR, Clark RE (2004) Spatial memory, recognition memory, and the hippocampus. Proc Natl Acad Sci U S A 101:14515-14520.

Burrone J, Murthy VN (2003) Synaptic gain control and homeostasis. Curr Opin Neurobiol 13:560-567.

Burrone J, O'Byrne M, Murthy VN (2002) Multiple forms of synaptic plasticity triggered by selective suppression of activity in individual neurons. Nature 420:414-418.

Campbell RE, Tour O, Palmer AE, Steinbach PA, Baird GS, Zacharias DA, Tsien RY (2002) A monomeric red fluorescent protein. Proc Natl Acad Sci U S A 99:7877-7882.

Carter AG, Sabatini BL (2004) State-dependent calcium signaling in dendritic spines of striatal medium spiny neurons. Neuron 44:483-493.

Cassel JC, Cassel S, Galani R, Kelche C, Will B, Jarrard L (1998) Fimbria-fornix vs selective hippocampal lesions in rats: effects on locomotor activity and spatial learning and memory. Neurobiol Learn Mem 69:22-45.

Chen HX, Otmakhov N, Lisman J (1999) Requirements for LTP induction by pairing in hippocampal CA1 pyramidal cells. J Neurophysiol 82:526-532.

Colbran RJ, Brown AM (2004) Calcium/calmodulin-dependent protein kinase II and synaptic plasticity. Curr Opin Neurobiol 14:318-327.

Collingridge GL, Kehl SJ, McLennan H (1983) Excitatory amino acids in synaptic transmission in the Schaffer collateral-commissural pathway of the rat hippocampus. J Physiol 334:33-46.

Couve A, Thomas P, Calver AR, Hirst WD, Pangalos MN, Walsh FS, Smart TG, Moss SJ (2002) Cyclic AMP-dependent protein kinase phosphorylation facilitates GABA(B) receptor-effector coupling. Nat Neurosci 5:415-424.

Cryan JF, Kaupmann K (2005) Don't worry 'B' happy!: a role for GABA(B) receptors in anxiety and depression. Trends Pharmacol Sci 26:36-43.

Cunningham MD, Enna SJ (1996) Evidence for pharmacologically distinct GABAB receptors associated with cAMP production in rat brain. Brain Res 720:220-224.

Davies CH, Collingridge GL (1996) Regulation of EPSPs by the synaptic activation of GABAB autoreceptors in rat hippocampus. J Physiol 496 (Pt 2):451-470.

Davies CH, Starkey SJ, Pozza MF, Collingridge GL (1991) GABA autoreceptors regulate the induction of LTP. Nature 349:609-611.

De Paola V, Holtmaat A, Knott G, Song S, Wilbrecht L, Caroni P, Svoboda K (2006) Cell type-specific structural plasticity of axonal branches and boutons in the adult neocortex. Neuron 49:861-875.

Debanne D, Gahwiler BH, Thompson SM (1999) Heterogeneity of synaptic plasticity at unitary CA3-CA1 and CA3-CA3 connections in rat hippocampal slice cultures. J Neurosci 19:10664-10671.

Deisz RA, Billard JM, Zieglgansberger W (1997) Presynaptic and postsynaptic GABAB receptors of neocortical neurons of the rat in vitro: differences in pharmacology and ionic mechanisms. Synapse 25:62-72.

Denk W, Svoboda K (1997) Photon upmanship: why multiphoton imaging is more than a gimmick. Neuron 18:351-357.

Denk W, Strickler JH, Webb WW (1990) Two-photon laser scanning fluorescence microscopy. Science 248:73-76.

Denk W, Yuste R, Svoboda K, Tank DW (1996) Imaging calcium dynamics in dendritic spines. 6:372-378.

Desai NS, Cudmore RH, Nelson SB, Turrigiano GG (2002) Critical periods for experience-dependent synaptic scaling in visual cortex. Nat Neurosci 5:783-789.

Diez-Garcia J, Akemann W, Knopfel T (2007) In vivo calcium imaging from genetically specified target cells in mouse cerebellum. Neuroimage 34:859-869.

Dinkel A, Aicher WK, Warnatz K, Burki K, Eibel H, Ledermann B (1999) Efficient generation of transgenic BALB/c mice using BALB/c embryonic stem cells. J Immunol Methods 223:255-260.

Dosemeci A, Tao-Cheng JH, Vinade L, Winters CA, Pozzo-Miller L, Reese TS (2001) Glutamate-induced transient modification of the postsynaptic density. Proc Natl Acad Sci U S A 98:10428-10432.

Durand GM, Kovalchuk Y, Konnerth A (1996) Long-term potentiation and functional synapse induction in developing hippocampus. Nature 381:71-75.

Elgersma Y, Fedorov NB, Ikonen S, Choi ES, Elgersma M, Carvalho OM, Giese KP, Silva AJ (2002) Inhibitory autophosphorylation of CaMKII controls PSD association, plasticity, and learning. Neuron 36:493-505.

Engert F, Bonhoeffer T (1997) Synapse specificity of long-term potentiation breaks down at short distances. Nature 388:279-284.

Engert F, Bonhoeffer T (1999) Dendritic spine changes associated with hippocampal long-term synaptic plasticity. Nature 399:66-70.

Erondu NE, Kennedy MB (1985) Regional distribution of type II Ca2+/calmodulin-dependent protein kinase in rat brain. J Neurosci 5:3270-3277.

Feldman DE (2000) Timing-based LTP and LTD at vertical inputs to layer II/III pyramidal cells in rat barrel cortex. Neuron 27:45-56.

Fong DK, Rao A, Crump FT, Craig AM (2002) Rapid synaptic remodeling by protein kinase C: reciprocal translocation of NMDA receptors and calcium/calmodulin-dependent kinase II. J Neurosci 22:2153-2164.

Gasparini S, Magee JC (2006) State-dependent dendritic computation in hippocampal CA1 pyramidal neurons. J Neurosci 26:2088-2100.

Gasparini S, Saviane C, Voronin LL, Cherubini E (2000) Silent synapses in the developing hippocampus: lack of functional AMPA receptors or low probability of glutamate release? Proc Natl Acad Sci U S A 97:9741-9746.

Gassmann M, Shaban H, Vigot R, Sansig G, Haller C, Barbieri S, Humeau Y, Schuler V, Muller M, Kinzel B, Klebs K, Schmutz M, Froestl W, Heid J, Kelly PH, Gentry C, Jaton AL, Van der Putten H, Mombereau C, Lecourtier L, Mosbacher J, Cryan JF, Fritschy JM, Luthi A, Kaupmann K, Bettler B (2004) Redistribution of GABAB(1) protein and atypical GABAB responses in GABAB(2)-deficient mice. J Neurosci 24:6086-6097.

Gemignani A, Paudice P, Bonanno G, Raiteri M (1994) Pharmacological discrimination between gamma-aminobutyric acid type B receptors regulating cholecystokinin and somatostatin release from rat neocortex synaptosomes. Mol Pharmacol 46:558-562.

Giese KP, Fedorov NB, Filipkowski RK, Silva AJ (1998) Autophosphorylation at Thr286 of the alpha calcium-calmodulin kinase II in LTP and learning. Science 279:870-873.

Grace CR, Perrin MH, DiGruccio MR, Miller CL, Rivier JE, Vale WW, Riek R (2004) NMR structure and peptide hormone binding site of the first extracellular domain of a type B1 G protein-coupled receptor. Proc Natl Acad Sci U S A 101:12836-12841.

Gustafsson B, Wigstrom H, Abraham WC, Huang YY (1987) Long-term potentiation in the hippocampus using depolarizing current pulses as the conditioning stimulus to single volley synaptic potentials. J Neurosci 7:774-780.

Hanson PI, Schulman H (1992) Inhibitory autophosphorylation of multifunctional Ca2+/calmodulin-dependent protein kinase analyzed by site-directed mutagenesis. J Biol Chem 267:17216-17224.

Harris KM, Stevens JK (1989) Dendritic spines of CA 1 pyramidal cells in the rat hippocampus: serial electron microscopy with reference to their biophysical characteristics. J Neurosci 9:2982-2997.

Harris KM, Kater SB (1994) Dendritic spines: cellular specializations imparting both stability and flexibility to synaptic function. Annu Rev Neurosci 17:341-371.

Harris KM, Sultan P (1995) Variation in the number, location and size of synaptic vesicles provides an anatomical basis for the nonuniform probability of release at hippocampal CA1 synapses. Neuropharmacology 34:1387-1395.

Harris KM, Jensen FE, Tsao B (1992) Three-dimensional structure of dendritic spines and synapses in rat hippocampus (CA1) at postnatal day 15 and adult ages: implications for the maturation of synaptic physiology and long-term potentiation. Journal of Neuroscience 12:2685-2705.

Harris KM, Fiala JC, Ostroff L (2003) Structural changes at dendritic spine synapses during long-term potentiation. Philos Trans R Soc Lond B Biol Sci 358:745-748.

Hartman KN, Pal SK, Burrone J, Murthy VN (2006) Activity-dependent regulation of inhibitory synaptic transmission in hippocampal neurons. Nat Neurosci 9:642-649.

Hausser M, Smith SL (2007) Neuroscience: controlling neural circuits with light. Nature 446:617-619.

Hayashi Y, Shi SH, Esteban JA, Piccini A, Poncer JC, Malinow R (2000) Driving AMPA receptors into synapses by LTP and CaMKII: requirement for GluR1 and PDZ domain interaction. Science 287:2262-2267.

Helmchen F, Fee MS, Tank DW, Denk W (2001) A miniature head-mounted two-photon microscope. high-resolution brain imaging in freely moving animals. Neuron 31:903-912.

Heynen AJ, Yoon BJ, Liu CH, Chung HJ, Huganir RL, Bear MF (2003) Molecular mechanism for loss of visual cortical responsiveness following brief monocular deprivation. Nat Neurosci 6:854-862.

Holthoff K, Tsay D, Yuste R (2002) Calcium dynamics of spines depend on their dendritic location. Neuron 33:425-437.

Holtmaat A, Wilbrecht L, Knott GW, Welker E, Svoboda K (2006) Experience-dependent and cell-type-specific spine growth in the neocortex. Nature 441:979-983.

Horton AC, Ehlers MD (2003) Neuronal polarity and trafficking. Neuron 40:277-295.

Huang YY, Kandel ER (1998) Postsynaptic induction and PKA-dependent expression of LTP in the lateral amygdala. Neuron 21:169-178.

Hudmon A, Schulman H (2002a) Neuronal CA2+/calmodulin-dependent protein kinase II: the role of structure and autoregulation in cellular function. Annu Rev Biochem 71:473-510.

Hudmon A, Schulman H (2002b) Structure-function of the multifunctional Ca2+/calmodulin-dependent protein kinase II. Biochem J 364:593-611.

Isaac JT, Nicoll RA, Malenka RC (1995) Evidence for silent synapses: implications for the expression of LTP. Neuron 15:427-434.

Isaac JT, Luthi A, Palmer MJ, Anderson WW, Benke TA, Collingridge GL (1998) An investigation of the expression mechanism of LTP of AMPA receptor-mediated synaptic transmission at hippocampal CA1 synapses using failures analysis and dendritic recordings. Neuropharmacology 37:1399-1410.

Ishizuka T, Kakuda M, Araki R, Yawo H (2006) Kinetic evaluation of photosensitivity in genetically engineered neurons expressing green algae light-gated channels. Neurosci Res 54:85-94.

Johnson JW, Ascher P (1987) Glycine potentiates the NMDA response in cultured mouse brain neurons. Nature 325:529-531.

Kanaseki T, Ikeuchi Y, Sugiura H, Yamauchi T (1991) Structural features of Ca2+/calmodulin-dependent protein kinase II revealed by electron microscopy. J Cell Biol 115:1049-1060.

Kasai H, Matsuzaki M, Noguchi J, Yasumatsu N, Nakahara H (2003) Structure-stability-function relationships of dendritic spines. Trends Neurosci 26:360-368.

Kaupmann K, Huggel K, Heid J, Flor PJ, Bischoff S, Mickel SJ, McMaster G, Angst C, Bittiger H, Froestl W, Bettler B (1997) Expression cloning of GABA(B) receptors uncovers similarity to metabotropic glutamate receptors. Nature 386:239-246.

Kaupmann K, Malitschek B, Schuler V, Heid J, Froestl W, Beck P, Mosbacher J, Bischoff S, Kulik A, Shigemoto R, Karschin A, Bettler B (1998) GABA(B)-

receptor subtypes assemble into functional heteromeric complexes. Nature 396:683-687.

Kennedy MB, Bennett MK, Erondu NE (1983) Biochemical and immunochemical evidence that the "major postsynaptic density protein" is a subunit of a calmodulin-dependent protein kinase. Proc Natl Acad Sci U S A 80:7357-7361.

Kim KJ, Kim HE, Lee KH, Han W, Yi MJ, Jeong J, Oh BH (2004) Two-promoter vector is highly efficient for overproduction of protein complexes. Protein Sci 13:1698-1703.

Knott GW, Holtmaat A, Wilbrecht L, Welker E, Svoboda K (2006) Spine growth precedes synapse formation in the adult neocortex in vivo. Nat Neurosci 9:1117-1124.

Koester HJ, Sakmann B (1998) Calcium dynamics in single spines during coincident pre- and postsynaptic activity depend on relative timing of back-propagating action potentials and subthreshold excitatory postsynaptic potentials. Proc Natl Acad Sci U S A 95:9596-9601.

Kolodziej SJ, Hudmon A, Waxham MN, Stoops JK (2000) Three-dimensional reconstructions of calcium/calmodulin-dependent (CaM) kinase IIalpha and truncated CaM kinase IIalpha reveal a unique organization for its structural core and functional domains. J Biol Chem 275:14354-14359.

Kopec CD, Li B, Wei W, Boehm J, Malinow R (2006) Glutamate receptor exocytosis and spine enlargement during chemically induced long-term potentiation. J Neurosci 26:2000-2009.

Kugler S, Meyn L, Holzmuller H, Gerhardt E, Isenmann S, Schulz JB, Bahr M (2001) Neuron-specific expression of therapeutic proteins: evaluation of different cellular promoters in recombinant adenoviral vectors. Mol Cell Neurosci 17:78-96.

Kulik A, Nakadate K, Nyiri G, Notomi T, Malitschek B, Bettler B, Shigemoto R (2002) Distinct localization of GABA(B) receptors relative to synaptic sites in the rat cerebellum and ventrobasal thalamus. Eur J Neurosci 15:291-307.

Kulik A, Vida I, Lujan R, Haas CA, Lopez-Bendito G, Shigemoto R, Frotscher M (2003) Subcellular localization of metabotropic GABA(B) receptor subunits GABA(B1a/b) and GABA(B2) in the rat hippocampus. J Neurosci 23:11026-11035.

Kulik A, Vida I, Fukazawa Y, Guetg N, Kasugai Y, Marker CL, Rigato F, Bettler B, Wickman K, Frotscher M, Shigemoto R (2006) Compartment-dependent colocalization of Kir3.2-containing K+ channels and GABAB receptors in hippocampal pyramidal cells. J Neurosci 26:4289-4297.

Kullmann DM (1994) Amplitude fluctuations of dual-component EPSCs in hippocampal pyramidal cells: implications for long-term potentiation. Neuron 12:1111-1120.

Lang C, Barco A, Zablow L, Kandel ER, Siegelbaum SA, Zakharenko SS (2004) Transient expansion of synaptically connected dendritic spines upon induction of hippocampal long-term potentiation. Proc Natl Acad Sci U S A 101:16665-16670.

Lee MY, Song H, Nakai J, Ohkura M, Kotlikoff MI, Kinsey SP, Golovina VA, Blaustein MP (2006) Local subplasma membrane Ca2+ signals detected by a tethered Ca2+ sensor. Proc Natl Acad Sci U S A 103:13232-13237.

Lehtinen MJ, Meri S, Jokiranta TS (2004) Interdomain contact regions and angles between adjacent short consensus repeat domains. J Mol Biol 344:1385-1396.

Lei S, McBain CJ (2003) GABA B receptor modulation of excitatory and inhibitory synaptic transmission onto rat CA3 hippocampal interneurons. J Physiol 546:439-453.

Lev-Ram V, Wong ST, Storm DR, Tsien RY (2002) A new form of cerebellar long-term potentiation is postsynaptic and depends on nitric oxide but not cAMP. Proc Natl Acad Sci U S A 99:8389-8393.

Liao D, Hessler NA, Malinow R (1995) Activation of postsynaptically silent synapses during pairing-induced LTP in CA1 region of hippocampal slice. Nature 375:400-404.

Liao D, Zhang X, O'Brien R, Ehlers MD, Huganir RL (1999) Regulation of morphological postsynaptic silent synapses in developing hippocampal neurons. Nat Neurosci 2:37-43.

Lisman J, Schulman H, Cline H (2002) The molecular basis of CaMKII function in synaptic and behavioural memory. Nat Rev Neurosci 3:175-190.

Lisman JE, Zhabotinsky AM (2001) A model of synaptic memory: a CaMKII/PP1 switch that potentiates transmission by organizing an AMPA receptor anchoring assembly. Neuron 31:191-201.

Lisman JE, McIntyre CC (2001) Synaptic plasticity: a molecular memory switch. Curr Biol 11:R788-791.

Lledo PM, Hjelmstad GO, Mukherji S, Soderling TR, Malenka RC, Nicoll RA (1995) Calcium/calmodulin-dependent kinase II and long-term potentiation enhance synaptic transmission by the same mechanism. Proc Natl Acad Sci U S A 92:11175-11179.

Luscher C, Jan LY, Stoffel M, Malenka RC, Nicoll RA (1997) G protein-coupled inwardly rectifying K+ channels (GIRKs) mediate postsynaptic but not presynaptic transmitter actions in hippocampal neurons. Neuron 19:687-695.

Luthi A, Schwyzer L, Mateos JM, Gahwiler BH, McKinney RA (2001) NMDA receptor activation limits the number of synaptic connections during hippocampal development. Nat Neurosci 4:1102-1107.

Majewska AK, Newton JR, Sur M (2006) Remodeling of synaptic structure in sensory cortical areas in vivo. J Neurosci 26:3021-3029.

Malenka RC, Nicoll RA (1999) Long-term potentiation--a decade of progress? Science J1 - Sci 285:1870-1874.

Malenka RC, Kauer JA, Perkel DJ, Nicoll RA (1989) The impact of postsynaptic calcium on synaptic transmission--its role in long-term potentiation. Trends Neurosci 12:444-450.

Maletic-Savatic M, Malinow R, Svoboda K (1999) Rapid dendritic morphogenesis in CA1 hippocampal dendrites induced by synaptic activity. Science J1 - Sci 283:1923-1927.

Malinow R, Malenka RC (2002) AMPA receptor trafficking and synaptic plasticity. Annu Rev Neurosci 25:103-126.

Malinow R, Schulman H, Tsien RW (1989) Inhibition of postsynaptic PKC or CaMKII blocks induction but not expression of LTP. Science 245:862-866.

Malitschek B, Ruegg D, Heid J, Kaupmann K, Bittiger H, Frostl W, Bettler B, Kuhn R (1998) Developmental changes of agonist affinity at GABABR1 receptor variants in rat brain. Mol Cell Neurosci 12:56-64.

Markram H, Tsodyks M (1996) Redistribution of synaptic efficacy between neocortical pyramidal neurons. Nature 382:807-810.

Marshall FH, Jones KA, Kaupmann K, Bettler B (1999) GABAB receptors - the first 7TM heterodimers. Trends Pharmacol Sci 20:396-399.

Martin SJ, Grimwood PD, Morris RG (2000) Synaptic plasticity and memory: an evaluation of the hypothesis. Annu Rev Neurosci 23:649-711.

Matsuzaki M, Honkura N, Ellis-Davies GC, Kasai H (2004) Structural basis of long-term potentiation in single dendritic spines. Nature 429:761-766.

Matsuzaki M, Ellis-Davies GC, Nemoto T, Miyashita Y, Iino M, Kasai H (2001a) Dendritic spine geometry is critical for AMPA receptor expression in hippocampal CA1 pyramidal neurons. Nature Neuroscience 4:1086-1092.

Matsuzaki M, Ellis-Davies GC, Nemoto T, Miyashita Y, Iino M, Kasai H (2001b) Dendritic spine geometry is critical for AMPA receptor expression in hippocampal CA1 pyramidal neurons. Nat Neurosci 4:1086-1092.

Matus A (2000) Actin-based plasticity in dendritic spines. Science 290:754-758.

McLatchie LM, Fraser NJ, Main MJ, Wise A, Brown J, Thompson N, Solari R, Lee MG, Foord SM (1998) RAMPs regulate the transport and ligand specificity of the calcitonin-receptor-like receptor. Nature 393:333-339.

Merrill MA, Chen Y, Strack S, Hell JW (2005) Activity-driven postsynaptic translocation of CaMKII. Trends Pharmacol Sci 26:645-653.

Miller SG, Kennedy MB (1985) Distinct forebrain and cerebellar isozymes of type II Ca2+/calmodulin-dependent protein kinase associate differently with the postsynaptic density fraction. J Biol Chem 260:9039-9046.

Mintz IM, Bean BP (1993) GABAB receptor inhibition of P-type Ca2+ channels in central neurons. Neuron 10:889-898.

Mohler H, Fritschy JM (1999) GABAB receptors make it to the top--as dimers. Trends Pharmacol Sci 20:87-89.

Morris R (1984) Developments of a water-maze procedure for studying spatial learning in the rat. J Neurosci Methods 11:47-60.

Morrisett RA, Mott DD, Lewis DV, Swartzwelder HS, Wilson WA (1991) GABAB-receptor-mediated inhibition of the N-methyl-D-aspartate component of synaptic transmission in the rat hippocampus. J Neurosci 11:203-209.

Mukherji S, Soderling TR (1994) Regulation of Ca2+/calmodulin-dependent protein kinase II by inter- and intrasubunit-catalyzed autophosphorylations. J Biol Chem 269:13744-13747.

Muller RU, Kubie JL, Ranck JB, Jr. (1987) Spatial firing patterns of hippocampal complex-spike cells in a fixed environment. J Neurosci 7:1935-1950.

Nagai T, Sawano A, Park ES, Miyawaki A (2001) Circularly permuted green fluorescent proteins engineered to sense Ca2+. Proc Natl Acad Sci U S A 98:3197-3202.

Nagel G, Szellas T, Kateriya S, Adeishvili N, Hegemann P, Bamberg E (2005) Channelrhodopsins: directly light-gated cation channels. Biochem Soc Trans 33:863-866.

Nagel G, Szellas T, Huhn W, Kateriya S, Adeishvili N, Berthold P, Ollig D, Hegemann P, Bamberg E (2003) Channelrhodopsin-2, a directly light-gated cation-selective membrane channel. Proc Natl Acad Sci U S A 100:13940-13945.

Nakai J, Ohkura M, Imoto K (2001) A high signal-to-noise Ca(2+) probe composed of a single green fluorescent protein. Nat Biotechnol 19:137-141.

Neveu D, Zucker RS (1996) Postsynaptic levels of Ca^{2+} needed to trigger LTD and LTP. Neuron 16:619-629.

Nevian T, Sakmann B (2004) Single spine Ca2+ signals evoked by coincident EPSPs and backpropagating action potentials in spiny stellate cells of layer 4 in the juvenile rat somatosensory barrel cortex. J Neurosci 24:1689-1699.

Nicoll RA, Malenka RC (1995) Contrasting properties of two forms of long-term potentiation in the hippocampus. Nature 377:115-118.

Nicoll RA, Malenka RC (1999) Expression mechanisms underlying NMDA receptor-dependent long-term potentiation. 868:515-525.

Nikonenko I, Jourdain P, Muller D (2003) Presynaptic remodeling contributes to activity-dependent synaptogenesis. J Neurosci 23:8498-8505.

Nimchinsky EA, Sabatini BL, Svoboda K (2002) Structure and function of dendritic spines. Annu Rev Physiol 64:313-353.

Noguchi J, Matsuzaki M, Ellis-Davies GC, Kasai H (2005) Spine-neck geometry determines NMDA receptor-dependent Ca2+ signaling in dendrites. Neuron 46:609-622.

Nusser Z, Lujan R, Laube G, Roberts JD, Molnar E, Somogyi P (1998) Cell type and pathway dependence of synaptic AMPA receptor number and variability in the hippocampus. Neuron 21:545-559.

O'Keefe J, Dostrovsky J (1971) The hippocampus as a spatial map. Preliminary evidence from unit activity in the freely-moving rat. Brain Res 34:171-175.

Oertner TG, Sabatini BL, Nimchinsky EA, Svoboda K (2002) Facilitation at single synapses probed with optical quantal analysis. Nature Neuroscience 5:657-664.

Oheim M, Beaurepaire E, Chaigneau E, Mertz J, Charpak S (2001) Two-photon microscopy in brain tissue: parameters influencing the imaging depth. J Neurosci Methods 111:29-37.

Olton DS (1987) The radial arm maze as a tool in behavioral pharmacology. Physiol Behav 40:793-797.

Otmakhov N, Tao-Cheng JH, Carpenter S, Asrican B, Dosemeci A, Reese TS, Lisman J (2004) Persistent accumulation of calcium/calmodulin-dependent protein kinase II in dendritic spines after induction of NMDA receptor-dependent chemical long-term potentiation. J Neurosci 24:9324-9331.

Palmer MJ, Isaac JT, Collingridge GL (2004) Multiple, developmentally regulated expression mechanisms of long-term potentiation at CA1 synapses. J Neurosci 24:4903-4911.

Per Andersen RM, David Amaral, Tim Bliss, & John O'Keefe (2007) The Hippocampus Book: Oxford University Press.

Perez-Garci E, Gassmann M, Bettler B, Larkum ME (2006) The GABAB1b isoform mediates long-lasting inhibition of dendritic Ca2+ spikes in layer 5 somatosensory pyramidal neurons. Neuron 50:603-616.

Petersen CC, Malenka RC, Nicoll RA, Hopfield JJ (1998) All-or-none potentiation at CA3-CA1 synapses. Proc Natl Acad Sci U S A 95:4732-4737.

Petersen JD, Chen X, Vinade L, Dosemeci A, Lisman JE, Reese TS (2003) Distribution of postsynaptic density (PSD)-95 and Ca2+/calmodulin-dependent protein kinase II at the PSD. J Neurosci 23:11270-11278.

Petreanu L, Huber D, Sobczyk A, Svoboda K (2007) Channelrhodopsin-2-assisted circuit mapping of long-range callosal projections. Nat Neurosci 10:663-668.

Pineda VV, Athos JI, Wang H, Celver J, Ippolito D, Boulay G, Birnbaumer L, Storm DR (2004) Removal of G(ialpha1) constraints on adenylyl cyclase in the hippocampus enhances LTP and impairs memory formation. Neuron 41:153-163.

Pologruto TA, Sabatini BL, Svoboda K (2003) ScanImage: Flexible software for operating laser scanning microscopes. Biomed Eng Online 2:13.

Pologruto TA, Yasuda R, Svoboda K (2004) Monitoring neural activity and [Ca2+] with genetically encoded Ca2+ indicators. J Neurosci 24:9572-9579.

Poncer JC, McKinney RA, Gahwiler BH, Thompson SM (1997) Either N- or P-type calcium channels mediate GABA release at distinct hippocampal inhibitory synapses. Neuron 18:463-472.

Pozza MF, Manuel NA, Steinmann M, Froestl W, Davies CH (1999) Comparison of antagonist potencies at pre- and post-synaptic GABA(B) receptors at inhibitory synapses in the CA1 region of the rat hippocampus. Br J Pharmacol 127:211-219.

Prosser HM, Gill CH, Hirst WD, Grau E, Robbins M, Calver A, Soffin EM, Farmer CE, Lanneau C, Gray J, Schenck E, Warmerdam BS, Clapham C, Reavill C, Rogers DC, Stean T, Upton N, Humphreys K, Randall A, Geppert M, Davies CH, Pangalos MN (2001) Epileptogenesis and enhanced prepulse inhibition in GABA(B1)-deficient mice. Mol Cell Neurosci 17:1059-1070.

Sakaba T, Neher E (2003) Direct modulation of synaptic vesicle priming by GABA(B) receptor activation at a glutamatergic synapse. Nature 424:775-778.

Salin PA, Malenka RC, Nicoll RA (1996) Cyclic AMP mediates a presynaptic form of LTP at cerebellar parallel fiber synapses. Neuron 16:797-803.

Sampo B, Kaech S, Kunz S, Banker G (2003) Two distinct mechanisms target membrane proteins to the axonal surface. Neuron 37:611-624.

Sanhueza M, McIntyre CC, Lisman JE (2007) Reversal of synaptic memory by Ca2+/calmodulin-dependent protein kinase II inhibitor. J Neurosci 27:5190-5199.

Scanziani M (2000) GABA spillover activates postsynaptic GABA(B) receptors to control rhythmic hippocampal activity. Neuron 25:673-681.

Schuler V, Luscher C, Blanchet C, Klix N, Sansig G, Klebs K, Schmutz M, Heid J, Gentry C, Urban L, Fox A, Spooren W, Jaton AL, Vigouret J, Pozza M, Kelly PH, Mosbacher J, Froestl W, Kaslin E, Korn R, Bischoff S, Kaupmann K, van der Putten H, Bettler B (2001) Epilepsy, hyperalgesia, impaired memory, and loss of pre- and postsynaptic GABA(B) responses in mice lacking GABA(B(1)). Neuron 31:47-58.

Scimemi A, Fine A, Kullmann DM, Rusakov DA (2004) NR2B-containing receptors mediate cross talk among hippocampal synapses. J Neurosci 24:4767-4777.

Scoville WB, Milner B (1957) Loss of recent memory after bilateral hippocampal lesions. J Neurol Neurosurg Psychiatry 20:11-21.

Shaner NC, Steinbach PA, Tsien RY (2005) A guide to choosing fluorescent proteins. Nat Methods 2:905-909.

Sharma K, Fong DK, Craig AM (2006) Postsynaptic protein mobility in dendritic spines: long-term regulation by synaptic NMDA receptor activation. Mol Cell Neurosci 31:702-712.

Shen K, Meyer T (1999) Dynamic control of CaMKII translocation and localization in hippocampal neurons by NMDA receptor stimulation. Science 284:162-166.

Shen K, Teruel MN, Connor JH, Shenolikar S, Meyer T (2000) Molecular memory by reversible translocation of calcium/calmodulin-dependent protein kinase II. Nat Neurosci 3:881-886.

Shepherd GM, Harris KM (1998) Three-dimensional structure and composition of CA3-->CA1 axons in rat hippocampal slices: implications for presynaptic connectivity and compartmentalization. Journal of Neuroscience 18:8300-8310.

Shi S, Hayashi Y, Esteban JA, Malinow R (2001) Subunit-specific rules governing AMPA receptor trafficking to synapses in hippocampal pyramidal neurons. Cell 105:331-343.

Silva AJ, Stevens CF, Tonegawa S, Wang Y (1992a) Deficient hippocampal long-term potentiation in alpha-calcium-calmodulin kinase II mutant mice. Science 257:201-206.

Silva AJ, Paylor R, Wehner JM, Tonegawa S (1992b) Impaired spatial learning in alpha-calcium-calmodulin kinase II mutant mice. Science 257:206-211.

Sineshchekov OA, Jung KH, Spudich JL (2002) Two rhodopsins mediate phototaxis to low- and high-intensity light in Chlamydomonas reinhardtii. Proc Natl Acad Sci U S A 99:8689-8694.

Smith MA, Ellis-Davies GC, Magee JC (2003) Mechanism of the distance-dependent scaling of Schaffer collateral synapses in rat CA1 pyramidal neurons. J Physiol 548:245-258.

Sobczyk A, Scheuss V, Svoboda K (2005) NMDA receptor subunit-dependent [Ca2+] signaling in individual hippocampal dendritic spines. J Neurosci 25:6037-6046.

Soderling TR, Derkach VA (2000) Postsynaptic protein phosphorylation and LTP. Trends Neurosci 23:75-80.

Soderling TR, Chang B, Brickey D (2001) Cellular signaling through multifunctional Ca2+/calmodulin-dependent protein kinase II. J Biol Chem 276:3719-3722.

Steiger JL, Bandyopadhyay S, Farb DH, Russek SJ (2004) cAMP response element-binding protein, activating transcription factor-4, and upstream stimulatory factor differentially control hippocampal GABABR1a and GABABR1b subunit gene expression through alternative promoters. J Neurosci 24:6115-6126.

Stewart MG, Medvedev NI, Popov VI, Schoepfer R, Davies HA, Murphy K, Dallerac GM, Kraev IV, Rodriguez JJ (2005) Chemically induced long-term potentiation increases the number of perforated and complex postsynaptic densities but does not alter dendritic spine volume in CA1 of adult mouse hippocampal slices. Eur J Neurosci 21:3368-3378.

Stoppini L, Buchs PA, Muller D (1991) A simple method for organotypic cultures of nervous tissue. Journal of Neuroscience Methods 37:173-182.

Strack S, Choi S, Lovinger DM, Colbran RJ (1997) Translocation of autophosphorylated calcium/calmodulin-dependent protein kinase II to the postsynaptic density. J Biol Chem 272:13467-13470.

Svoboda K, Yasuda R (2006) Principles of two-photon excitation microscopy and its applications to neuroscience. Neuron 50:823-839.

Svoboda K, Denk W, Kleinfeld D, Tank DW (1997) In vivo dendritic calcium dynamics in neocortical pyramidal neurons. Nature 385:161-165.

Takao K, Okamoto K, Nakagawa T, Neve RL, Nagai T, Miyawaki A, Hashikawa T, Kobayashi S, Hayashi Y (2005) Visualization of synaptic Ca2+ /calmodulin-dependent protein kinase II activity in living neurons. J Neurosci 25:3107-3112.

Takumi Y, Ramirez-Leon V, Laake P, Rinvik E, Ottersen OP (1999) Different modes of expression of AMPA and NMDA receptors in hippocampal synapses. Nat Neurosci 2:618-624.

Tallini YN, Ohkura M, Choi BR, Ji G, Imoto K, Doran R, Lee J, Plan P, Wilson J, Xin HB, Sanbe A, Gulick J, Mathai J, Robbins J, Salama G, Nakai J, Kotlikoff MI (2006) Imaging cellular signals in the heart in vivo: Cardiac expression of

the high-signal Ca2+ indicator GCaMP2. Proc Natl Acad Sci U S A 103:4753-4758.

Tanaka J, Matsuzaki M, Tarusawa E, Momiyama A, Molnar E, Kasai H, Shigemoto R (2005) Number and density of AMPA receptors in single synapses in immature cerebellum. J Neurosci 25:799-807.

Thalhammer A, Rudhard Y, Tigaret CM, Volynski KE, Rusakov DA, Schoepfer R (2006) CaMKII translocation requires local NMDA receptor-mediated Ca2+ signaling. Embo J 25:5873-5883.

Theer P, Hasan MT, Denk W (2003) Two-photon imaging to a depth of 1000 microm in living brains by use of a Ti:Al2O3 regenerative amplifier. Opt Lett 28:1022-1024.

Toni N, Buchs PA, Nikonenko I, Bron CR, Muller D (1999) LTP promotes formation of multiple spine synapses between a single axon terminal and a dendrite. Nature 402:421-425.

Umeda T, Ebihara T, Okabe S (2005) Simultaneous observation of stably associated presynaptic varicosities and postsynaptic spines: morphological alterations of CA3-CA1 synapses in hippocampal slice cultures. Mol Cell Neurosci 28:264-274.

Vigot R, Barbieri S, Brauner-Osborne H, Turecek R, Shigemoto R, Zhang YP, Lujan R, Jacobson LH, Biermann B, Fritschy JM, Vacher CM, Muller M, Sansig G, Guetg N, Cryan JF, Kaupmann K, Gassmann M, Oertner TG, Bettler B (2006) Differential Compartmentalization and Distinct Functions of GABA(B) Receptor Variants. Neuron 50:589-601.

West AE, Griffith EC, Greenberg ME (2002) Regulation of transcription factors by neuronal activity. Nat Rev Neurosci 3:921-931.

Whitlock JR, Heynen AJ, Shuler MG, Bear MF (2006) Learning induces long-term potentiation in the hippocampus. Science 313:1093-1097.

Xavier GF, Oliveira-Filho FJ, Santos AM (1999) Dentate gyrus-selective colchicine lesion and disruption of performance in spatial tasks: difficulties in "place strategy" because of a lack of flexibility in the use of environmental cues? Hippocampus 9:668-681.

Xiao MY, Wasling P, Hanse E, Gustafsson B (2004) Creation of AMPA-silent synapses in the neonatal hippocampus. Nat Neurosci 7:236-243.

Yamada K, Yu B, Gallagher JP (1999) Different subtypes of GABAB receptors are present at pre- and postsynaptic sites within the rat dorsolateral septal nucleus. J Neurophysiol 81:2875-2883.

Yasuda R, Nimchinsky EA, Scheuss V, Pologruto TA, Oertner TG, Sabatini BL, Svoboda K (2004) Imaging calcium concentration dynamics in small neuronal compartments. Sci STKE 2004:pl5.

Yuste R, Bonhoeffer T (2001) Morphological changes in dendritic spines associated with long-term synaptic plasticity. Annu Rev Neurosci 24:1071-1089.

Zamanillo D, Sprengel R, Hvalby O, Jensen V, Burnashev N, Rozov A, Kaiser KM, Koster HJ, Borchardt T, Worley P, Lubke J, Frotscher M, Kelly PH, Sommer B, Andersen P, Seeburg PH, Sakmann B (1999) Importance of AMPA receptors for hippocampal synaptic plasticity but not for spatial learning. Science 284:1805-1811.

Zhang YP, Oertner TG (2007) Optical induction of synaptic plasticity using a light-sensitive channel. Nat Methods 4:139-141.

Zhou Q, Homma KJ, Poo MM (2004) Shrinkage of dendritic spines associated with long-term depression of hippocampal synapses. Neuron 44:749-757.

Zipfel WR, Williams RM, Webb WW (2003) Nonlinear magic: multiphoton microscopy in the biosciences. Nat Biotechnol 21:1369-1377.

Zuo Y, Yang G, Kwon E, Gan WB (2005) Long-term sensory deprivation prevents dendritic spine loss in primary somatosensory cortex. Nature 436:261-265.

Abbreviations

ACSF	artificial cerebrospinal fluid
AMPAR	α-amino-3-hydroxy-5-methylisoxazole-4- propionic acid receptor
AP	action potential
bAP	backpropagating action potential
CA	*Cornu Ammonis*
CaMKII	calcium/calmodulin-dependent protein kinase II
CFP	cyan fluorescent protein
ChR2	channelrhodopsin-2
cpGFP	circularly permuted green fluorescent protein
CV	coefficient of variation
DG	dentate gyrus
EC	entorhinal cortex
EM	electron microscope
EPSCs	excitatory postsynaptic currents
EPSPs	excitatory postsynaptic potentials
GABA	γ-aminobutyric acid
GFP	green fluorescent protein
IPSCs	inhibitory postsynaptic currents
LTP	long-term potentiation
NMDAR	N-methyl-D-aspartate receptors
PBS	phosphate buffered saline
Pr	release probability
PSD	postsynaptic density
RFP	red fluorescent protein
TTX	tetrodotoxin
YFP	yellow fluorescent protein
2-P	Two-photon

Acknowledgements

Dr. Thomas Oertner

for this wonderful project and great guidance, support, advice and care.

Dr. Andreas Lüthi

for great support and critical discussions.

Daniela Gerosa-Erni

for excellent technical assistance. No work can be done without your nice cultures.

Aaron Ponti & Ursin Stauss

for writing the 3D spine analysis program and helping me with Matlab programming.

Nunu Mchedlishvili

for writing the automatic contact finding program (ContactChecker).

Francois Grenier

for critical reading of the manuscript.

Åsa Müller-Grunditz and Niklaus Holbro

for helping me with synaptic calcium imaging and two-photon uncaging experiments. It is a lot fun to work with you.

my parents, my brother and Martin

for enormous understanding, encouragement and support during all times.

Curriculum Vitae

Personal Profile:

Name:	Yan-Ping Zhang
Date of birth:	7 Apr. 1978
Place of birth:	Shanghai, China
e-mail:	yan-ping.zhang@fmi.ch
Address:	Haltingerstrasse 13, CH-4057, Basel, Switzerland
Telephone:	+41 616978274

Education:

2003- present	Basel University (Switzerland) PhD thesis work at Friedrich Miescher Institute
2001- 2003	Leiden University (the Netherlands) Major in Bio-Pharmaceutical Sciences (MSc)
1996- 2001	Fudan University (China) Major in Pharmacology (BM)

Awards:

Jun 2007	EMBO long term fellowship
July 2003	S.E. de Jongh Award (the Netherlands)
Sep 2001- July 2003	China Scholarship Council (CSC) Scholarship for Studying Abroad
Jun 2001	"Excellent" (*i.e. cum laude*) Graduate Award of Shanghai (China)

Publications:

1) YP. Zhang and T.G. Oertner: Optical induction of synaptic plasticity using a light-sensitive channel. **Nature Methods** 4(2):139-41, 2007.

2) YP. Zhang, N. Holbro, T.G. Oertner: Single synapse LTP reveals input-specific accumulation of αCaMKII. **Submitted**, 2007.

3) M. Galic, A. Kriz, J. Reinhard, R. Vigot, YP Zhang, G. Bezakova, C.F. Bentzinger, D. Cloëtta, M. Stebler, B. Bettler, T.G. Oertner, M.A. Ruegg: Regulation of dendritic spine morphogenesis and synapse formation by Copine family members. **Submitted**, 2007.

4) R. Vigot, S. Barbieri, H. Bräuner-Osborne, R. Turecek, R. Shigemoto, YP. Zhang, R. Lujan, L.H. Jacobson, B. Biermann, JM. Fritschy, CM. Vacher, M. Müller, G. Sansig, N. Guetg, J.F. Cryan, K. Kaupmann, M. Gassmann M, T.G. Oertner, B. Bettler: Differential compartmentalization and distinct functions of GABA(B) receptor variants. **Neuron** 50(4): 589-601, 2006.

5) YP. Zhang, K. Deisseroth, T.G. Oertner: Optical induction of synaptic plasticity using channel rhodopsin-2. Program No. 39.7. Atlanta, GA: Society for Neuroscience, 2006. Online.

6) YP. Zhang, T.G. Oertner: Activity-dependent translocation of αCaMKII at individual synapses in the hippocampus. Program No. 739.1. San Diego, CA: Society for Neuroscience, 2004. Online.

7) X. Lin, ZM. Ma, X. Yao, YP. Zhang, YM. Wen: Replication efficiency and sequence analysis of full-length hepatitis B virus isolates from hepatocellular carcinoma tissues. **Int J Cancer** 102(5): 487-91, 2002.

References:

Dr. T. Oertner: Friedrich Miescher Institute Maulbeerstrasse 66, 4058 Basel,
Tel: +41 616978273

Prof. Dr. E. R. de Kloet: Division of Medical Pharmacology, Gorlaeus Laboratories,
P.O. Box 9502, Einsteinweg 55, 2300 RA Leiden,
the Netherlands, Tel: + 31 71 5274715